Freie Universität Berlin

Aspects of the zonally asymmetric Southern Hemispheric Circulation and Representation in the MPI Earth System Model

Dissertation

zur Erlangung des Grades eines
Doktors der Naturwissenschaften
am Fachbereich Geowissenschaften
der Freien Universität Berlin

vorgelegt von
Stella Babian
Berlin, April 2018

Erstgutachter	Prof. Dr. Ulrich Cubasch Institut für Meteorologie Freie Universität Berlin
Zweitgutachter	Prof. Dr. Henning Rust Institut für Meteorologie Freie Universität Berlin
Tag der Disputation	21. Juni 2018

Abstract

Due to the characteristic land-sea distribution of the southern hemisphere (SH) its atmospheric circulation is generally more zonally symmetric than its northern hemispheric equivalent. Distinct deviances from its symmetric nature, however, play an important role with regard to weather and climate on the regional scale, e.g. on the Antarctic sea ice distribution over the Amundsen Sea (Lefebvre et al., 2004). Thus the SH represents an ideal research area for the investigation of different aspects of the zonally asymmetric components of the circulation.

As the Antarctic Oscillation (AAO) is the leading mode of tropospheric variability an adequate representation in earth system models is essential. Therefore the first goal of this thesis is evaluating to what extent the AAO and its related precipitation patterns are represented in the MPI Earth System Model (MPI-ESM). This is done by comparing the spatial patterns of the AAO (given as EOFs) with their associated principal components (PCs) and precipitation patterns of the MPI-ESM to three different reanalyses. A comparison between the leading EOFs of the MPI-ESM and ERA-Interim indicates shifted and less pronounced centers of action in the MPI-ESM. Similarly the spectral density estimates of the associated PCs in the ESM show reduced variability for periods between 4 to 5 months. The relation between AAO and SH precipitation is assessed via composite and correlation analysis. Altogether the MPI-ESM underestimates the relation of AAO and SH precipitation but exhibits the same sign and spatial distribution of correlation values. These findings suggest a lack of El Niño-Southern Oscillation (ENSO) variability in the MPI-ESM and related teleconnections towards Antarctica, which accounts for the reduced variability over the Amundsen Sea.

One of the most prominent asymmetric features of the SH circulation is the split jet over Australia and New Zealand in Austral winter. Previous studies have developed indices to describe to what degree the upper-level mid-latitude westerlies are split. Furthermore, these studies have investigated the relationship of the split jet to the AAO and ENSO. The results of these studies, however, are fairly inconsistent in their message so that the relationship between the SH wintertime split jet and climate variability indices remains unclear. The scope of this thesis is a more thorough investigation of this link.

So far, all established split jet indices are based on a definition that is focused on the specific region in which the jet split is recognizable. In this thesis, the split jet is considered to be of a hemispheric nature rather than of a regional. Therefore a new, hemispherically defined index based on the principal components (PCs) of the zonal wind field for the Austral winter is proposed. A linear combination of PC2 and PC3 (PSI = PC2 – PC3) of the anomalous monthly (JAS) zonal wind is used to identify the split jet condition. The newly defined index indicates a strong coherence with the AAO. A regression analysis with the Multivariate ENSO Index indicates a non-linear relationship between PSI and ENSO, i.e. split jets occur

during strong positive and negative phases of ENSO but hardly under "normal" conditions.

The 2^{nd} and 3^{rd} PCA-mode of the geopotential height variability in 500 hPa are defined as the Pacific South American patterns. They exhibit only a weak correlation with the PSI, but they show a significant correlation with the individual components (PCs) of the PSI, thereby uncovering an indirect influence on the SH split jet variability. This leads to the conclusion that a positive AAO phase, as well as both flavors of ENSO and the PSA-1 pattern, produce favorable conditions for a SH split event.

The MPI-ESM's ability to reproduce the zonally asymmetric components of the SH circulation was further evaluated by an investigation of the split variability in the model. Modes larger than the first order in the zonal wind anomalies over the SH in Austral winter are found to be not distinguishable according to North's "rule of thumb". Nevertheless, PC1 and PC3 of the 200 hPa zonal wind field are found to contain the "model-intern" split variability. A composite analysis reveals, that the split variability is simulated insufficiently in the MPI-ESM. It is deduced that the split variability of the higher order PCs is mixed by the model. A likely cause for this difference compared to the reanalysis could be a low-pressure system over the Amundsen Sea, i.e. the Amundsen Sea Low (ASL). The model lacks ASL variability due to insufficiently simulated ENSO and its teleconnections which are known to reach and impact the ASL region. This can be confined by considering the climatologies and standard deviations of two associated fields (U_{200} and Z_{500}). Furthermore, it was analysed to what extent the model is able to reproduce the zonally asymmetric component by comparing the deviations from the zonal mean in both fields (U_{200} and Z_{500}). The zonal asymmetric part of the total variability is underestimated in the model especially over the ASL region and south of Australia, i.e. where the split jet is located. A composite analysis of the zonal asymmetric AAO component (i.e. the transient eddy portion) reveals that the model lacks substantial parts of the asymmetric AAO component. The composite's spatial distribution of significant values resembles approximately the PSA patterns in the reanalysis which are traditionally seen as the primary mechanism for the poleward transport of tropical signals. As this spatial structure is largely absent in the model, it is deduced that the deficiencies of the model in simulating the zonal asymmetric part of the SH circulation originate from the inadequate representation of ENSO variability including the high-latitude teleconnections to the ASL region. Consequently, improving the ability of the model to simulate the discussed variability modes would improve the representation of the SH split variability (and likely other asymmetric aspects of the SH atmospheric circulation) in the MPI-ESM.

Zusammenfassung

Aufgrund der charakteristischen Land- und Ozeanverteilung der südlichen Hemisphäre (SH) weist die atmosphärische Zirkulation verglichen mit der Nordhalbkugel eine größere zonale Symmetrie auf. Trotzdem gibt es deutliche Abweichungen von der symmetrischen Natur der SH Zirkulation, die auf regionaler Skala einen bedeutenden Einfluss auf das Klima und Wetter haben, z.B. auf die Antarktische Seeeis-Verteilung in der Amundsen See Region (Lefebvre et al., 2004). Die SH ist folglich ein ideales Forschungsgebiet, um verschiedene Aspekte der zonal asymmetrischen Komponenten der Zirkulation zu untersuchen.

Da die Antarktische Oszillation (AAO) als die erste Hauptkomponente der troposphärischen Variabilität definiert ist, ist eine adäquate Darstellung der AAO in Erdsystemmodellen (ESM) von großer Bedeutung. Die Evaluierung, inwieweit die AAO und die mit ihr verbundenen Niederschlagsmuster im MPI-ESM repräsentiert sind, ist folglich das erste Ziel dieser Arbeit. Dazu werden die räumlichen Muster der AAO (gegeben als EOFs) und ihre zugehörigen Hauptkomponenten (PCs) sowie die assoziierten Niederschlagsmuster des MPI-ESM mit drei verschiedenen Reanalysen verglichen. Der Vergleich zwischen den ersten Hauptkomponenten des MPI-ESM und der ERA-Interim Reanalyse zeigt, dass die charakteristischen „Aktionszentren“ der ersten Hauptkomponente im MPI Modell weniger betont und leicht verschoben sind. Konsistent mit diesem Ergebnis zeigt die spektrale Dichte der ersten PC im Modell reduzierte Variabilität für Perioden zwischen 4 und 5 Monaten im Vergleich zur Reanalyse. Der Zusammenhang zwischen AAO und Niederschlag wird mit Hilfe von einer Korrelations- und Kompositeanalyse evaluiert. Insgesamt unterschätzt das MPI-ESM die Beziehung zwischen AAO und dem Niederschlag über der SH, aber weist das korrekte Vorzeichen und eine ähnliche räumliche Verteilung der Korrelationswerte auf. Diese Ergebnisse suggerieren, dass die Darstellung der Variabilität der El Niño-Southern Oscillation (ENSO) sowie ihrer Telekonnektionen in die Antarktis im MPI-ESM mangelhaft ist und zu einer reduzierten Variabilität über der Amundsen See führt.

Eine der wichtigsten asymmetrischen Besonderheiten der SH Zirkulation ist der Split Jet über Australien und Neuseeland, der im südlichen Winter auftritt. Bisherige Studien haben Indizes entwickelt, die erfassen, zu welchem Grad die westlichen Winde in den höheren Schichten der Troposphäre gesplittet sind. Diese Studien haben weiterhin die Beziehungen zwischen dem Split Jet und der AAO sowie ENSO evaluiert. Die Ergebnisse dieser Studien sind jedoch inkonsistent untereinander, sodass die Zusammenhänge zwischen SH Split Jet Variabilität und den großskaligen Klimaindizes unklar bleiben. Ein weiteres Ziel dieser Arbeit ist daher die Untersuchung dieser Beziehungen.

Bis jetzt basieren alle gängigen Split Jet Indizes auf einer Definition, die auf die Region fokussiert ist, über der der Split Jet auftritt. In dieser Arbeit wird der SH Split Jet hingegen als ein hemisphärisches statt regionales Phänomen angenommen.

Deshalb wird ein neuer, hemisphärischer Index, basierend auf den PCs des zonalen Windes des südlichen Winters, vorgeschlagen. Eine lineare Kombination aus PC2 und PC3 (PSI = PC2 – PC3) der monatlichen Anomalien des zonalen Windes im Winter (JAS) dient der Identifikation des Split Jets. Der neu definierte Index weist auf eine starke Kohärenz mit der AAO hin. Eine Regressionsanalyse mit dem Multivariaten ENSO Index (MEI) zeigt einen nicht-linearen Zusammenhang zwischen PSI und ENSO, d.h., Split Jets treten unter stark positiven und negativen ENSO Phasen auf, aber seltener unter „normalen“ Bedingungen.

Die zweite und dritte Komponente der Variabilität des Geopotentials in der Höhe von 500 hPa sind als die PSA Muster definiert. Diese weisen eine schwache Korrelation zum PSI, aber eine signifikante zu den einzelnen Komponenten (PCs) des PSI auf und weisen so auf einen indirekten Einfluss auf die SH Split Jet Variabilität hin. Es wird geschlussfolgert, dass eine positive AAO Phase, sowie beide Ausprägungen der ENSO und des PSA-1 Musters begünstigende Bedingungen für ein Split Jet Ereignis darstellen.

Die Fähigkeit des MPI-ESM, die zonal asymmetrische Komponente der SH Zirkulation darzustellen, wurde weiterhin im Kontext des SH Split Jets im Modell untersucht. Die höheren Moden der zonalen Windvariabilität im SH Winter sind nach der „Daumenregel “ von North et al. (1982) im Modell nicht voneinander unterscheidbar. Dennoch enthalten PC1 und PC3 des 200 hPa Windfeldes die „modellinterne“ SH Split Jet Variabilität. Eine Kompositeanalyse zeigt jedoch, dass die Split Variabilität unzureichend im Modell simuliert wird. Ein wahrscheinlicher Grund für die Differenzen zwischen Modell und Reanalyse ist die unzureichende Modellierung des Tiefdruckgebiets über der Amundsen See (ASL). Die unzulängliche Simulation dieses Tiefs resultiert aus der unvollständigen Repräsentation der ENSO und ihrer Telekonnektionen, die bis in die Antarktis (ASL Region) reichen. Dies kann aus dem Vergleich der Klimatologien und der Standardabweichungen assoziierter Felder (U_{200} und Z_{500}) abgeleitet werden.

Das Fehlen von ASL Variabilität führt zu einem stärkeren (schwächeren) Subtropischen Jet (Polar Front Jet) im Vergleich zur ERA-Interim Reanalyse. Weiterhin wurde untersucht, inwieweit das Modell in der Lage ist, die zonal asymmetrischen Anteile der Zirkulation darzustellen, indem die Abweichungen vom zonalen Mittel in zwei assoziierten Feldern (U_{200} und Z_{500}) mit der Reanalyse verglichen wurde. Insgesamt unterschätzt das Modell die zonal asymmetrische Komponente der Zirkulation, vor allem über der ASL Region und südlich von Australien, wo sich der Split Jet befindet. Eine Kompositeanalyse der zonal asymmetrischen Komponente der AAO (d.h. der transienten Eddy Komponente) macht deutlich, dass im MPI-ESM wesentliche Teile der asymmetrischen AAO fehlen. Eine Kompositeanalyse der asymmetrischen AAO Komponenten in der Reanalyse zeigt weiterhin, dass die räumliche Struktur den PSA Mustern ähnelt. Diese sind in der Literatur mit der Kommunikation von tropischen Signalen in die polaren Regionen verbunden. Da dieses Muster im Modell weniger ausgeprägt ist, wird gefolgert, dass die

Defizite des Modells von der unvollständigen ENSO Simulation, inkl. der Telekonnektionen in die polaren Gebiete, stammen. Eine Verbesserung der Simulation der diskutierten Oszillationen würde folglich auch die Repräsentation des SH Split Jet (und vermutlich andere asymmetrische Aspekte der atmosphärischen SH Zirkulation) verbessern.

Abbreviations

AAO	Antarctic Oscillation
ASL	Amundsen Sea Low
BE	Split jet index as defined by Bals-Elsholz et al. (2001)
ENSO	El Niño-Southern Oscillation
EOF	Empirical Orthogonal Function
ESM	Earth System Model
HLM	High Latitude Mode
IH	Split jet index as defined by Inatsu and Hoskins (2006)
MPI	Max Planck Institute for Meteorology in Hamburg
PC	Principal Component
PSA	Pacific South American Modes (also referred to as PSA Patterns)
PSI	PC based Split Jet Index
SAM	Southern Annular Mode
SH	Southern Hemisphere
U	Zonal wind velocity (m/s) at a specific level
YC	Split jet index as defined by Yang and Chang (2006)
Z	Geopotential height (m) at a specific level

Contents

1 Introduction

1.1 Motivation

The Southern Hemisphere (SH) exhibits a unique landmass distribution, which is characterised by fewer landmasses and more water (roughly 80%) compared to its northern hemispheric counterpart. This has implications for the atmospheric circulation, especially over the high latitudes where the circulation is thereby nearly zonally symmetric. The zonal symmetry is only broken by the presence of the continental masses of Australia, South America and southern Africa and the huge Antarctic continent, which is shaped by elevations of up to 4892 m (Mount Vinson, Ellsworth Mountains near the Antarctic Peninsula). These orographic barriers induce notable zonal variations in the time-mean flow, which have large impact on weather and climate on the regional scale (e.g. Renwick et al., 1998). The main goal of this thesis is the examination of different aspects of these zonal asymmetric features of the SH tropospheric circulation in reanalysis data as well as in the earth system model (ESM) of the Max-Planck-Institute (MPI) in Hamburg.

The most important pattern of the tropospheric variability on timescales from weeks to decades (Kidson, 1999) in the SH middle and high latitudes is the "Antarctic Oscillation" (AAO; Gong and Wang (1999)). When the AAO is in its positive phase negative pressure anomalies prevail over Antarctica and positive pressure anomalies over the SH mid-latitudes. The AAO can thus be interpreted as the periodical strengthening and weakening of the circumpolar vortex, the belt of tropospheric westerlies surrounding the Antarctic continent (van den Broeke and van Lipzig, 2004).

The impacts of the AAO on the SH climate have been extensively examined in numerous studies in observations (e.g. Lorenz and Hartmann, 2001) as well as in models (e.g. Lu et al., 2007). Several climatological parameters were found to be associated with the AAO: the strength and location of the westerlies (Kidson, 1988), the Antarctic surface temperature (Marshall and Bracegirdle, 2015; Kwok and Comiso, 2002; van den Broeke and van Lipzig, 2004), sea surface temperatures in the southern oceans (Mo, 2000), Antarctic sea ice (Renwick, 2002; Baba and

Renwick, 2017; Kohyama and Hartmann, 2016), precipitation over South Africa (Reason and Rouault, 2005) and New Zealand / Australia (Pezza et al., 2008; Meneghini et al., 2007; Ummenhofer and England, 2007). A realistic representation of the large-scale variability in the MPI-ESM is therefore highly desirable.

The term "annular" mode captures the appearance of the AAO as a near-zonally symmetric pattern across the high southern latitudes in its mean state. The zonally symmetric structure exists primarily because the contributions of the eddy activity to the jet stream are roughly equal across all longitudes (Hall and Visbeck, 2002; Fogt et al., 2012). However, the phrase "annular" is only to some extent accurate, since the AAO describes a seesaw in geopotential height between the high- and mid-latitudes (Gong and Wang, 1999) and reveals regionally significant deviations from the zonally symmetric AAO structure. In particular over the southern Pacific Ocean and during Austral winter, there exist considerable anomalies relative to the zonal mean in both, geopotential height and zonal wind (Fogt et al., 2012).

Non-stationary impacts of the leading mode in tropospheric circulation have been found in temperatures over the Pacific sector including the Antarctic Peninsula where temperature anomalies are tied to the zonally asymmetric structure of the tropospheric variability (Fogt et al., 2012). Similar results were found by Marshall and Bracegirdle (2015) who examined the relationship between the AAO and the surface temperature at Halley Station (Antarctica). Changes in surface temperatures and sea ice have important implications for the stability of the Antarctic ice sheet and thus for the meridional temperature gradient which is the main driver for the SH zonal circulation. Therefore, the examination of the ability of earth system models to capture the symmetric and asymmetric components of the AAO is worthwhile, especially in the context of global climate models demonstrating an unrealistic high degree of zonal symmetry in the monthly AAO structure (Fyfe, 2003).

A further particular exception from the nearly zonal symmetry of the SH circulation is the presence of the wintertime split jet over the longitudes of Australia and New Zealand. The SH split jet is composed of a Subtropical Jet (STJ) on its northern flank, a Polar Front Jet (PFJ) at its poleward side and a pronounced "gap" of reduced zonal wind variability between those. A number of attempts have been made in the past to describe that split jet variability in terms of indices in different meteorological fields and vertical levels (Bals-Elsholz et al., 2001; Yang and Chang, 2006; Inatsu and Hoskins, 2006). These indices are constructed similarly, i.e. their definitions are based on the regions accounting for the two branches (STJ, PFJ) and the gap between those. A major goal of this thesis is the development

of a new PC based split jet index, without the rigid regional definitions and gives new insight into the relationships between the SH split jet and the large-scale teleconnection patterns (AAO, ENSO, PSA). These relationships which were found to be inconsistent in literature and the remaining open research question is thus aim of this thesis.

The presence of the SH split jet is (via eddy-mean flow interaction) strongly related to the location and intensity of storm tracks (Hio and Hirota, 2002) which in turn have large impact on regional climate, e.g. on the distribution of precipitation, cloudiness and radiation (Bengtsson et al., 2006). Small model errors in the latitudinal position of these features can lead to large local biases (e.g. Ceppi et al., 2012). Since the split jet is further associated with the extensively studied blocking situations over New Zealand (Trenberth and Mo, 1985; Mo et al., 1987; Renwick et al., 1998) it is of critical importance to simulate this asymmetric feature of the SH circulation in climate and earth system models.

To sum up, on monthly to seasonal timescales the SH circulation variability exhibits a pronounced asymmetric structure with a prominent center of low-frequency variance over the southern Pacific Ocean (Fogt et al., 2012). The main reason for a concentration of low-frequency variability over the Pacific sector appears to be the influence of teleconnections associated with the El Niño-Southern Oscillation (ENSO; e.g. Kidson (1999); Renwick (2002)) and the Pacific South American modes (PSA; e.g. Mo (2000); Hobbs and Raphael (2010)). Since it is specifically this region which coincides with the climatological location of the SH wintertime split jet, it is an exciting and convenient domain for the investigation of zonally symmetric and asymmetric features of the SH circulation in reanalyses as well as in climate models.

1.2 Fundamentals

1.2.1 Southern Hemispheric Circulation

The weather and climate in the mid-latitudes of both hemispheres is characterised by the existence of westerly jet streams, the Subtropical Jet (STJ) and the Polar Front Jet (PFJ). One of the key differences between the two jets is their vertical structure. The STJ is relatively shallow and confined to the upper branch of the Hadley cell whereas the eddy-driven PFJ extends throughout the depth of the troposphere. The STJ is driven by angular momentum transport from the tropics, which results in a westerly jet stream in the upper levels at the poleward edge of

the Hadley cell. The PFJ evolves as a result of the momentum and heat forcing arising from transient mid-latitude (baroclinic) eddies which balance the meridional temperature gradient induced by differential solar heating (e.g. Lee and Kim, 2003). Since the eddy forcing of the PFJ is distributed approximately equally across the SH longitudes, as there are fewer orographic effects compared to the northern hemisphere, the SH circulation is more zonally symmetric. The presence and the predominant regime of the jets is further governed by the seasonal cycle of the SH atmosphere.

Figure 1.1 shows the climatological 200 hPa zonal wind seasonal cycle for the SH. The maximum wind zones in the transitional seasons (SON and MAM) are characterised by a distinct spiral structure: a pronounced PFJ extends from longitudes around eastern Pacific to the Indian Ocean. Isochronal expands a STJ from about 70° E to nearly 90° W which is confined to the latitudes around 30° S.

In austral summer (DJF) a strong mid-latitude jet is established according to the weaker and wider Hadley circulation during that season. The zone of maximum wind speeds is nearly circumpolar (zonally symmetric) with a peak at approximately 30° S and highest zonal wind values occurring between the longitudes of the southern South Atlantic Ocean and south of Australia. During the summer season, the mid-latitude jet is weak over the western South Pacific Ocean but reestablishes towards the eastern South Pacific Ocean.

In contrast, the Austral winter (JJA) circulation is characterised by a strong STJ with a zone of maximum wind speeds between the longitudes of the Southern Indian Ocean and the biggest part of the central South Pacific Ocean. A distinct characteristic of the Austral winter circulation is the zonally asymmetric structure with the typical time-mean split jet occurring at the longitudes of New Zealand and Australia. The split jet is composed of a pronounced STJ over Australia (between 25° and 30° S), which is paralleled by a second jet, the PFJ (around 60° S) developing over the southern Indian Ocean and a zone of weak westerlies (gap) between both jets.

Additionally to the seasonal variability, the wintertime SH atmospheric circulation exhibits strong year-to-year variability in the zonal wind field. Although the time-mean upper-tropospheric flow exhibits the asymmetric split jet structure, there are winter months which lack the typical split jet feature and are rather characterised by a merged or "non-split" jet regime. Figure 1.2 shows two (monthly mean) fields of the zonal wind at 200 hPa. The left panel of Fig. 1.2 illustrates a typical split jet event as occurred in July 2015 and the right panel shows an exemplary month of a"non-split" regime which took place in July 2009.

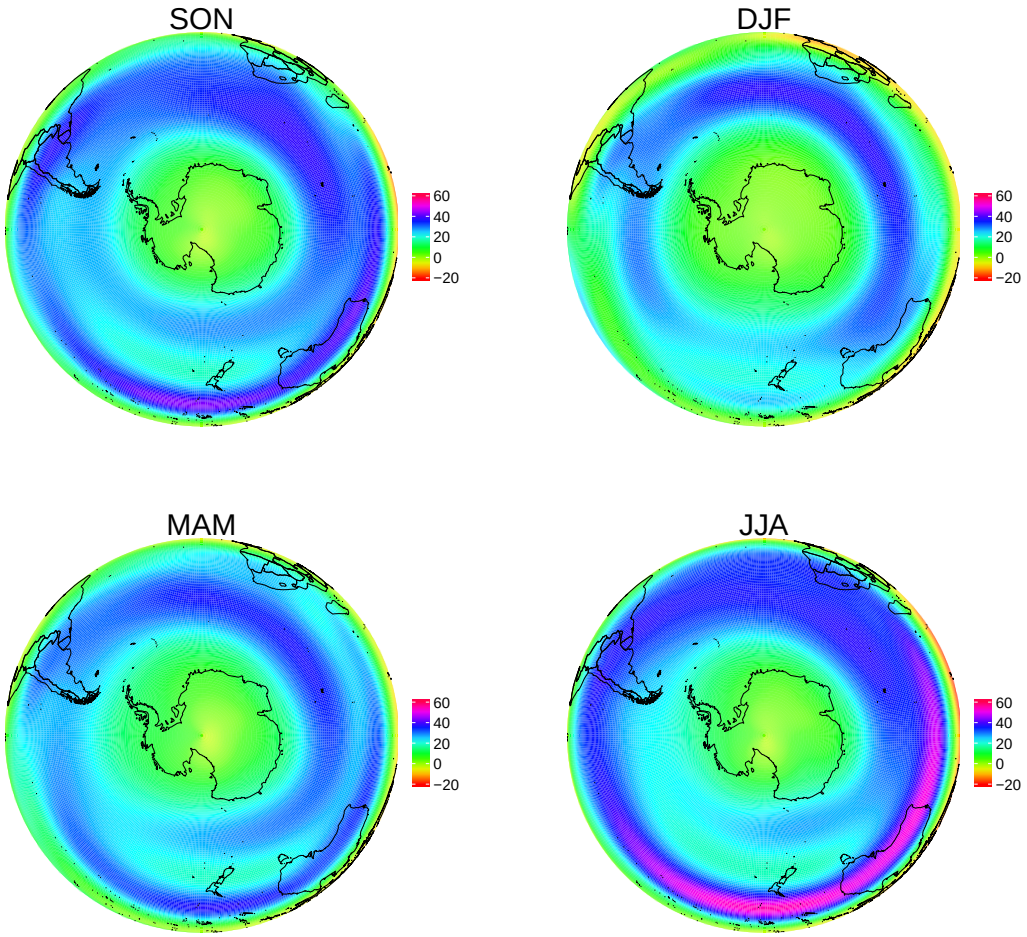

Figure 1.1: *Seasonal SH zonal wind climatologies [m/s] at 200 hPa level for SON (top left), DJF (top right), MAM (bottom left) and JJA (bottom right) based on ERA-Interim reanalysis data and averaged for the 1979–2015 period, respectively.*

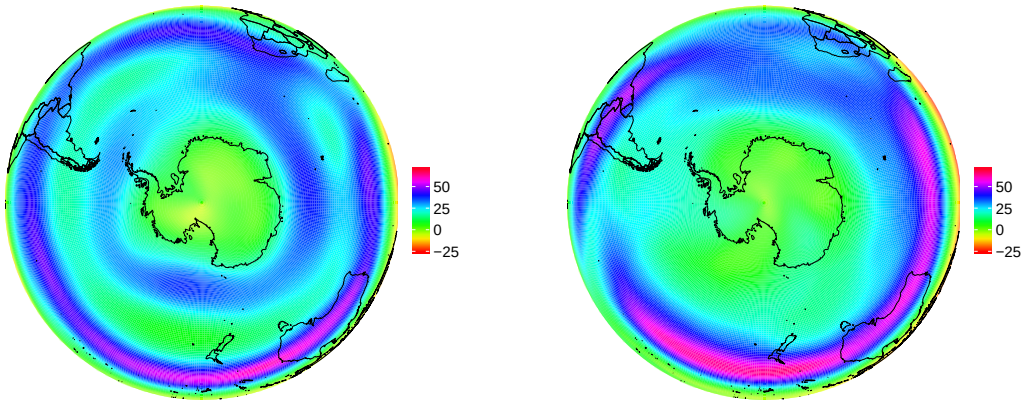

Figure 1.2: *Exemplary split and non-split jet months in July 2015 (strong split event, lhs) and in July 2009 (non-split flow, rhs). The data of both panels stem from the monthly mean zonal wind [m/s] at 200 hPa of the ERA-Interim reanalysis.*

1.2.2 Large-scale teleconnection patterns

Antarctic Oscillation

The leading mode of tropospheric variability on timescales from weeks to decades (Kidson, 1999) in the SH middle and high latitudes is the "Antarctic Oscillation" (AAO, that terminology is used in this thesis hereafter; Gong and Wang (1999)), which is in literature also referred to as the "High Latitude Mode" (HLM; Rogers and Van Loon (1982)) or the Southern Annular Mode (SAM). As the dominant mode of SH extra-tropical (south of 20° S) variability, the AAO is defined as the first principal component (PC) or leading empirical orthogonal function (EOF) of geopotential height (with a nearly barotropic structure) from the sea level throughout the troposphere (see Methods, Chap. 3). It represents roughly 35 % of the total variance in the SH troposphere.

The spatial structure of the AAO is characterised by pressure anomalies of one sign over the polar region, surrounded by a band of anomalies of the opposing polarity over the mid-latitudes between 40° to 50° S. The AAO reflects the strength and position of the westerly winds over the mid-latitudes that circle the Antarctic continent, following the meridional atmospheric pressure gradient (Thompson and Wallace, 2000). The positive phase of the AAO can thus be interpreted in terms of a poleward shift of the PFJ relative to its climatological position around 45° S. This

structure is sustained by a positive feedback from transient high-frequency eddies (Codron, 2007). The importance of the AAO to the PFJ was in literature further highlighted by Gerber et al. (2008) who found that the annular modes characterize both, the spatial and the temporal properties of the (eddy-driven) polar front jet streams in both hemispheres.

During southern summer the AAO is found to be largely zonally symmetric whereas during Austral winter it exhibits increased zonal wave number 2-3 variability. This asymmetric part of the AAO is most pronounced near the Drake Passage where the high terrain of both southern South America and the Antarctic Peninsula act to create a regional asymmetry over the Amundsen and Bellingshausen Seas (Lefebvre et al., 2004). Fogt et al. (2012) cautioned therefore to consider both, the zonally symmetric and asymmetric components of the AAO structure, especially when examining seasonal variations of the SH tropospheric variability.

The large-scale and manifold impacts of the symmetric and asymmetric components of the AAO on the SH climate have been introduced and summarised in detail in the previous section and are thus not repeated here. The interested reader is referred to e.g. Gong and Wang (1999); Thompson and Wallace (2000); Fogt et al. (2012).

The Austral summer (DJF) and autumn (SON) AAO as calculated from observation and reanalysis data are found to exhibit significant positive trends during recent decades (e.g. Fyfe et al., 1999) due to greenhouse gas increases and ozone depletion over Antarctica (Zhang et al., 2014). Therefore, the Austral wintertime AAO was tested prior to any analysis in the context of this thesis for significant trends (see Methods, Chap. 3). However, there was no detectable trend in the Austral wintertime during the analysis period of 1979–2015.

El Niño-Southern Oscillation

The El Niño-Southern Oscillation (hereafter ENSO) is a coupled ocean-atmosphere phenomenon and a leading climate mode in the tropical sea surface temperature (hereafter SST) variability that has significant impacts on ecosystems and global climate (Kim et al., 2017; Trenberth and Caron, 2000, and references therein) on the interannual time scale.

During El Niño (La Niña) phases the tropical SSTs raise at all longitudes which result in increased (equatorial) convection and a stronger Hadley cell. It follows that the STJ (PFJ) strengthens on its equatorward flank (Seager et al., 2003) and simultaneously the PFJ (STJ) weakens (Karoly, 1989; Chen et al., 1996; Kitoh,

1994). This results in an equatorward shift of the jet and the associated storm track. Although the AAO appears as a main modulator of the latitude and strength of the PFJ, influencing to a minor extent its subtropical counterpart, the ENSO was found to influence properties of the PFJ, i.e. the ENSO cycle modifies the latitude, strength and preferred wavenumber of the PFJ (Gallego et al., 2005).

Pacific South American Patterns

As previously mentioned, the leading EOF of the geopotential height in several tropospheric levels is (per definition) the AAO which exhibits nearly zonally symmetric, although opposing height anomalies at high- and mid-latitudes.

The Pacific South American (PSA) modes are represented by two higher order EOF patterns (2^{nd} and 3^{rd} EOF correspond to the PSA1 and PSA2 modes, respectively) of the SH 500 hPa geopotential height anomalies (Mo, 2000). Both modes are in quadrature with each other and depict a zonal wavenumber 3 structure which is associated with a wave train expanding from the tropical Pacific to Argentina (Ding et al., 2016; Irving and Simmonds, 2016).

The PSA has been found to be associated with variations in the upper-level zonal wind over the South Pacific, which may then affect other meteorological fields, i.e. precipitation patterns over New Zealand as well as surface temperatures and sea ice cover over the Antarctic Peninsula (Ding et al., 2016; Kwok and Comiso, 2002; Yuan, 2004).

1.3 Objectives

The main objective of this thesis is the investigation of the symmetric and different aspects of the asymmetric features of the SH extra-tropical circulation. To this end, the following summary gives an overview of the research questions posed prior to the analysis. The three major research questions (bold face) refer to the three main parts of this thesis and refer to the chapters 4, 5 and 6, respectively.

Chap. 4: Is the MPI-ESM able to reproduce the spatial patterns of the Antarctic Oscillation (AAO) and related precipitation?

- How is the leading EOF in SH geopotential height at 700 hPa represented in the MPI-ESM?

- Can mechanisms be identified which cause the deficiencies in the MPI-ESM?
- How are the SH precipitation patterns related to the AAO in the MPI-ESM?

Chap. 5: Can a hemispheric index be defined which clarifies the relationships between the SH wintertime split jet variability and the large-scale teleconnection patterns ENSO, AAO and PSA?

- Can a SH wintertime split jet index be found which is superior to the rigid regional definitions used for established indices?
- Is the SH wintertime split jet related to the large-scale teleconnection indices (i.e. ENSO, AAO and PSA)?

Chap. 6: Is the MPI-ESM able to reproduce the SH wintertime split jet variability?

- Can a PC based split jet index be applied in the MPI-ESM as in ERA-Interim?
- Can causes be identified which account for potential shortcomings of the model in representing the SH split jet variability?
- Are the zonal asymmetric components of the SH circulation depicted by the MPI-ESM?

1.4 Outline

In the following sections, a detailed study of aspects of asymmetric features of the SH circulation in reanalysis data as well as in the MPI earth system model will be presented. This thesis is therefore structured into three main parts, which can be read largely independent of each other. The first part of this thesis (Chap. 4) was published in the context of a special issue concerned with the evaluation of the MPI earth system model in the journal *Meteorologische Zeitschrift*.[1] The second part of this thesis (Chap. 5) was published in the *Atmospheric Physics and Chemistry*

[1] **Babian, S., Rust, H. W., Grieger, J., and Cubasch, U. (2016).** *Representation of the Antarctic Oscillation and related precipitation in the MPI Earth System Model.* Meteorol. Z., 17:12635, doi: 10.1127/metz/2016/0661

journal.[2] If the phrase "this study" is used in the following, the corresponding chapter is referred to these papers.

- Chapter 2 provides an overview of the reanalysis data used throughout this thesis as well as the model data utilised in the second (Chap. 4) and third part (Chap. 6) of this thesis.

- Chapter 3 gives information about the calculation of Empirical Orthogonal Functions (EOFs), which are the essential part of Chap. 4. The methods to compute three established split jet indices as well as the new proposed PC based split index are presented in Sec. 3.4. In order to investigate further symmetric and asymmetric components of the SH, several statistical analysis approaches, i.e. spectral, correlation and composite analysis were described in this chapter.

- In Chapter 4 the ability of the MPI-ESM to represent the AAO and related precipitation patterns over the SH is evaluated and compared to three reanalysis data sets.

- Chapter 5 deals with the SH wintertime split jet variability. A new PC based split jet index (PSI) is introduced and compared to three established split jet indices. The PSI is then used to investigate the relationship between the SH split jet variability and the large-scale teleconnection indices (AAO, ENSO and PSA).

- Chapter 6 evaluates the potential of the MPI-ESM to reproduce the SH wintertime split jet variability. A method to compute a respective PSI in the model is suggested and possible causes for differences between the model and the ERA-Interim reanalysis in illustrating the split jet variability are examined.

- The main results of this thesis are finally summarised and discussed in Chapter 7. An overview of potential future work is given in Chapter 8.

[2] **Babian, S., Grieger, J., and Cubasch, U. (2017).** *A New Index for the Wintertime Southern Hemispheric Split Jet.* Atmospheric Chemistry and Physics Discussions, 2017:1–19, doi: https://doi.org/10.5194/acp-2017-840

2 Data

2.1 Reanalyses

Three reanalyses data sets provide the reference for the first part of this thesis (Chap. 4): the National Center for Environmental Prediction and National Center for Atmospheric Research (NCEP/NCAR) reanalysis (Kalnay et al., 1996; Kistler et al., 2001), the ERA-40 (Uppala et al., 2005), and ERA-Interim (Dee et al., 2011) reanalysis data from the European Centre for Medium Range Weather Forecast (ECMWF). Table 2.1 gives further details on the three reanalysis data sets and the MPI-ESM (see Sec. 2.2).

The monthly mean geopotential height at 700 hPa (Z_{700}) is the basis for defining the AAO pattern and index (Sec. 3.5). The monthly precipitation rate from NCEP/NCAR and the monthly total precipitation sums from the ECMWF products ERA-40 and ERA-Interim provide reliable precipitation data for the SH (Bracegirdle and Marshall, 2012).

The second part of this thesis (Chap. 5) makes use only of the ERA-Interim (Dee et al., 2011) reanalysis data sets from the European Centre for Medium Range Weather Forecast (ECMWF). ERA-Interim was selected from the above mentioned reanalysis data sets because ECMWF products (e.g. mean sea level pressure and

Model/Data	**horizontal resolution**	**vertical levels**	**time period available**
NCEP/NCAR	2.5°	17	1948 – 2005
ERA-40	3.75°	23	1958 – 2001
ERA-Interim	1.5°	37	1979 – 2013
MPI-ESM (Atm./Ocean)	1.88°(T63)/0.4°	95/40	1850 – 2005

Table 2.1: *Resolution, levels and available time periods of NCEP/NCAR, ERA-Interim, ERA-40 and of the historical run of the MPI-ESM. The resulting common period of reanalyses and model run is 1979–2001.*

geopotential height at 500 hPa from ERA-Interim) were found to be the most reliable data, in particular over the Antarctic region (Bracegirdle and Marshall, 2012). Monthly zonal wind and geopotential height data were used covering the winter seasons which are defined here for the months from July to September (JAS) in accordance with earlier studies concerned with the SH split jet variability (Bals-Elsholz et al., 2001; Yang and Chang, 2006; Inatsu and Hoskins, 2006). All fields were used on a 0.75° grid and were analysed for the period from 1979 to 2015.

The last part of this thesis (Chap. 6) investigates both, the ERA-Interim reanalysis described above, as well as the MPI-ESM-MR model zonal wind and geopotential height data for the SH split jet variability. For the purpose of comparison, the analysis period was set to 1979–2005 to account for the common period of ERA-Interim and the model run.

2.2 MPI Earth System Model

Various initialization techniques have been used to perform decadal prediction experiments (Müller et al., 2012; Pohlmann et al., 2013; Kruschke et al., 2015) with the Max-Planck-Institute's Earth System Model (MPI-ESM, Giorgetta et al., 2013). The MPI-ESM consists of an atmospheric component, ECHAM6 (Stevens et al., 2013), an ocean and sea ice model MPIOM (Marsland et al., 2003; Giorgetta et al., 2013) coupled with OASIS3 (Valcke, 2013). Furthermore, the subsystems JSBACH (Raddatz et al., 2007) and HAMOCC (Ilyina et al., 2013) contribute the biosphere and the bio-geochemical processes.

Here, the MPI-ESM-MR (mixed resolution) with a T63 resolution in the atmosphere is considered, similar to the LR (low resolution) version of the MPI-ESM but with an extended vertical resolution of 95 levels (instead of 47 levels in LR) reaching up to 0.01 hPa. The horizontal resolution corresponds to a 1.88°×1.88° grid. The oceanic component of the model is available on a 0.4°×0.4° grid and 40 vertical levels (Marotzke et al., 2016).

The so-called historical run (MPI-ESM-MR-hist) with the radiative forcing given by the observed forcing for the period from 1850 to 2005 and an interactive carbon cycle is used (boundary conditions). These uninitialised historical runs of the particular model with prescribed boundary conditions serve as reference experiments within the MiKlip project (see Chap. 4) to quantify predictive power (skill) of initialised over uninitialised runs.

2.3 Climate Indices

The monthly resolved teleconnection indices used in the second part of this thesis (Chap. 5), namely the Antarctic Oscillation Index and the Multivariate ENSO Index are both freely available from NOAA's website (`http://www.noaa.gov/`). The website was last visited in January 2018.

3 Methods

Consistent with the majority of existing literature, this thesis focuses on the monthly timescale. Monthly anomalies were obtained by removing the monthly mean quantity with respect to the considered time period (i.e. 1979–2001 for the first, 1979–2015 for the second part and 1979–2005 for the last major part of this thesis, accounting for different lengths of the model and reanalysis data sets, respectively). Many time series used in this thesis are standardised which means that they have a mean of zero and a standard deviation of one. All time series have been tested with a Mann-Kendall trend test for significant trends prior to the application of the methods described in the following.

3.1 Spectral Analysis

The characteristics of time series that have been Fourier-transformed are often summarised using a plot known as a periodogram or Fourier line spectrum (Wilks, 2011). The characteristic plot of a spectrum consists of the squared amplitudes C_k^2 as a function of the frequencies ω_k. The spectrum reveals the proportions of variation in the original data series accounting for oscillations (the harmonic frequencies) but lacks information concerning the time domain, i.e. when these oscillations are expressed (Wilks, 2011).

A spectral analysis of the principal components (PCs, see Sec. 3.3) reveals their activity on various time scales. The classical Fourier periodogram is in this thesis obtained from the index time series, tapered with a split cosine for 10 % of the data at both ends. An associated consistent estimate of the spectral density can be obtained in two ways: either parametrically, using auto-regressive processes of order p (AR[p]) or non-parametrically using kernel smoothing (e.g., Priestley, 1992; Venables and Ripley, 2002). AR[p] processes with the Yule-Walker-equations were used to estimate the associated parameters (e.g., Brockwell and Davis, 1991; Box and Jenkins, 1976); the Akaike-Information Criterion (AIC, e.g. deLeeuw, 1992; Venables and Ripley, 2002) guides the selection of orders p. Additionally, a modified Daniell kernel is used as a non-parametric density estimate with the

degree of smoothness defined such that it roughly corresponds to the flexibility of the associated AR-process. Spectral density estimates are based on the R-functions `spec.pgram()` and `spec.ar()` (R Core Team, 2013).

3.2 Composite and Correlation Analysis

Composite mean fields are calculated throughout this thesis for various temporal subsets (e.g. all times corresponding to the positive or negative phase of the PSI). The positive composite of a monthly time series of an index (e.g. the PSI) is defined as the values (time steps) exceeding a certain threshold of the respective index, and vice versa for the negative composite. In this thesis, monthly index values exceeding (undercutting) the normalised index mean over the respective time period about plus (minus) one standard deviation (e.g. Hendon et al., 2007) were defined as positive (negative) composite, respectively. The values (time steps) which are defined in this way as an element of a positive / negative composite (e.g. corresponding to the high or low PSI values) are then used to calculate composite maps in different meteorological fields (e.g. zonal wind at 200 hPa).

The monthly composites with an anomalous high or low index allow the examination of the dominant spatial pattern of the anomalies associated with the behavior of the (e.g.) PSI and are then used for investigating the potential mechanisms associated with the zonally symmetric and asymmetric parts of the SH variability.

In order to get the composite anomalies, the periods' monthly mean was removed afterward from the composites. Lastly, two-sided, one sample t-tests were applied at each grid point to examine the null hypothesis that the composite mean anomaly had been drawn from a population centered on zero.

Spearman's rank correlation coefficient quantifies the relationship between different teleconnection indices and the time series of monthly reanalysis and model data (Wilks, 2011). The Spearman's rank correlation coefficient is in literature known as the Pearson correlation coefficient computed using the ranks of the data:

$$r_{rank} = 1 - \frac{6 \sum_{i=1}^{n} D_i^2}{n(n^2 - 1)}, \tag{3.1}$$

where D_i is the difference in ranks between the ith pair of data values and n is the sample size.

3.3 Empirical Orthogonal Function (EOF) Analysis

Analysis of atmospheric circulation patterns can be done by means of an Empirical Orthogonal Functions Analysis (EOF) which is in literature also referred to as Principal Component Analysis (PCA) (Jolliffe, 2002; Hannachi et al., 2007).

The original purpose of the EOF Analysis was to reduce the large number of variables of an original data set to a few variables, while retaining much of the explained variance (Hannachi et al., 2007). Lately, however, EOF analysis has been used to extract individual modes of variability such as the Antarctic Oscillation (AAO) (Thompson and Wallace, 2000). The following description of how the EOFs are defined and derived follows Jolliffe (2002).

Presume a vector $\boldsymbol{x}$ of p random variables which are centered (i.e. their average is zero). The variable x_i denotes in this thesis typically a time series of zonal wind or geopotential height values at a certain grid point i. The first step in a PCA is then to look for a linear function $\boldsymbol{\alpha}_1'\boldsymbol{x}$ of the elements of $\boldsymbol{x}$ which maximizes the variance of $\boldsymbol{\alpha}_1'\boldsymbol{x}$, where $\boldsymbol{\alpha}_1$ is a vector of p constants and the inverted comma ($'$) denotes a transposed vector:

$$\boldsymbol{\alpha}_1'\boldsymbol{x} = \alpha_{11}x_1 + \alpha_{12}x_2 + \ldots + \alpha_{1p}x_p = \sum_{j=1}^{p} \alpha_{1j}x_j. \tag{3.2}$$

In the next step a linear function $\boldsymbol{\alpha}_2'\boldsymbol{x}$ is wanted which is uncorrelated with (i.e. orthoganal to) $\boldsymbol{\alpha}_1'\boldsymbol{x}$, while having the maximum variance, and so on, so that at the kth stage a linear function $\boldsymbol{\alpha}_k'\boldsymbol{x}$ is found that has maximum variance and is uncorrelated with $\boldsymbol{\alpha}_1'\boldsymbol{x}$, $\boldsymbol{\alpha}_1'\boldsymbol{x}$,..., $\boldsymbol{\alpha}_{k-1}'\boldsymbol{x}$. The derived variable $\boldsymbol{\alpha}_k'\boldsymbol{x}$ is called the kth PC. In general, it is expected that the first m PCs, where $m \ll p$, account for most of the variance found in the data set.

In order to find the first PC, $\mathrm{Var}(\boldsymbol{\alpha}_1'\boldsymbol{x}) = \boldsymbol{\alpha}_1'\boldsymbol{\Sigma}\boldsymbol{\alpha}_1'$ is maximized, where $\boldsymbol{\Sigma}$ is the covariance matrix of $\boldsymbol{x}$. The maximum will not be archived for finite $\boldsymbol{\alpha}_1$. So a normalization constraint must be imposed: $\boldsymbol{\alpha}_1 = 1$. The standard approach to maximize $\boldsymbol{\alpha}_1'\boldsymbol{\Sigma}\boldsymbol{\alpha}_1$ is to use Lagrange multipliers. Maximize

$$\boldsymbol{\alpha}_1'\boldsymbol{\Sigma}\boldsymbol{\alpha}_1 - \lambda(\boldsymbol{\alpha}_1'\boldsymbol{\alpha}_1 - 1) \tag{3.3}$$

where λ is the Lagrange multiplier. Afterwards Eq. 3.3 is differentiated with respect to $\boldsymbol{\alpha}_1$ which gives

$$\boldsymbol{\Sigma}\boldsymbol{\alpha}_1 - \lambda\boldsymbol{\alpha}_1 = 0 \tag{3.4}$$

or

$$(\boldsymbol{\Sigma} - \lambda \boldsymbol{I})\boldsymbol{\alpha}_1 = 0, \tag{3.5}$$

where $\boldsymbol{I}$ is the identity matrix. λ is an eigenvalue of $\boldsymbol{\Sigma}$ and $\boldsymbol{\alpha}_1$ the corresponding eigenvector. It can be shown that all p linear functions $\boldsymbol{\alpha}_j'$ are eigenvectors of the covariance matrix $\boldsymbol{\Sigma}$. Furthermore, the sign of the basis vectors are arbitrary and have no meaning.

A more detailed description of the theoretical background of the EOF analysis can the interested reader find for example in Wilks (2011); Jolliffe (2002); Hannachi et al. (2007).

Unfortunately, the eigenvalues are not necessarily distinct due to sampling issues. North et al. (1982) provide a "rule of thumb" for determining if a particular eigenvalue (mode) is distinct from its nearest neighbor. An approximation for a "typical" error of the estimated EOFs can be expressed by

$$\Delta\boldsymbol{\alpha}_i \approx \sqrt{\frac{2}{n}} \sum_{j=1, j\neq i}^{m} \frac{c}{\lambda_j - \lambda_i}\boldsymbol{\alpha}_j, \tag{3.6}$$

where c is a constant, λ_j is the closest eigenvalue to λ_i and n is the number of independent samples. By combining the "typical" error in λ_i ($\Delta\lambda_i \approx \lambda_i\sqrt{\frac{2}{n}}$) with Eq.3.6, North et al. (1982) finally obtain

$$\Delta\boldsymbol{\alpha}_i \approx \frac{c\Delta\lambda_i}{\lambda_j - \lambda_i}\boldsymbol{\alpha}_j. \tag{3.7}$$

"The rule is simply that if the sampling error of a particular eigenvalue is comparable to or larger than the spacing between λ and a neighboring eigenvalue, then the sampling errors for the EOF associated with λ will be comparable to the size of the neighboring EOF. The interpretation is that if a group of true eigenvalues lie within one or two $\delta\lambda$ of each other, then they form an "effectively degenerate multiplet", and sample eigenvectors are a random mixture of the true eigenvectors" (North et al., 1982).

Prior to the variability analysis of the SH zonal wind, the seasonal cycle was removed by taking the anomalies with respect to a mean annual cycle which was obtained by an average of the individual winter months of the year. The individual grid cells are then centered and scaled with the square-root of their latitude to account for different grid cell sizes. An EOF analysis of the 111 winter months from the period 1979–2015 was then performed. The time series of each EOF mode

(the associated PC) are determined by projecting the spatially weighted anomalies onto the derived eigenvectors.

3.4 Split Jet Index Definitions

Figure 5.1 shows the 200 hPa climatological SH winter (JAS) zonal mean wind and the typical time-mean split jet, composed of a subtropical (at 30° S) and a polar branch (roughly at 60° S) as well as the characteristic zonal wind minimum in between.

The three established split jet indices are based on flow characteristics for the specific regions of Australia and New Zealand (see Fig. 3.1). Each index is based on a Subtropical Jet (STJ) and a Polar Front Jet (PFJ) component and a gap between these two branches except the index of Yang and Chang (2006) which lacks the subtropical part. Table 3.1 provides information about these areas and gives an overview of the particular data sets used in the split jet references.

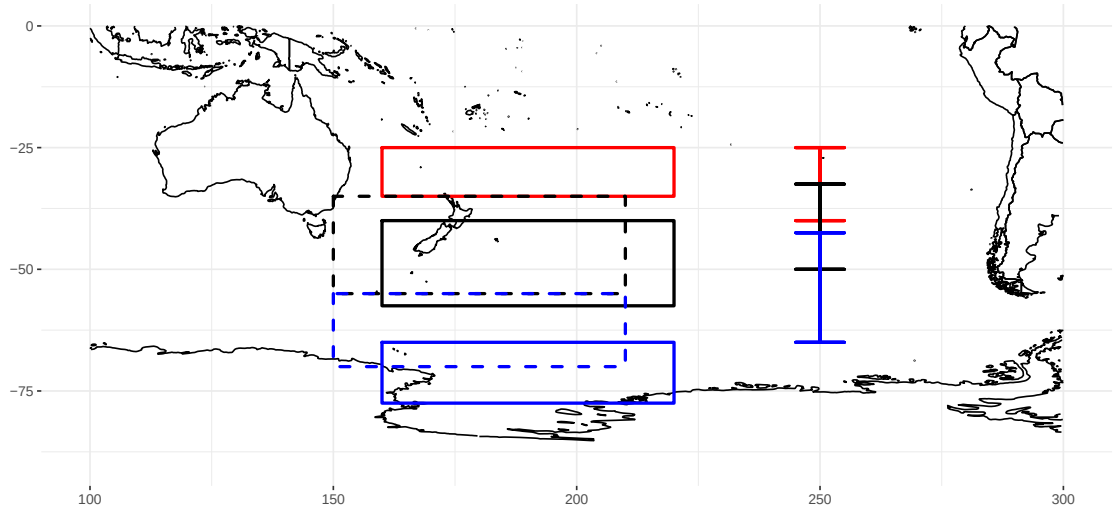

Figure 3.1: *Area definitions of three previous studies. Red lines show the STJ part, blue lines the PFJ part and the black lines the gap between the two branches defined by the different studies. Continuous lines refer to the SFI of Bals-Elsholz et al. (2001) and dashed lines mark the two regions defined in Yang and Chang (2006). The right side shows the meridional boundaries used in the split index defined by Inatsu and Hoskins (2006).*

	SFI (BE)	**STJ (YC)**	**STJ (IH)**	**PSI**
Reference	Bals-Elsholz et al. (2001)	Yang and Chang (2006)	Inatsu and Hoskins (2006)	Babian et al. (2017)
Data sets				
Variable	relative vorticity	zonal wind	zonal mean wind	zonal wind
Level	200 hPa	300 hPa	mean of 200 and 300 hPa	200 hPa
Data Source	NCEP NCAR	ERA15	ERA40	ERA-Interim
Period	1958 – 2000	1979 – 1993	1979 – 2001	1979–2015
Regions used for definitions				
STJ	25° – 35° S	–	25° – 40° S	SH
GAP	40° – 57.5° S	35° – 55° S	32.5° – 50° S	
PFJ	65° – 77.5° S	55° – 70° S	42.5° – 65° S	

Table 3.1: *List of split jet definition constraints as suggested in three earlier studies. The indices resemble specific areas depicting the equatorward branch of the split (STJ), the gap between the jets (GAP) and the Polar Front Jet part (PFJ).*

3.4.1 Split-flow Index (SFI)

Bals-Elsholz et al. (2001) developed the very first split index to evaluate the structure and evolution of the SH split jet structure. A Split-Flow Index (SFI) based on the relative vorticity (ζ) at 200 hPa in three neighboring regions (Fig. 3.1) was designed as follows:

$$SFI = \zeta_{PFJ} + \zeta_{STJ} - \zeta_{GAP} \tag{3.8}$$

The normalised monthly index gives large negative (positive) values for split (non-split) years. Split flow regimes similar to the climatological mean have normalised SFI values near zero.

3.4.2 Normalised Monthly Split-Jet Index (NMSJI)

The Yang and Chang (2006) Split Jet Index (SJI) is based on the difference in 300 hPa time-mean zonal wind anomalies (U) in two adjoining areas (PFJ, GAP). The index is normalised then by subtracting the climatological mean and by dividing its standard deviation.

$$SJI = \overline{U}_a^{PFJ} - \overline{U}_a^{GAP} \tag{3.9}$$

$$NMSJI = \frac{MSJI - \overline{MSJI}}{\sigma} \tag{3.10}$$

3.4.3 Split Jet Index (SJI)

The Split Jet Index published by Inatsu and Hoskins (2006) was defined as the difference of the 200 hPa and 300 hPa zonal mean zonal wind (U) between the (overlapping) latitudinal boundaries given in Tab. 3.1 and illustrated in Fig. 3.1.

$$SJI = U_{STJ} - 2 \cdot U_{GAP} + U_{PFJ} \tag{3.11}$$

In agreement with the weighting of the wind minimum between the jets by 2, the index values rise for both, a strong STJ and/or PFJ and reduce or even reverse if there is a strong single jet centered in the (gap) region between the two jets.

3.5 Climate Indices

3.5.1 Definition of the Antarctic Oscillation Index

The AAO is most commonly defined as the leading empirical orthogonal function (EOF) of a near-surface geopotential height anomaly field south of 20° S (e.g. Thompson and Wallace, 2000). In this thesis, the first EOF of a principal component analysis (Jolliffe, 2002; Hannachi et al., 2007) of the monthly mean Z_{700} anomalies south of 20° S over the SH defines the spatial pattern of the AAO (Thompson and Wallace, 2000; Mo, 2000; Climate Prediction Center, 2014). The associated principal component (PC) gives the AAO index time series. The geopotential height anomalies are taken with respect to a mean annual cycle obtained by averaging individual month of the year for the respective time period. The individual grid cells are centered and scaled with the square-root of their latitude to account for different grid cell sizes.

3.5.2 Pacific South American Patterns

By definition, the PSA modes are the second and third EOF of the 500 hPa geopotential height anomalies over the SH (Mo, 2000). The associated PCs give the PSA-1 (2^{nd} PC) and PSA-2 (3^{rd} PC) time series. The calculation of the EOF patterns and the associated time series (PCs) was carried out analogous to the procedure to calculate the AAO (see Sec. 3.5.1 and Sec. 3.3).

4 Representation of the Antarctic Oscillation and related precipitation in the MPI-ESM

This chapter has been published in Meteorologische Zeitschrift.[1] *The co-authors supervised the work on the manuscript. The remaining work was carried out by Stella Babian.*

The most important pattern of climate variability in the Southern Hemisphere (SH) middle and high latitudes is the Antarctic Oscillation (AAO). This variability mode is defined as the leading empirical orthogonal function (EOF) of the 700 hPa geopotential height anomaly field south of 20° S (Thompson and Wallace, 2000; Mo, 2000). The predominant pattern (leading EOF) of the AAO is roughly circular with its center at the south pole (zonally symmetric) and changes sign between 40° S to 50° S (Thompson and Wallace, 2000; Kidson, 1999; Climate Prediction Center, 2014). Phases with a positive AAO index are by convention associated with positive geopotential height anomalies over the mid-latitudes and negative anomalies over Antarctica; vice versa for negative phases. The temporally evolving meridional geopotential height gradient results in periodical strengthening and weakening of the circumpolar vortex in the SH which, in turn, affects other meteorological fields.

As the leading mode of temporal variability of atmospheric circulation in the SH, the AAO has remarkable impacts on regional climate (Rashid and Simmonds, 2005). Several studies examined selected climatological parameters with respect to potential connections with the AAO: changes in strength and location of the westerlies (Kidson, 1988), storm tracks and extra-tropical cyclones (Pezza et al.,

[1] **Babian, S., Rust, H. W., Grieger, J., and Cubasch, U. (2016).** *Representation of the Antarctic Oscillation and related precipitation in the MPI Earth System Model.* Meteorol. Z., 17:12635, doi: 10.1127/metz/2016/0661

2008), connections to air temperatures in Antarctica (van den Broeke and van Lipzig, 2004), sea surface temperatures in the southern oceans (Mo, 2000), and temperature and precipitation over southern South America (Silvestri and Vera, 2003; Moy et al., 2009; Carvalho et al., 2005; Berman et al., 2012, 2013; Silvestri and Vera, 2009), western South Africa (Reason and Rouault, 2005; Gillett et al., 2006) and New-Zealand-Australia (Renwick and Thompson, 2006; Ummenhofer and England, 2007; Meneghini et al., 2007) were established.

Given the importance of the AAO for the SH, an adequate representation in a climate model is highly desirable. Here, the Max-Planck-Institute's Earth System Model (Giorgetta et al., 2013) is assessed for its potential to represent the AAO and related precipitation patterns. A primary aim of this thesis is thus to contribute a new important aspect to the validation of the MPI-ESM. The MPI-ESM participated in the 5^{th} Coupled Model Intercomparison Project (CMIP5 Taylor et al., 2012) for climate projections and for the associated decadal prediction experiments. The latter has been part of CMIP for the first time in CMIP5. The MPI-ESM is also the basis of the German national initiative for decadal prediction (MiKlip, *Mittelfristige Klimaprognose*) (Marotzke et al., 2016; Müller et al., 2012; Pohlmann et al., 2013; Kruschke et al., 2014)[2].

This work compares the AAO spatial pattern (EOFs), the spectral properties of the associated PCs, and AAO-related precipitation patterns as found in the MPI-ESM to three reanalysis data sets: the European Centre for Medium Range Weather Forecast's 40-year (Uppala et al., 2005) and ERA-Interim reanalysis projects (Dee et al., 2011) as well as the National Center for Environmental Prediction and National Center for Atmospheric Research 40-year reanalysis project (Kalnay et al., 1996; Kistler et al., 2001).

4.1 Spatial variability patterns

The leading spatial patterns of variability (first EOFs) for Z_{700} anomalies (Fig. 4.1 (a), (b)) account for roughly 26 % of the total variability for the MPI-ESM, for the three reanalyses (Fig. 4.1(d)) the portion of variability is slightly lower. The subsequent EOFs represent about 10 % and less of the total variability; here the 2^{nd} and 3^{rd} EOF associated with the MPI-ESM represent slightly less variability than their counterparts from the reanalyses and thus compensating for the larger portion associated with the first EOF (Fig. 4.1(d)).

[2]See also `http://www.fona-miklip.de/index.php`

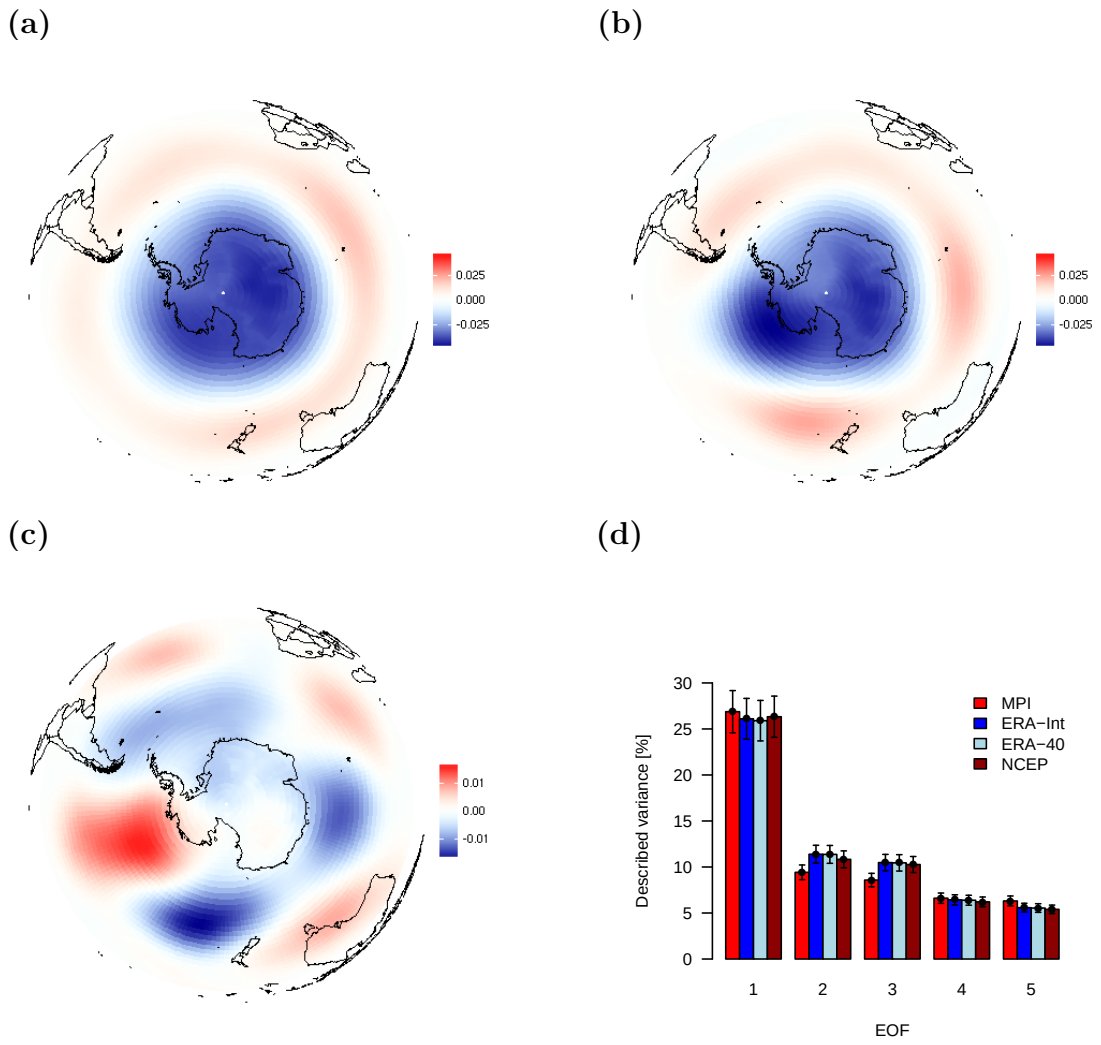

Figure 4.1: *First EOF of Z_{700} anomalies from (a) MPI-ESM and (b) ERA-Interim reanalysis for the period 1979–2001. (c) Difference plot of the first EOFs of MPI-ESM and ERA-Interim: $EOF1_{\text{MPI-ERA}}$ (shown in (a) and (b)) for the Z_{700} field and the same period. (d) Proportion of the total variance [%] associated with the first 5 EOFs for MPI-ESM model and ERA-Interim, ERA-40 and NCEP/NCAR reanalyses. Error bars are estimates of sampling errors in EOF computation according to "North's rule of thumb" (North et al., 1982).*

Figure 4.1(a) and (b) show the spatial patterns for MPI-ESM and ERA-Interim, respectively. Both show a strong zonal symmetry resulting in an almost concentrically structure around the South Pole. This pattern is known as the positive phase of the AAO pattern (Thompson and Wallace, 2000). The typical three centers of action (Mo, 2000) in the southern oceans break the circular symmetry and lie along 40° S, located at about 90° E, 50° W, and 170° W and are readily visible for the AAO pattern obtained for ERA-Interim (Fig. 4.1(b)). The MPI-ESM shows a stronger circular symmetry and consequently, these three centers are less pronounced. Furthermore, a slight shift compared to the reanalysis becomes evident in a difference plot in Fig. 4.1(c). The centers in the Pacific sector (170° W) and Indian sector (90° E) are shifted anti-clockwise. The difference pattern of the leading EOFs of the reanalysis and the MPI-ESM-MR shows four prominent features, Fig. 4.1: a strong positive signal over the Bellingshausen and Amundsen Sea, a slightly negative signal over the Weddell Sea, and two negative regions over the Ross Sea and the southern Indian Ocean. Jungclaus et al. (2013) also identified the first two features and reported a too strong low-pressure system in the Amundsen Sea region and significant differences in air-pressure distribution over the Weddell Sea. These two regions correspond to the location of the Antarctic Dipole (Yuan, 2004, and references therein); this dipole coins the reanalysis AAO pattern but is not a prominent feature of the MPI-ESM-MR's AAO pattern. However, the characteristic signature of this dipole can be found in MPI-ESM-MR's EOF2 (not shown). Thus, the model is in principle able to reproduce the dipole's pattern but not with 1) a comparable amplitude and 2) the proper connection to the model's AAO.

4.2 Seasonal cycle of AAO index variability

The annual cycle in the variability (variance) of the AAO index time series (first PC) peaks in the cold season (JJA). Figure 4.2 shows the annual cycle obtained for ERA-Interim (blue solid line) with 95 % confidence intervals (blue shading).

The MPI-ESM (red solid line and shading) reproduces this cycle to a large extent. Discrepancies are particularly present in May where the MPI-ESM shows lower variance, followed by a steeper increase in June and July. The subsequent decay of variability in August, September and October is slower for the MPI-ESM than for ERA-Interim. However, confidence intervals largely overlap and differences are not statistically significant (i.e., $p \not< 0.05$).

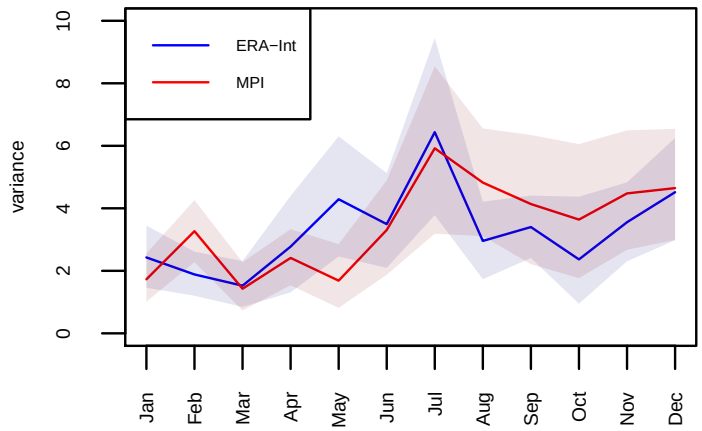

Figure 4.2: *Variances of monthly mean AAO index for MPI-ESM (red solid line) and ERA-Interim (blue solid line) for the 1979–2001 period. The shading depicts a 95 % confidence interval for monthly mean variances.*

4.3 Spectral Density of PCs

Figure 4.3 compares spectral density estimates for the first PC of ERA-Interim (light and dark blue) and MPI-ESM (light and dark red).

To give an impression of the uncertainty, the dotted line in the background shows the (unsmoothed) Fourier-periodogram of the first PC derived for ERA-Interim. A description with AR-processes of order $p = 1, \ldots, 15$ yields a smallest value for the AIC-value at $p = 1$, closely followed by $p = 6$ and $p = 7$. The result is highly similar for NCEP/NCAR and ERA-40 (not shown), however here the AIC prefers larger orders $p = 6$ and $p = 7$ over $p = 1$. As it is difficult to discriminate between the low order $p = 1$ and the larger orders $p = 6$ and $p = 7$ for the given reanalysis data sets, Fig. 4.3 gives the spectral densities for orders $p = 1$ (solid lines, dark colours) and $p = 7$ (solid lines, light colours) for ERA-Interim (light and dark blue) and MPI-ESM (light and dark red). Note that a corresponding order selection with AIC for the MPI-ESM yields order $p = 1$; here higher orders (e.g., $p = 6$ or $p = 7$) are not as compatible with $p = 1$ as it is the case for the reanalyses.

Irrespective of the ambiguity of orders, the variability associated with frequencies larger than $f = 2/12$ (two months) is underrepresented in the MPI-ESM. The higher order AR-process (AR[7], or low degree of smoothing) suggests that particularly the variability at frequencies between $f = 4/12$ and $f = 5/12$, i.e. at periods

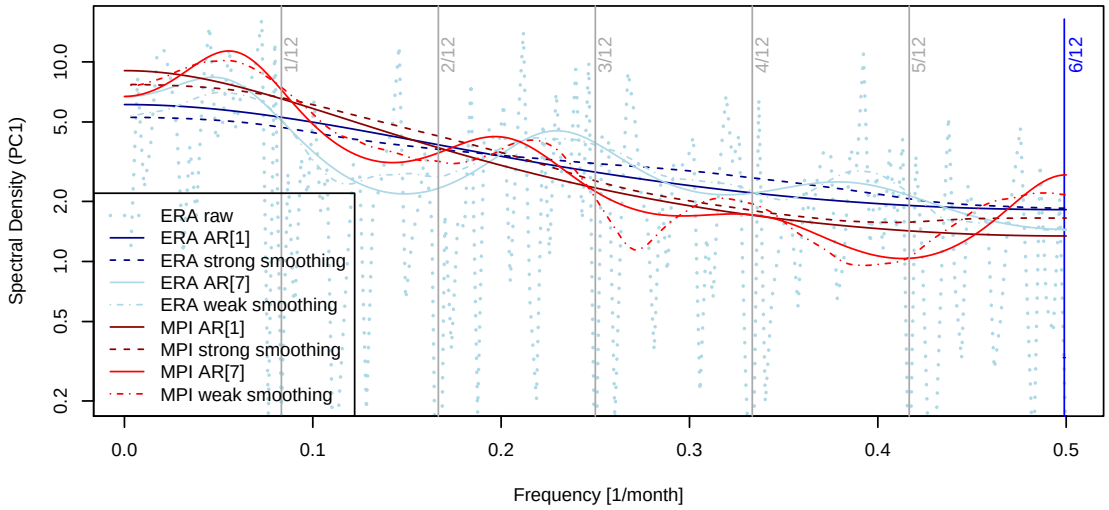

Figure 4.3: *Spectral density estimates for the first PC obtained from ERA-Interim (light blue and dark blue) and MPI-ESM (light red and dark red). Solid lines show density estimates based on AR[1] (dark) and AR[7] (light); dashed lines give estimates based on smoothing with a modified Daniell kernel with high (dark colours) and low degree of smoothing (light colours). The light blue dotted line depicts the associated unsmoothed Fourier periodogram for ERA-Interim. The vertical lines mark the frequency of the annual cycle and higher harmonics* $f = k/12, k = 1, \ldots, 6$.

Model / Data	**AAO$^-$**	**AAO$^+$**
NCEP/NCAR	45	41
ERA-40	42	44
ERA-Interim	45	46
MPI-ESM	46	47

Table 4.1: *Counts of monthly AAO indices exceeding (AAO$^+$) or undercutting (AAO$^-$) the 1979–2001 mean value about one standard deviation, respectively.*

of 4 to 5 months is underrepresented.

4.4 Link to Southern Hemispheric Precipitation

Table 4.1 gives the counts of anomalously high and low AAO index values (larger / smaller one standard deviation with reference to the 1979 – 2001 mean).

The months with positive (AAO$^+$) and negative (AAO$^-$) indices define positive (Fig. 4.4 (a), (c)) and negative (Fig. 4.4 (b), (d)) composites of precipitation anomalies for MPI-ESM and ERA-Interim, respectively.

Both model and reanalysis composites suggest that negative AAO phases are associated with a band of precipitation increase in the mid-latitudes (30° S – 50° S) and dryer conditions south of 50° S (Fig. 4.4 (b), (d)). This "wet band" disappears for positive AAO phases (Fig. 4.4 (a), (c)). During these phases, the MPI-ESM overestimates precipitation anomalies in the Indonesian region and underestimates precipitation over the Antarctic Peninsula.

The model does recover ERA-Interim's spatial precipitation pattern during negative phases quite well. However, the MPI-ESM overestimates rainfall anomalies over a region around Western Indonesia and the "wet band" of precipitation is less pronounced in the central South Atlantic and the central South Pacific (Fig. 4.4 (b), (d)).

Additionally to positive / negative AAO composites, Fig. 4.5, shows maps of the Spearman rank correlation coefficient estimated for the AAO index time series and monthly precipitation.

The strong zonal pattern of significant negative correlation between 40° S and 50° S in Fig. 4.5(a) fits well with the "wet band" identified in Fig. 4.4(b) for negative AAO phases. Positive correlation dominates the mid-latitudes to polar regions in

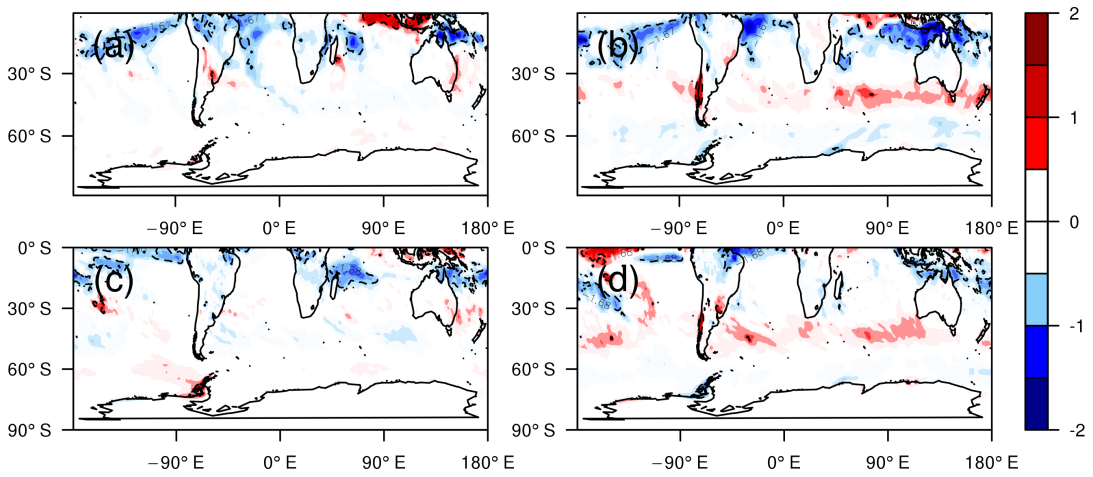

Figure 4.4: *Composite anomalies (w.r.t. 1979–2001 mean) of monthly precipitation [mm per day]: (a) MPI-ESM during positive phases and (b) negative phases of the model AAO; (c) ERA-Interim reanalysis for positive phases and (d) negative phases. The dotted lines depict the 95 % confidence interval, respectively.*

both model and reanalyses (NCEP/NCAR, ERA-40, not shown) and indicates an increase in precipitation here for positive phases. Discrepancies are most dominant in the Weddell Sea: positive correlation is weaker in the model which is associated with negative rainfall anomalies for a negative AAO index. Van den Broeke and van Lipzig (2004) found that the western Antarctic Peninsula becomes drier when the AAO index is low; hence implying a positive correlation between precipitation and the index time series. As the correlation is reduced here for MPI-ESM, this mechanism is not as prominent in the model as in reanalyses. A lack of negative correlation over Marie Byrd Land (West Antarctica) and the adjacent Ross Sea is found for the MPI-ESM. The source of this asymmetric response in precipitation is determined by the direction of flow anomalies with respect to the Antarctic topography (van den Broeke and van Lipzig, 2004). Overall, the correlation is less pronounced (positive and negative) which indicates a weaker link between AAO and precipitation in the model.

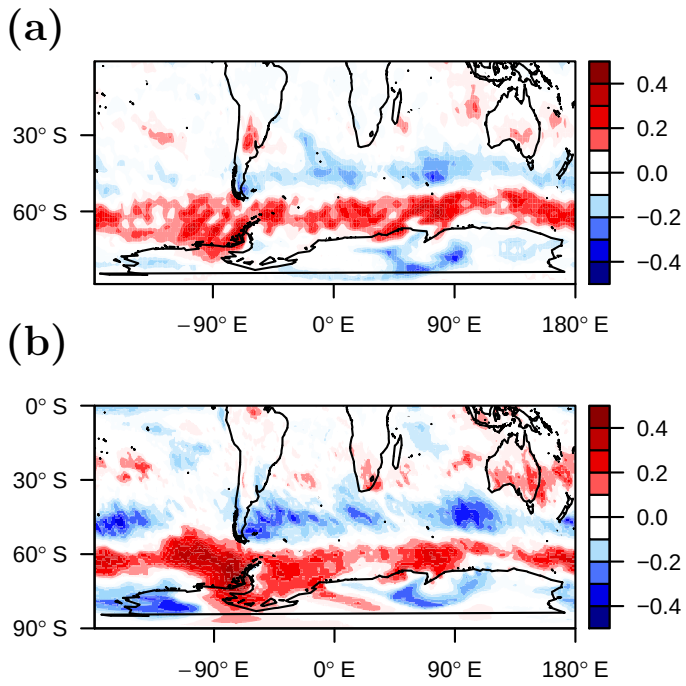

Figure 4.5: *Spearman correlation coefficient between monthly precipitation means and the AAO index time series of (a) MPI-ESM and (b) ERA-Interim for the period 1979 – 2001. White indicates correlation being compatible with 0 at a 5 % level of significance.*

4.5 Summary and discussion

It is investigated to what extent the Antarctic Oscillation (AAO / SAM) is represented in the MPI Earth System Model (MPI-ESM-MR-hist) by comparing to three reanalyses (NCEP/NCAR, ERA-40, ERA-Interim). The leading EOF of monthly mean 700 hPa geopotential height anomalies defines the mode's spatial pattern and the associated PC defines the index time series. The leading EOF describes 27 % (MPI-ESM) and 26 % (ERA-Interim) of the total variance of the geopotential height anomaly field. The spatial patterns are roughly circular (zonally symmetric) due to landmass distribution in the SH. The AAO's characteristic three centers of action are less pronounced in the MPI-ESM-MR and slightly shifted (Mo, 2000).

The differences pattern of the first EOFs shows distinct features over the Amundsen Sea, the Weddell Sea (i.e., the Antarctic Dipole, ADP) and two regions with stronger differences over the Ross Sea and the southern Indian Ocean. This indicates that the variability of the geopotential height contrast in the reanalyses in these locations is not adequately reproduced in the MPI-ESM. As Yuan (2004) suggests that the ADP is influenced by ENSO, a hypothesis about deficits in MPI-ESM-MR's ENSO simulation emerges and this might be responsible for part of the difference in the AAO patterns. Jungclaus et al. (2013) reports that the MPI-ESM-MR is superior in ENSO modeling compared to the CMIP3 version of the MPI model but does not reproduce the appropriate seasonal modulation of the ENSO strength and neither the right ratio of El Niño and La Niña events. Thus improving these ENSO deficits might improve also MPI-ESM-MR's AAO characteristics.

For the absence of variability over the Ross Sea and the southern Indian Ocean a hypothesis connected to the ADP can be formulated: the centers of action are less pronounced (if at all present) in the model, geopotential height anomalies are either not so pronounced and / or are not associated with a fixed location. This can be thought as a consequence of the wavenumber-3-pattern (Mo, 2000) being rather a progressing than a standing wave in the MPI-ESM. A propagating wave does not coin the stationary variability pattern (EOF1) as the standing wave in the ERA-Interim does. It is expected furthermore that the well pronounced ADP in the reanalyses favors a standing wavenumber-3-pattern. Consequently, the same mechanisms are expected to be responsible for a weak ADP in the MPI-ESM-MR leading also to the observed differences over the Ross Sea and the southern Indian Ocean.

The characteristic annual cycle of AAO index variability with the characteristic peak in the cold season is well reproduced by the MPI-ESM. A spectral analysis of

the index time series reveals a lack of variability in the intra-seasonal range (periods of 4 to 5 months).

The relation between the AAO and precipitation over the SH is furthermore assessed through composites for negative and positive AAO phases and a correlation analysis. An increasing (decreasing) AAO index implies an increasing (decreasing) equatorward directed meridional pressure gradient with poleward (equatorward) shifted westerlies and an extension (contraction) of the mean mid-latitude storm track (Thompson and Wallace, 2000). The northward shift of westerlies causes increased precipitation between 30° to 50° S; this "wet band" of precipitation disappears for high AAO indices. The MPI-ESM underestimates precipitation during positive AAO phases over the Antarctic Peninsula and overestimates precipitation anomalies in the Indonesian region. Underestimation of precipitation over the peninsula could result from reduced air-pressure over the Amundsen sea in MPI-ESM via changes in the circulation and related precipitation.

Correlation plots quantify the link between the monthly AAO time series and southern hemispheric precipitation: the reanalysis correlation maps are to a large extent reproduced by the model. However, over southern Australia, the Weddell Sea and the Antarctic Peninsula the MPI-ESM underestimates the strong link between AAO and precipitation. The missing dipolar-like structure in the correlation pattern between Weddell Sea and Antarctic Peninsula on the one hand and Amundsen Sea and West Antarctica on the other hand in the reanalysis is explained by the already mentioned underestimation of the low pressure system over Amundsen Sea. The prominent (surface) Amundsen Sea Low (ASL) is one of three climatological low pressure centers around Antarctica. The climatological ASL contributes wet and warm (cold) air to the eastern (western) part of the Antarctic peninsula. This mechanism is less distinct in the model and therefore accounts for missing positive and negative precipitation correlation in the west Antarctic area.

In conclusion, the MPI-ESM in MR mode is in general able to reproduce central features of the AAO and related precipitation as found in the reanalyses, i.e. the dominant mode of atmospheric variability in the SH is roughly captured. The models exaggerated zonal symmetry and the slight shift of the centers of action in the first EOF might result from the model's difficulties in reproducing properly the ENSO characteristics. These deficiencies of the model lead to the differences in precipitation distribution compared to the ERA-Iterim reanalysis.

5 A new index for the wintertime SH split jet

This chapter has been published online in the Atmospheric Physics and Chemistry journal.[1] *The co-authors supervised the work on the manuscript. The remaining work was carried out by Stella Babian.*

The circulation in the Southern Hemisphere (SH) is generally more zonally symmetric than its Northern Hemisphere counterpart, but there are significant zonal variations in the upper-tropospheric time-mean flow. A unique asymmetric feature of the SH winter circulation is the climatological split jet over Australia and New Zealand (Fig. 5.1).

The split is composed of two distinguishable branches: the northern branch, the subtropical jet (STJ) is located over the South Indian Ocean extending eastwards to the South Pacific Ocean between the latitudes of 25° and 30° S. The STJ is paralleled by the weaker Polar Front Jet (PFJ), which lies over the South Pacific Ocean up to ca. 60° S. A distinct feature of the split structure is a pronounced "gap" between these two branches, characterizing a zone of weak upper-level westerly winds over New Zealand (Bals-Elsholz et al., 2001).

Several past studies have addressed the existence, location and variability of the wintertime SH split jet. An early study by Taljaard (1972) has linked the existence and strength of the split jet to the outflow from the Asiatic monsoon anticyclone of the Northern Hemisphere. Other studies have variously suggested that the split jet is associated with cold air outbreaks (Mo et al., 1987), the breakdown

[1] **Babian, S., Grieger, J., and Cubasch, U. (2017).**, *A new index for the wintertime southern hemispheric split jet.* Atmospheric Chemistry and Physics Discussions, 2017:1–19, doi: https://doi.org/10.5194/acp-2017-840

of the Antarctic polar vortex in late spring (Mechoso et al., 1988), phases of ENSO (Karoly, 1989; Chen et al., 1996), and the AAO (Yang and Chang, 2006).

The AAO, which is in literature also referred to as Southern Annular Mode (SAM), is the dominant climate mode of the extra-tropical SH circulation variability and describes the out-of-phase pressure anomalies in polar and mid-latitude regions (e.g. Lorenz and Hartmann (2001), Thompson and Wallace (2000)). Positive (negative) phases of the AAO are linked to a poleward (equatorward) shift and strengthening (weakening) of the PFJ. The AAO was found to be the main modulator of the PFJ strength and location (Limpasuvan and Hartmann, 1999) and is thus expected to play a major role in the formation of the split jet.

The ENSO has an impact on both the STJ and the PFJ by directly affecting the Hadley circulation: while El Niño events are linked to increased (equatorial) convection and the PFJ, La Niña phases are marked by a stronger (weaker) PFJ (STJ) (Karoly, 1989; Chen et al., 1996; Kitoh, 1994). Gallego et al. (2005) have confirmed that the ENSO impact on the PFJ attributes (strength, wavenumber, average latitude) is mainly confined to the Pacific sector where the split jet is located.

Bals-Elsholz et al. (2001) have developed a vorticity-based split index and investigated its relationship to both ENSO and the AAO. Their study reveals that the existence of the split jet is dependent upon the presence of the PFJ branch as the STJ is a quasi-permanent feature of the SH winter circulation. The PFJ branch of the split index is indeed correlated with the AAO, but the STJ branch shows no correlation. Thus, overall their index correlates weakly with the AAO. A subsequent study (Inatsu and Hoskins, 2006) suggested a split index based on zonal mean of zonal wind variations; its correlation with the AAO is significant but low ($r = 0.43$). Both studies also investigated the relationship between the split jet and the ENSO; neither the index from Bals-Elsholz et al. (2001) nor the one developed by Inatsu and Hoskins (2006) correlated on a significant level with the Southern Oscillation Index (SOI).

The ongoing debate about the relationships between AAO, ENSO and the SH split jet in the published studies raise the question if an index could be defined that clarifies the relationships between the SH split jet and the large-scale teleconnection indices viz. ENSO and AAO?

In previous studies (Bals-Elsholz et al. (2001) (hereafter BE), Inatsu and Hoskins (2006) (IH)) and in the work of Yang and Chang (2006) (YC), indices were developed to detect the characteristics of the SH climatological split in the Austral winter.

These indices represent the split structure in several meteorological variables and at different but comparable levels: 200 hPa vorticity (BE), 300 hPa zonal wind anomalies (YC), 200 – 300 hPa difference in the zonal mean zonal wind (IH). The similarity in the construction of all these split indices is a definition based on the regions accounting for the two branches of the split jet (STJ, PFJ) and the gap between them over the Australian / New Zealand region. Although these indices are similarly constructed, the respective studies revealed inconsistent relationships with the AAO and ENSO.

Additionally, there remains a lack of clarity about the link between split jet variability and the Pacific South American (PSA) patterns, although the latter were found to be associated with ENSO and the AAO teleconnection indices. The PSA patterns are conventionally seen as Rossby wave trains emanating in quadrature to each other from the tropical Pacific towards Argentina and serve simultaneously as a waveguide for eddies moving south. On interannual time scales the PSA-1 mode is tied to ENSO, while the PSA-2 pattern is associated with the quasi-biennial component of ENSO (e.g., Mo, 2000). Furthermore, although called an "annular" mode, the AAO contains asymmetries, which are most pronounced in Austral winter and over the Pacific sector. This (tropically forced) component of the AAO is related to a fixed active Rossby wave source and resembles the spatial structure of the PSA patterns (Ding et al., 2012).

The lack of knowledge about the relationship between the split jet variability and the PSA patterns, and the inconsistencies about its connection to ENSO and the AAO have motivated this study to develop an improved SH split jet index. The split jet is one of the most important features of the interannual variability in the SH winter circulation and its pattern is not only centered over the Australian / New Zealand region but bears also hemispheric signatures (Yang and Chang, 2006). Consequently, it is assumed that the split jet variability is already intrinsically contained in one or several leading modes of the SH winter zonal wind field.

In this study, a PC based methodology is provided to describe the SH wintertime split jet to clarify the relationship between the SH split jet and the large-scale teleconnection indices (ENSO and AAO). This chapter is organised as follows: the definition of the new index is proposed in Section 5.2. The PSI is then used to examine the relationships between split phases and the large-scale variability modes (ENSO, AAO and PSA) in Section 5.4. Finally, the main results are summarised and discussed in Section 5.5. The data and methodology which are the basis for the reconstruction of the earlier split jet indices and for the PSI definition are described in Chapter 2 and 3.

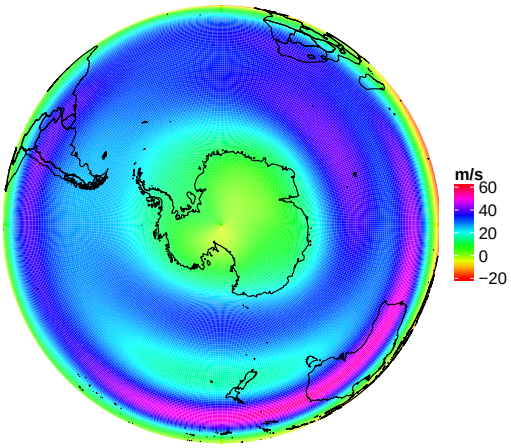

Figure 5.1: *Climatological zonal wind [m/s] in 200 hPa in Austral winter (JAS) averaged for the period 1979–2015.*

5.1 EOFs in SH zonal wind

As mentioned in Section 1, the wintertime split jet is the most prominent asymmetric feature of the mid-latitude SH circulation centered over the Pacific sector although it bears hemispheric signatures as well (Yang and Chang, 2006). In order to design a PC based split jet index, the three split jet indices defined earlier (Section 3.4) were reproduced, and their respective statistical relationships to the leading modes of the SH wintertime circulation (as depicted by zonal wind anomalies at 200 hPa) have been investigated in this section. The EOF modes showing the largest coherence with the split jet indices (as defined by the respective studies) are assumed to contain the main signals associated with the split variability.

The three leading spatial patterns of variability (EOFs) for U 200 hPa anomalies on the SH (0–90° S) account for roughly 19 %, 10 % and 9 % respectively of the total variability of the 200 hPa zonal wind field (Fig. 5.2). The 200 hPa pressure level was chosen due to the mechanisms associated with the jet(s) variability, which have their maximum at this level (e.g., Galvin, 2007). The subsequent EOFs (EOF4 and EOF5) represent about 6 % and less of the total variability and are not distinguishable from each other after "North's rule of thumb" (North et al., 1982).

Worth mentioning, the second and third EOF are effectively degenerate, which means that the eigenvalue's uncertainty is larger than the spacing between the

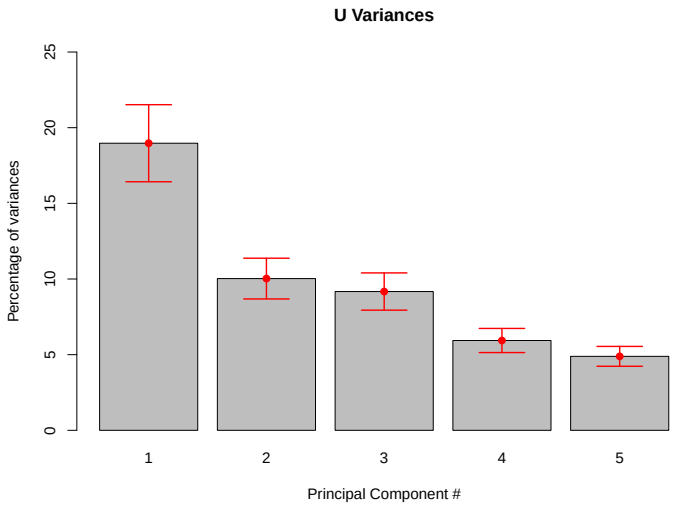

Figure 5.2: *Proportions of the total variance [%] associated with the leading 5 EOFs for the 200 hPa zonal wind field of ERA-Interim reanalysis. Error bars are estimates of sampling errors in EOF computation according to "North's rule of thumb" (North et al., 1982).*

	PC1	PC2	PC3	PC4	PC5	PSI
JAS – correlation values						
-BE	**-0.28**	**0.44**	**-0.36**	-0.09	-0.15	**0.56**
YC	-0.24	**0.56**	**-0.48**	-0.13	-0.09	**0.73**
IH	**-0.49**	**0.57**	**-0.43**	**0.26**	0.09	**0.71**
Mean	**-0.38**	**0.59**	**-0.48**	0.02	-0.05	**0.76**

Table 5.1: *Monthly (JAS) Pearson correlation coefficients of individual leading 5 PCs in the 200 hPa zonal wind as well as the PSI with the split jet indices introduced in the methods section (Sec. 3.4). By construction, the Bals-Elsholz et al. (2001) index becomes negative during split events and its sign is therefore reversed. Bold values are significant at the $\alpha = 1\%$ level.*

eigenvalues. By construction, a linear combination of the two EOFs (which describe respective equal amounts of the total variance) will explain the same amount of variance. With the aid of linear algebra, it can be shown that any orthogonal pair of such linear combinations is equally well qualified to be an EOF (Sahai et al., 2014).

The correlation between the leading 5 PCs and the split indices introduced earlier is shown in Table 5.1. PC1 correlates significantly (r = -0.49) with the zonal mean zonal wind-based index developed by Inatsu and Hoskins (2006) and weakly but significantly with the relative vorticity based index designed by Bals-Elsholz et al. (2001). The weaker correlation with the Yang and Chang (2006) index, which is also defined in the zonal wind, is because SJI lacks the STJ branch.

Whereas the fourth and fifth PC correlate poorly with any of the indices, the second and third PC show robust relations to split events. While PC2 is strongly positively correlated with the split indices with coefficient values ranging from r = 0.44 (BE) to r = 0.57 (IH), PC3 is negatively related with the split regimes. Pearson's correlation values of PC3 increase from r = -0.36 (BE) to r = -0.48 (YC). Generally, the correlation values associated with the relative vorticity based index designed by Bals-Elsholz et al. (2001) show the weakest links to PC2 and PC3 of the zonal wind field, but are nevertheless significant at the $\alpha = 1$ % level. The two zonal wind-based indices (IH and YC) produce the strongest correlation to PC2 and PC3, which is exceeded only by the mean of all three earlier split indices for PC2 (r = 0.59). Altogether, the splits in the westerlies show weaker correlation with PC1 but show an improved association with the higher order PCs in the 200 hPa zonal wind field.

5.2 Definition of the PC based Split Index (PSI)

From the correlation analysis of the PCs with the three split indices discussed in Section 5.1, it is apparent that PC2 and PC3 are associated with the SH wintertime split jet events and resemble the partly split variability. In order to develop a PC based split jet index, PC2 and PC3 which correlate well with the earlier split jet indices are linearly coupled. The monthly wintertime (JAS) PC based SH Split Jet Index (PSI) is then defined as follows:

$$PSI = PC2_{U_{200hPa}} - PC3_{U_{200hPa}} \tag{5.1}$$

The PSI is based on the second and third PC of the anomalous 200 hPa zonal

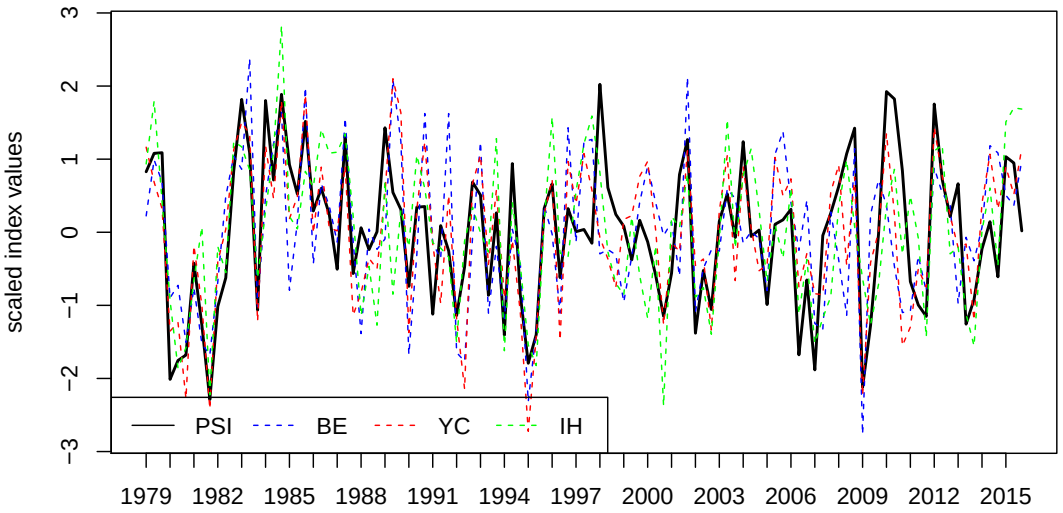

Figure 5.3: *PSI (PC2 - PC3) index in 200 hPa zonal wind and three earlier split jet indices defined by Bals-Elsholz et al. (2001) (BE), Yang and Chang (2006) (YC) and Inatsu and Hoskins (2006) (IH). All time series were scaled for illustration purposes.*

wind field over the whole SH during Austral winter (JAS). It appears that adding two constants c_1 and c_2 to the individual components of the linear combination ($PSI = c_1 PC2_{U_{200hPa}} - c_2 PC3_{U_{200hPa}}$) does not improve the ability of the PSI to show the split variability. The constants are thus omitted (set to 1 and -1, respectively) in the PSI definition. The PSI time series, as well as the split indices of the previous studies, are displayed in Fig. 5.3.

The correlation values between these indices and the PSI at 200 hPa are shown in the last column of Table 5.1. All indices are well correlated to the PSI with coefficients ranging from 0.56 (BE) to 0.73 (YC) and the mean of all the three earlier split indices raises Pearson's correlation coefficient to r = 0.76. This relationship is significant at the $\alpha = 1$ % level and shows that the linear combination of PC2 and PC3 exceeds values obtained from the performance of the individual PCs (Table 5.1).

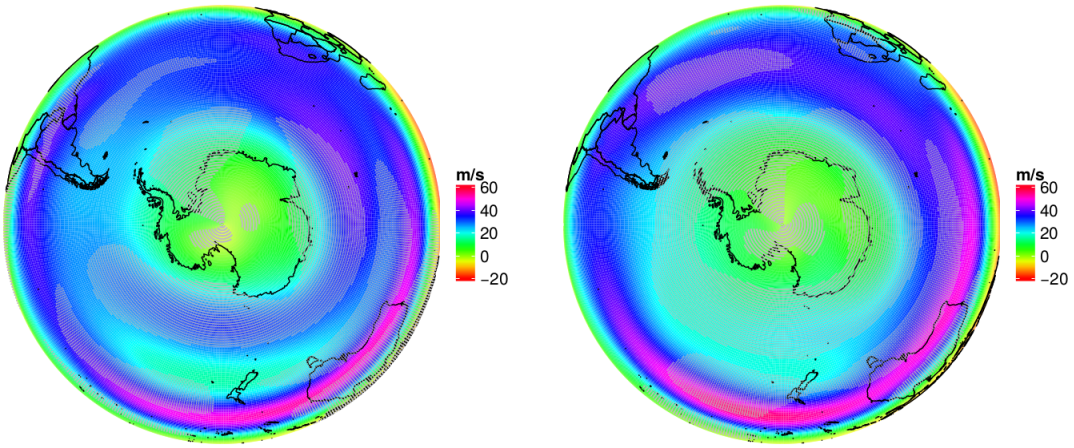

Figure 5.4: *Positive (left) and negative (right) composite of the PSI (PC2-PC3) index in 200 hPa zonal wind. Gray dotted areas are significant at the α = 1% level.*

5.3 Composite Analysis of U 200 hPa with PSI

Figure 5.4 shows the spatial patterns of U at 200 hPa for high (18 cases) and low (19 cases) PSI index phases. The positive composite affirms the characteristic split structure with an existing, but weak STJ, a pronounced PFJ, and a well-defined minima of zonal wind strength in between. The split composite shows that the PFJ strength is not limited to the Australian sector of the east Pacific, but is enhanced over the Indian Ocean and over the full width of the South Pacific Ocean. The low index composite displays a clear non-split or "merged" jet state with a strong STJ over the Australian continent and a missing PFJ. The spatial patterns of the split and non-split cases are captured well by the PSI and show results similar to the composites of the indices defined in Section 3.4 (compare Fig. 6.2 from Sec. 6.1).

To understand the independent contribution of both components of PSI, i.e. PC2 and PC3, a composite study of both PCs was also done separately. Figure 5.5 shows the appropriate composites of the second and third EOF in U 200 hPa. The positive composite of PC2 shows the typical split (left column) which developed over the Indian Ocean and strengthened in the western Pacific sector where a clear double jet structure with a pronounced minimum in U 200 hPa between the two jets is visible. The negative composite of PC2 displays a single jet formation (right

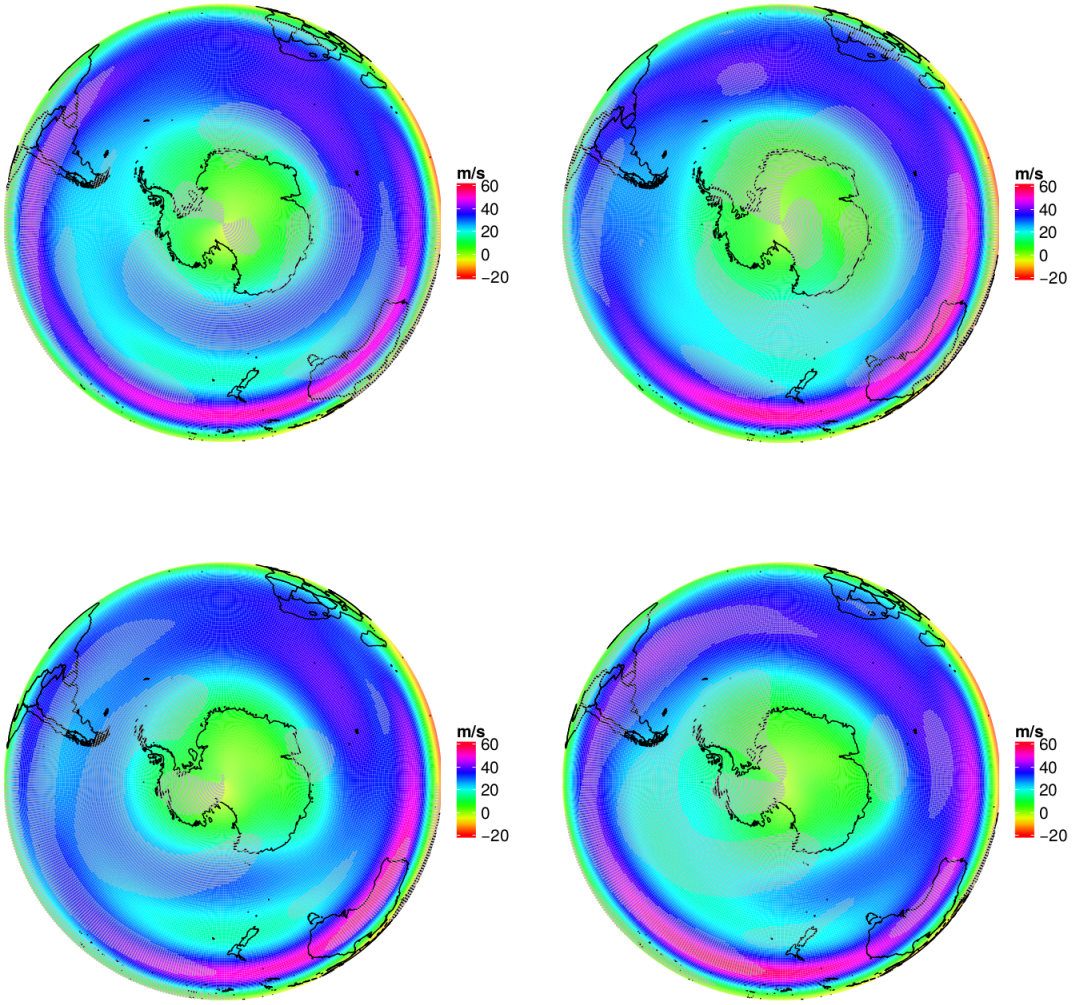

Figure 5.5: *Composites of positive (left) and negative (right) phases of PC2 (first summand of Eq. 5.1; top row) and -PC3 (second summand of Eq. 5.1; bottom row) time series of the SH zonal wind in 200 hPa. Gray dotted areas are significant at the $\alpha = 1\%$ level.*

column). The bottom row of Fig. 5.5 gives the equivalent composites of PC3. The most striking difference in the split composites (Fig. 5.5, top left) is the PFJ strength over the western Pacific Ocean and the Drake Passage, which is absent in the PC2 composite.

Additionally, the positive composite of PC3 shows an established double jet structure over the Atlantic Ocean, which breaks down south of South Africa and results in a strong STJ over the Australian / New Zealand region again (Fig. 5.5, bottom left). A further feature of the positive composite is the lack of annular structure compared to PC2. In literature, this known zonal wave number 3 pattern is often referred to as a modulator of e.g. blocking events in the New Zealand region, and Australian rainfall (Trenberth and Mo, 1985; Pook et al., 2013).

The negative composite (Fig. 5.5, bottom right) of the second term of Equation 5.1, i.e. -PC3 (non-split / single jet regime) bears resemblance to the appropriate composite of PC2 but describes a stronger STJ over the central and east South Pacific Ocean and South America. Additionally, the PFJ is weakened in the non-split composite, but south of the Australian / New Zealand region there are still traces of a PFJ.

Summarising, the positive PSI composite (Fig. 5.4, left) benefits from the combination of the double jet structure with a pronounced minimum between the jets associated with PC2(+) and the strong PFJ over the South Pacific Ocean associated with the "non-annular" component localised over the South Pacific Ocean of PC3(-).

5.4 Links between PSI and large-scale climate modes (AAO, ENSO and PSA)

In order to determine whether the PSI is modulated by large-scale phenomena, i.e. the AAO and the ENSO, correlations between the PSI and the teleconnection indices were computed. The respective time series are illustrated in Fig. 5.6 and the Pearson's correlation coefficients, based on 111 winter months, are summarised in Table 5.2.

The AAO, also referred to as the Southern Annular Mode (SAM) in literature, is defined here as the anomalous geopotential height at 700 hPa (NOAA's AAO) and describes a seesaw in pressure anomalies between polar and mid-latitude regions (e.g. Lorenz and Hartmann (2001), Thompson and Wallace (2000)). The arising meridional geopotential height gradient results in periodical shifting and

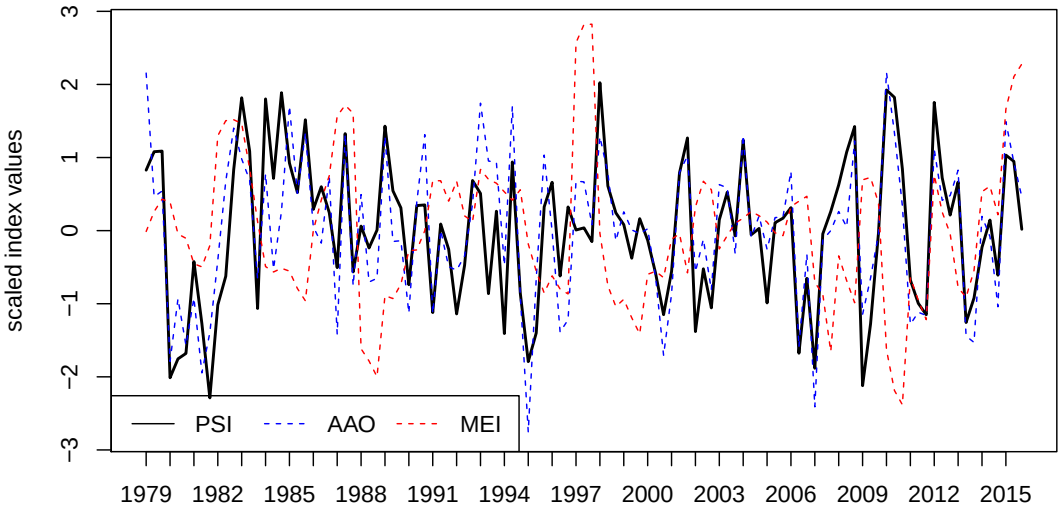

Figure 5.6: *Time series of PSI (black solid line), NOAA's AAO (blue dotted line) and NOAA's MEI (Multivariate ENSO Index, red dotted line) from 1979 to 2015.*

	PSI	PC2	PC3	BE	YC	IH	Mean
JAS – correlation values							
AAO	**0.81**	**0.65**	**-0.50**	**0.45**	**0.66**	**0.58**	**0.64**
MEI	-0.09	0.07	0.20	0.20	0.12	**0.34**	**0.25**
PSA-1	0.19	**-0.26**	**-0.55**	0.14	0.16	-0.17	0.05
PSA-2	0.06	0.20	0.13	0.22	0.20	-0.12	0.11

Table 5.2: *Monthly (JAS) Pearson correlation coefficients of the three split indices introduced in the methods section (Sec. 3.4), as well as the PSI with three major SH climate mode indices for the Antarctic Oscillation (AAO), ENSO (Multivariate ENSO Index) and the Pacific South American (PSA) patterns (PSA indices as defined in Mo (2000) for PSA-1 and PSA-2). Bold values are significant at the $\alpha = 1\%$ level.*

strengthening of the circumpolar vortex. The correlation analysis reveals a strong connection (r = 0.81) between the PSI (defined at 200 hPa) and the AAO. The highly significant correlation accounts for the large influence of the AAO on the PFJ variability, which in turn is associated with the split jet (Fyfe, 2003; Gallego et al., 2005).

Although PSI (split jet index) is significantly correlated with the AAO indicating a strong link with the PSI variability, the PSI has no such relationship with the Multivariate ENSO Index (MEI). Figure 5.7 shows a scatter plot of the monthly MEI values with respect to the PSI value. The correlation between the PSI and MEI is low (r = 0.04), but by comparing the top left and the top right quadrant of the scatter plot (Fig. 5.7) to the respective bottom quadrants it is evident that warm (red dots) and cold (red dots) ENSO events are both associated with positive (or neutral) values of the PSI. Altogether from 24 warm and cold ENSO events that occurred over 111 winter months, it is clear that there was no month with a negative PSI value. This asymmetric and non-linear behavior results in a low correlation coefficient.

Table 5.3 gives counts of positive (first column), negative (second column) and neutral (last column) PSI months and the corresponding predominant AAO and ENSO states. The box, which emerges when concentrating on the first six lines and columns of the same table, contains all possible AAO^+/PSI^+ and AAO^-/PSI^- cases during the analysis period. Although the AAO index is well correlated with the PSI, the last column of the same table shows that 5 AAO^+ months are marked

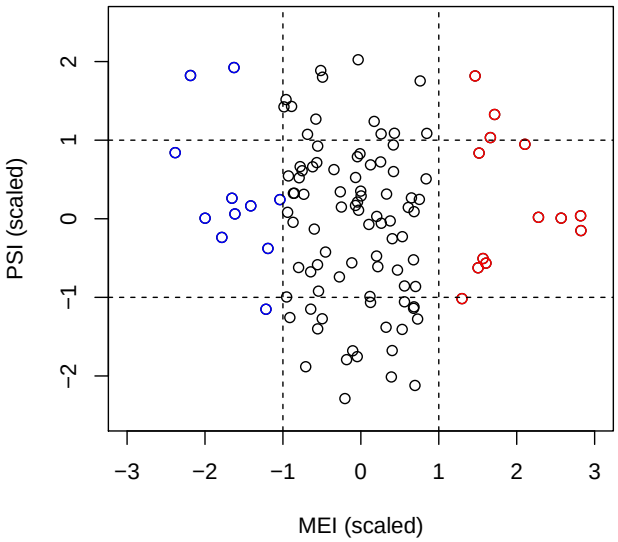

Figure 5.7: *Scatter plot of the new split index (PSI) and MEI, the Multivariate ENSO Index (each normalised to unit variance). Dashed lines give (minus) one standard deviation of MEI and PSI indices, respectively. Red (blue) dots mark warm (cold) ENSO events.*

Combination	**PSI$^+$**	**PSI$^-$**	**PSI^0**
AAO$^+$ MEI$^+$	3	–	–
AAO$^+$ MEI$^-$	2	–	–
AAO$^+$ MEI^0	8	–	5
AAO$^-$ MEI$^+$	–	–	1
AAO$^-$ MEI$^-$	–	1	–
AAO$^-$ MEI^0	–	12	6
AAO^0 MEI$^+$	2	–	7
AAO^0 MEI$^-$	–	–	8
AAO^0 MEI^0	3	6	47

Table 5.3: *The predominant jet regimes (PSI$^+$ = split jet, PSI$^-$ = single jet, PSI^0 = mixed jet regime) as counted during the 111 winter months of the 1979–2015 period, separated by occurred combinations of AAO and ENSO states.*

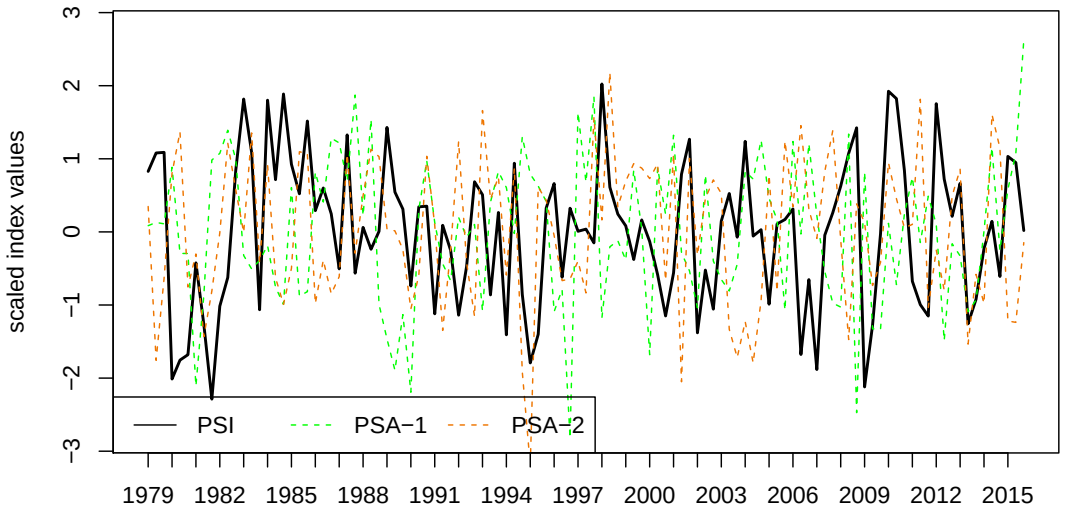

Figure 5.8: *Time series of PSI (black solid line), PSA-1 index (green dotted line) and PSA-2 index (orange dotted line) from 1979 to 2015.*

as neutral PSI months, and there are 5 months of PSI^+ and neutral AAO conditions. Consequently, the jet is able to split under neutral AAO conditions, and not every AAO^+ month necessarily leads to a split event. The negative phases of the AAO nearly mirror the conditions of its positive counterpart. Altogether 7 events occurred under AAO^-/PSI^0, likewise, 6 months were counted as AAO^0/PSI^- cases.

By revisiting these points in the investigated period between 1979 and 2015, it turns out that 3 months of the first case (AAO^+/PSI^0) occurred in a period during the 1980s and 3 of the latter cases (AAO^0/PSI^+) occurred sequentially in the 1990s (not shown). A spectral analysis of the time series of the differences between PSI and AAO index shows multiple frequencies over the 37 year period (not shown). Unfortunately, the study interval is too short to draw meaningful conclusions about decadal to centennial variabilities. Furthermore, the time series of differences is correlated neither with the ENSO nor to the known Pacific Decadal Oscillation (NOAA's PDO index, not shown).

The low correlative relationship between MEI and PSI mentioned above arises from the fact that 8 out of 18 split events occurred during any state of ENSO phases, while only one cold ENSO event occurred in a negative PSI phase. The last three rows of Table 5.3 reveal that there are 7 (8) ENSO warm (cold) events, including the extreme La Niña event in 1988 and the severe El Niño event from 1997, where a mixed jet (PSI^0) regime predominated.

Figure 5.8 shows the time series of both the PSA modes (see Section 1.2.2) and the PSI. Although the correlation between PSI and the PSA indices is low ($r_{PSA-1} = 0.19$ and $r_{PSA-2} = 0.06$), the PSA-1 mode is significantly correlated with the individual PCs of the SH zonal circulation variability (Table 5.2). Both PSI components (i.e. PC2 and PC3) are associated with the PSA-1 pattern. The spatial pattern of EOF2 was previously identified as resembling the dominant part of the split jet structure (Section 5.1) characterised by an intensified PFJ over the eastern hemisphere. Since the PSA-1 pattern is primarily associated with the variability over the central and western Pacific sectors, it can be concluded that PC2 describes less PSA-1 variability but contains a considerable part of the wind response associated with the AAO. PC3 accounts for the "non-annular" component of the PSI and contains most of the variability over the Pacific sector. However, only 3 cases were identified where both indices, PSI and PSA-1, exceeded the threshold of one standard deviation during the analysis period (not shown).

5.5 Summary and discussion

While several studies of the SH winter circulation examined the presence, origin, and structure of the climatological time-mean SH split jet which forms over the western South Pacific Ocean in the vicinity the South Australia / New Zealand region, only a few have developed indices capturing the SH split variability to quantify the relationships with the large-scale variabilities i.e. the AAO and the ENSO.

According to the literature review, until now there are three published studies (Bals-Elsholz et al. (2001); Inatsu and Hoskins (2006); Yang and Chang (2006)) suggesting a SH split jet index. All of which have used a region based definition, which contradicts the assumption that the SH split jet is a hemispheric feature rather than a regional effect. The most important advantage and the innovative aspect of the new PC based split index (PSI) compared to the existing indices is its independence from regional definitions: the PSI is defined by linearly combining the SH second and third principal component of the monthly (JAS) anomalous zonal wind at 200 hPa.

The PSI correlates well with the individual split indices and even the mean of all gives a significant correlation coefficient of 0.76 with the PSI. An analysis of Bals-Elsholz et al. (2001) showed that their SFI agreed favorably with a subjective classification of the split regime with the exception of 1998. This year was affected by a strong La Niña event and an anomalously weak STJ.

While the three earlier split indices failed to agree with the (subjective) split regime, the PSI value for July 1998 was high and was thus marked as one of 18 split events. From this fact, the correlation analysis, and the investigation of PSI composites in the 200 hPa zonal wind field, it is evident that the PC based split index is able to reproduce the SH wintertime split jet structure.

Separate composites of PC2 and PC3 reveal that both PCs are essential for the split representation. PC2 is associated with the jet strength (Lorenz and Hartmann, 2001) over the eastern hemisphere, whereas PC3 exhibits a “non-annular” component in both composites. It is proposed that the split events are connected to PC2 because it represents the jet strength, and to PC3 as it adds a “non-annular” component to the jet variability. Thus, the PC based split jet index (PSI) is a qualitative measure of the spatio-temporal variability of the split jet and can efficiently be used to investigate the relationships with the known climate variability modes i.e. AAO, ENSO, and PSA patterns.

Although not previously reported in studies involving the SH circulation (jet)

variability (e.g. Gallego et al. (2005)), it was expected that the SH split jet should exhibit a strong connection to the AAO. The newly developed PSI shows a highly significant correlation with the leading mode in the near-surface level of the geopotential height anomalies (NOAA's AAO at 700 hPa) with r = 0.81.

This highly significant relation of the PSI to the leading mode in geopotential reiterates the importance of the AAO to the PFJ variability (Fyfe, 2003; Gallego et al., 2005). The PFJ strength is enhanced under AAO^+ conditions in accordance with the negative pressure anomalies over the polar region occurring under AAO^+. Since the PFJ variability is more important for the representation of split events (Bals-Elsholz et al., 2001) than its subtropical counterpart, the AAO has a high correlation with the PSI (r = 0.81). Nevertheless, the AAO index has a neutral value in 5 out of 18 split events occurring in the analysis period between 1979 and 2015. It can be concluded that a positive AAO phase is a preferred condition for the SH split jet. However, the split jet is also able to arise in neutral AAO months.

The correlation between the MEI and the PSI is low, but 7 out of 18 split events occurred during a warm (5) or cold (2) ENSO month. The occurrence of both warm and cold ENSO events damps the correlation with the PSI, but the relative frequency of ENSO events is still 30 %. It seems likely that any kind of ENSO flavor is favorable for split events, which results in a non-linear relation between PSI and ENSO i.e. positive (negative) PSI values mainly occurred during warm or cold (neutral) ENSO states. From earlier studies it is known that El Niño (La Niña) phases enhance (reduce) the STJ strength over the South Pacific Ocean via advection of mean flow momentum flux (e.g. Chen et al. (1996)). This is consistent with the finding that 5 out of 18 split events occurred during a warm ENSO phase which enhances the STJ (PFJ) strength. Otherwise, there are strong ENSO events (El Niño of 1997 and La Niña in 1988) during the analysis period, which did not lead to a pronounced split event. Thus, an ENSO event alone is not able to reproduce the SH split jet variability. It is worth mentioning that published literature indicates that ENSO and AAO are also mutually dependent. There are reports that cold ENSO events are favored by positive phases of the AAO (e.g. Carvalho et al. (2005)). As these are in turn associated with split events, it is expected La Niña phases to occur more often than El Niño events during PSI^+ phases.

In contrast, the ENSO warm phase coincided more frequently (5 months) with the high PSI (split jet) phases than its cold counterpart (2 months), although both flavors of ENSO appeared roughly equally during the considered time period of 111 winter months. It is proposed that the ENSO induced Rossby wave dynamics are

beneficial for the SH split jet modulation, regardless of the sign of that oscillation. However, further work is needed here to clarify the complex relationship between ENSO and the SH split jet.

The traditional view suggests that the PSA patterns are part of a stationary Rossby wave train extending from the central Pacific to Argentina (e.g., Mo and Higgins, 1998). The PSA patterns, typically defined as the second and third modes of tropospheric geopotential height variability over the SH (e.g., Mo, 2000), have been attributed to ENSO (PSA-1) on interannual time scales and to the quasi-biennial component of ENSO and the Madden-Julian-Oscillation (PSA-2) respectively (Mo and Paegle, 2001).

The relationship between the PSA indices and the PSI revealed a low relationship to both indices ($r_{PSA-1} \approx 0.2$ and $r_{PSA-2} = 0.06$). In contrast, the individual PCs of the zonal circulation at 200 hPa correlate significantly with the PSA-1 index. Positive PSA phases are associated with a strong PFJ over the western Pacific sector (not shown) and the PSA-1 mode is consistently significantly correlated with the PC3(-) component which is (by definition) related to split events. Negative PSA events are associated with an enhanced PFJ over the eastern hemisphere which partly describes the EOF2 variability. It is proposed that PC3 represents both AAO and the PSA variability. However, the connection between the PSA-1 mode and the PSI is canceled out by the PC2 component, which is (as well as the PC3 component) negatively correlated with the PSA-1 mode.

To conclude, the relationship between the new PC based SH split jet index and the large-scale modes AAO and ENSO is non-linear. The highly significant relationship between the PSI and the AAO highlights the importance of the PFJ variability which is a determining factor in the split jet formation, while the ENSO and PSA effects are complex and relatively less important.

6 Representation of the wintertime SH split jet in the MPI-ESM

Despite continuous improvements in resolution and representation of complex processes, current state-of-the-art coupled global circulation models (CGCMs) and earth system models (ESMs) are known to exhibit significant biases in mean jet latitude towards a more poleward position than observed (e.g. Ceppi et al., 2012; Stevens et al., 2013). However, properties (e.g. strength, meridional extent and position) of the jets are strongly associated with the distribution of precipitation and clouds, mid-latitude storms, blocking events and the persistence of the annular modes (Barnes and Hartmann, 2010). Thus, small model errors in the latitudinal position of these features can lead to large local biases (e.g. Ceppi et al., 2012). Moreover, jet latitude biases are of importance in the context of climate change since the jets are predicted to shift due to increasing greenhouse gases (e.g. Kidston and Gerber, 2010). A realistic representation of jet properties in ESMs is therefore of crucial importance in climate modeling.

The results of Chap. 4 reveal a lack of geopotential height variability over the Amundsen Sea in the MPI earth system model compared to the ERA-Interim reanalysis. The MPI-ESM was found to be in general able to reproduce central properties of the leading mode of SH extra-tropical variability in a near-surface (700 hPa) geopotential height field (i.e. the AAO). Nevertheless, the three centers of action (Mo, 2000) (i.e. the "non-annular" component) are reproduced to a smaller magnitude in the model compared to the reanalysis data. Since the split jet is the most prominent asymmetric feature of the SH extra-tropical circulation it is assumed that the representation of the zonal asymmetric structures of the tropospheric circulation is fundamental for the depiction of the SH split variability. The questions to be focused on in this chapter are therefore: Is the MPI-ESM able to reproduce the SH wintertime split jet variability? Can an index be found which describes that variability as in ERA-Interim? And lastly, are deviations from the reanalysis attributable to the zonally asymmetric component of the SH circulation?

6.1 The SH wintertime split jet variability in the MPI-ESM

In order to evaluate the potential of the MPI-ESM to represent the wintertime SH split jet, a new PC based split index similarly to the PSI definition in ERA-Interim (Chap. 5) is desired. To this end, the three established split jet indices are computed (see Sec. 3.4) for the respective fields in the MPI model and fitted to the model run period of 1979–2005 (MPI-ESM-MR, historical run). For comparison purposes, the ERA-Interim data set is shortened as well and the resolution is reduced to the MPI-ESM-MR resolution of T63.

The composites of the established split jet indices in the 200 hPa zonal wind field in MPI-ESM are illustrated in Fig. 6.1. All three positive composites (left panels of Fig. 6.1) indicate a reduced PFJ strength and a less pronounced gap between the jets in the MPI-ESM compared to the ERA-Interim reanalysis (Fig. 6.2). Especially the region south of Australia reveals considerable differences compared to the reanalysis. The MPI-ESM lacks the strong PFJ which is apparent in the reanalysis composites north of the Antarctic Peninsula and south of South Africa. In contrast, the zonal wind over the split region is well represented in the MPI model as characterised by a strong STJ north and a weaker PFJ south of New Zealand.

The negative composites of the split jet indices in the MPI-ESM (right panels of Fig. 6.1) resemble the single jet regimes indicative of a strong STJ starting from the southern Indian Ocean towards the longitudes of South America. The structure of the "non-split" composites is well represented in the MPI model, although the subtropical jets are stronger in all three negative composites compared to the ERA-Interim reanalysis.

In summary, the MPI-ESM is able to represent a certain portion of the split variability of the SH circulation. Hence, it is appropriate to introduce an index capturing the model SH split jet variability (analogous to the ERA-Interim reanalysis) in the subsequent section.

6.2 PC based Split Index in the MPI-ESM (PSI_{MPI})

Figure 6.3 shows the described variances of the SH 200 hPa zonal wind anomaly field for the Austral winter season in the MPI-ESM. The leading mode (PC1) accounts for roughly 15 % of the total variance. The subsequent EOFs represent about 9 % and less of the total variability and are not distinguishable from each

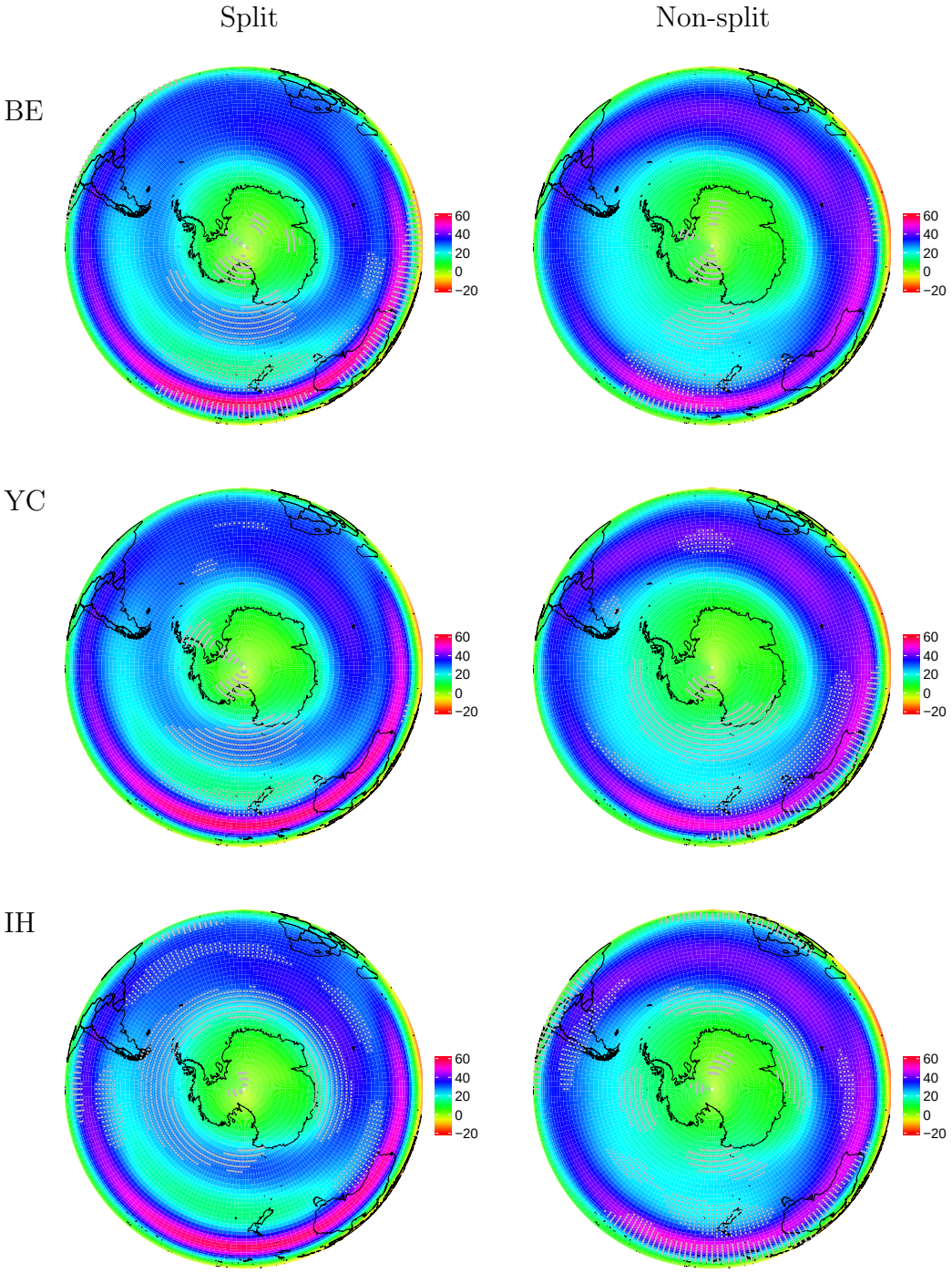

Figure 6.1: *Positive (left column) and negative (right column) composites of three established split jet indices defined by Bals-Elsholz et al. (2001) (first row), Yang and Chang (2006) (second row) and Inatsu and Hoskins (2006) (last row) in the 200 hPa zonal wind field [m/s] of the MPI-ESM for the 1979–2005 period. All indices were scaled for illustration purposes (see Chap. 3). Gray dotted areas are significant at the $\alpha = 1$ % level.*

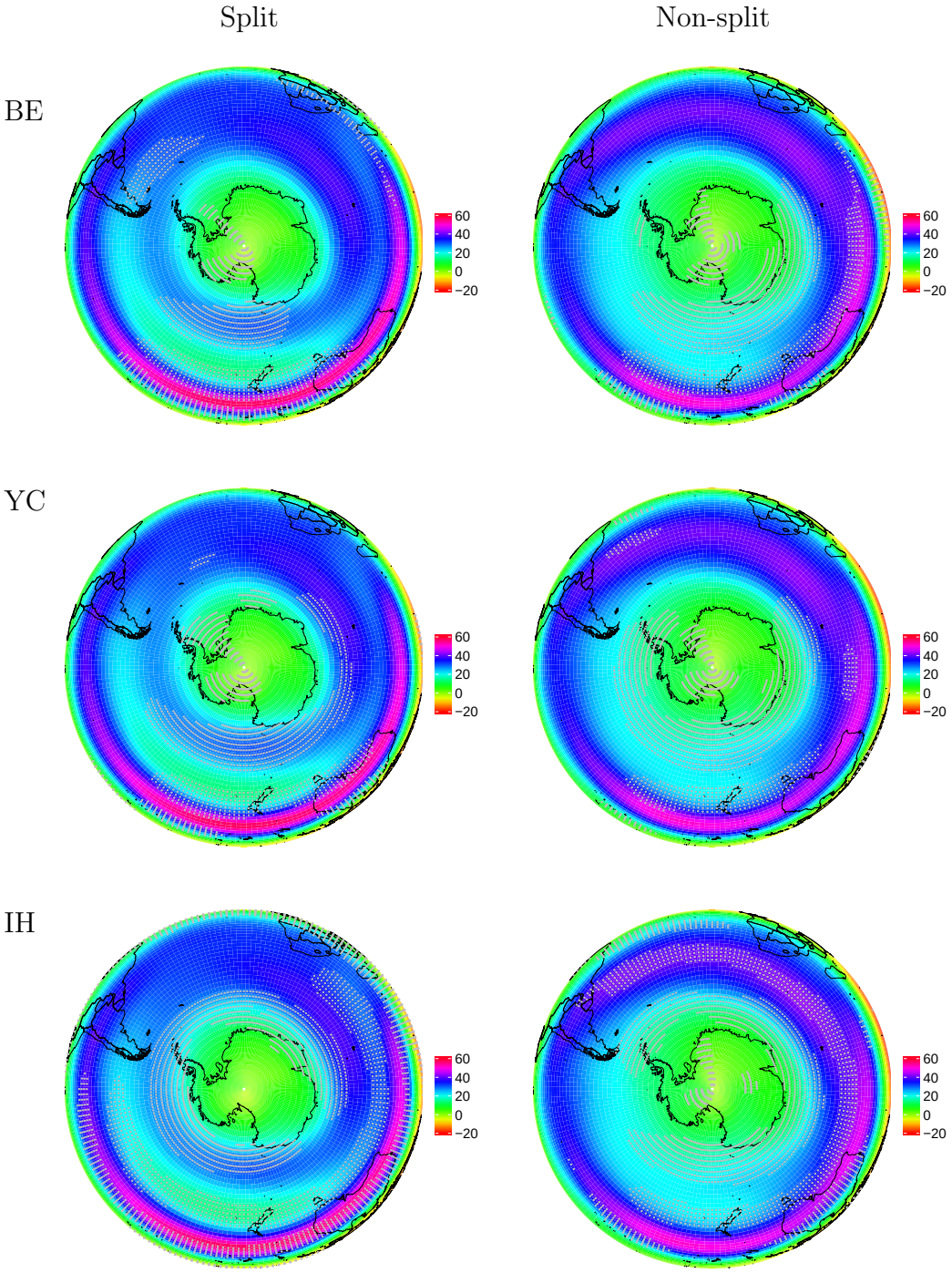

Figure 6.2: *Positive (left column) and negative (right column) composites of three established split jet indices defined by Bals-Elsholz et al. (2001) (first row), Yang and Chang (2006) (second row) and Inatsu and Hoskins (2006) (last row) in the 200 hPa zonal wind field [m/s] of the ERA-Interim reanalysis for the 1979–2005 period. All indices were scaled for illustration purposes (see Chap. 3). Gray dotted areas are significant at the $\alpha = 1$ % level.*

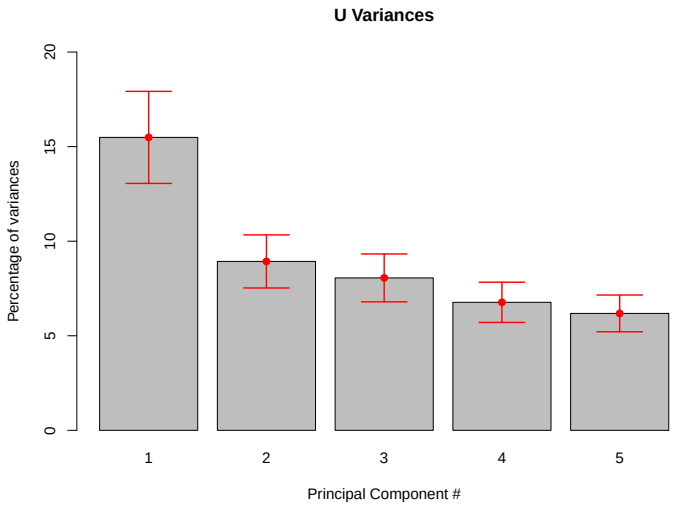

Figure 6.3: *Proportions of the total variance [%] associated with the leading 5 EOFs for the 200 hPa zonal wind field of the MPI-ESM. Error bars are estimates of sampling errors in EOF computation according to North's "rule of thumb" (North et al., 1982).*

other after North's "rule of thumb" (North et al., 1982), i.e. PC2 to PC5 are effectively degenerate. That means that the eigenvalues uncertainty is larger than the spacing between the eigenvalues. As mentioned in Chap. 5 it can be shown with the aid of linear algebra, that any orthogonal pair of such linear combinations is equally well qualified to be an EOF (Sahai et al., 2014).

In accordance with the procedure for calculating the PSI in the ERA-Interim reanalysis data set, a PC based split jet index is defined for the MPI model by correlating the individual leading five PCs of the SH 200 hPa zonal wind field in Austral winter (JAS) to the established split jet indices (Tab. 6.1). The leading and the third PC were identified to contain significant parts of the SH split jet variability in the MPI earth system model. The significant Pearson correlation coefficients range from r = 0.26 (YC) to r = 0.33 (IH) between PC1 and the traditional split indices. PC3 which is significantly correlated to all three split indices produces correlation values ranging from r = 0.26 (YC) to r = 0.49 (IH). The mean of all established split jet indices correlates significantly positive to PC1 (r = 0.36) and PC3 (r = 0.41). Nevertheless, the amount of the correlation coefficients in the MPI-ESM is overall smaller compared to ERA-Interim. This will be discussed in the last section (Sec. 7).

The correlation analysis between the individual PCs of the 200 hPa zonal wind field in the MPI-ESM and the three traditional split jet indices revealed that PC1 and PC3 contain the "model-intern" SH split variability and are thus linearly combined to the PSI_{MPI} as follows:

$$PSI_{MPI} = PC1_{U_{200hPa}} + PC3_{U_{200hPa}} \tag{6.1}$$

Worth mentioning, the 4^{th} PC of the MPI-ESM zonal wind field correlates negatively with the split jet indices defined by Bals-Elsholz et al. (2001) and Yang and Chang (2006), but simultaneously significantly positive (r = 0.49) to the split jet index designed by Inatsu and Hoskins (2006). Consequently, the mean of all established split jet indices shows no correlation (r = -0.05) to PC4. This behavior is approximately mirrored for PC5: the BE and the YC indices correlate weak but significantly positive to PC5 although the IH index shows no relationship to PC5 (r = -0.02). The split jet index suggested by Inatsu and Hoskins (2006) is based on the zonal mean zonal wind field (Sec. 3.4) in contrast to both other split indices (BE and YC) and lacks thus longitudinal variations which are of essential importance for the split jet representation.

The last column of Tab. 6.1 reveals Pearson's correlation values between the PSI_{MPI} and the established split jet indices. Although the correlation coefficients are significant for all earlier split jet indices and their mean, the amount of the values is relatively smaller compared to the PSI defined in the ERA-Interim reanalysis. The PSI_{MPI} time series, as well as the split indices of the previous studies, are displayed in Fig. 6.4 and show much less consensus compared to the split indices calculated from the ERA-Interim data (Fig. 5.3).

6.3 Composite Analysis of U 200 hPa with PSI_{MPI}

Figure 6.5 shows the spatial patterns of U_{200} for the high (9 cases) and low (13 cases) PSI_{MPI} phases identified during the 1979–2005 model simulation. The positive composite (Fig. 6.5, left panel) reveals a strong STJ from the southern Indian Ocean to the eastern South Pacific Ocean and a weak PFJ south of New Zealand which weakens further towards the longitudes of the Antarctic Peninsula region. Compared to the PSI composites of the ERA-Interim reanalysis (Fig. 5.4) the split jet structure is less pronounced. The right panel of Figure 6.5 shows the equivalent negative composite of the PSI_{MPI}. Although the figure contains the "non-split" (merged jet) cases it still reveals a weak PFJ over the South Pacific Ocean.

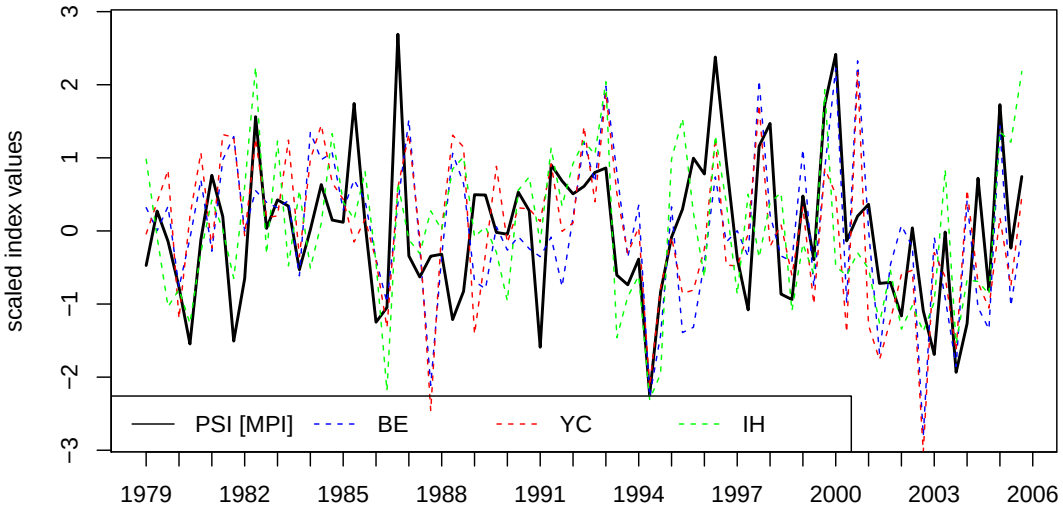

Figure 6.4: *PSI_{MPI} (PC1 + PC3) index in 200 hPa zonal wind and three established split jet indices defined by Bals-Elsholz et al. (2001) (BE), Yang and Chang (2006) (YC) and Inatsu and Hoskins (2006) (IH) and calculated for the MPI-ESM. All time series were scaled for illustration purposes (see Chap. 3).*

	$\mathbf{PC1}_{MPI}$	$\mathbf{PC2}_{MPI}$	$\mathbf{PC3}_{MPI}$	$\mathbf{PC4}_{MPI}$	$\mathbf{PC5}_{MPI}$	$\mathbf{PSI}_{MPI}$
JAS – correlation values						
-BE	**0.32**	0.02	**0.27**	**-0.31**	**0.26**	**0.42**
YC	**0.26**	-0.06	**0.26**	**-0.31**	**0.27**	**0.37**
IH	**0.33**	-0.16	**0.49**	**0.49**	-0.02	**0.56**
Mean	**0.36**	-0.08	**0.41**	-0.05	0.20	**0.53**

Table 6.1: *Monthly (JAS) Pearson correlation coefficients of individual leading 5 PCs of the MPI-ESM 200 hPa zonal wind, as well as the PSI_{MPI} (PC1 + PC3), with the split jet indices introduced in the methods chapter (see Sec. 3.4). By construction, the index defined by Bals-Elsholz et al. (2001) becomes negative during split events and its sign is therefore reversed. Bold values are significant at the $\alpha = 1$ % level.*

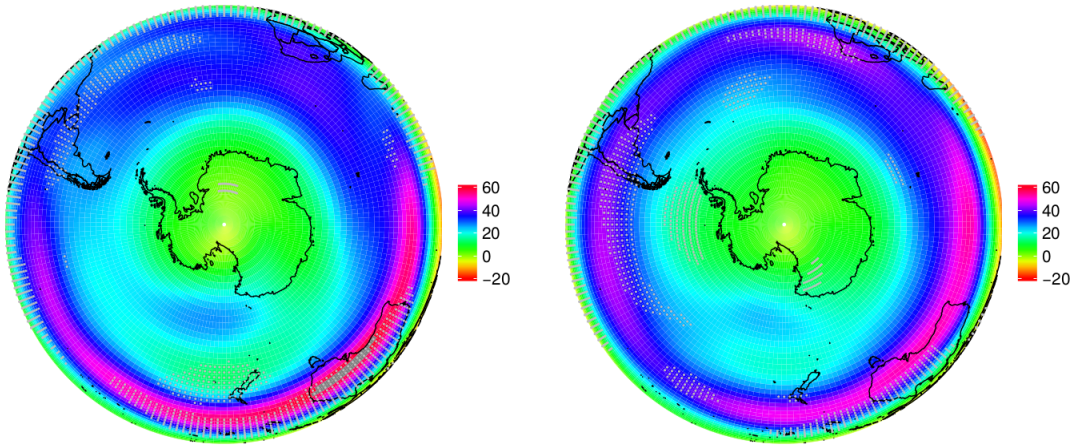

Figure 6.5: *Positive (left) and negative (right) composite of the PSI_{MPI} (PC1 + PC3) index in 200 hPa zonal wind. Gray dotted areas are significant at the $\alpha = 1$ % level.*

A composite analysis of both components of the PSI_{MPI}, i.e. PC1 and PC3, is considered to give further insight into the individual contributions of the PCs. The most prominent feature of the positive component of PC1 is a strong STJ which is accompanied by a weaker PFJ extending over the whole width of the Ross Sea. The PFJ south of Australia which is apparent in the positive composite of the PSI (and the individual components) in the ERA-Interim reanalysis is missing in the positive composite of PC1 in the MPI-ESM. The respective negative composite of PC1 shows a weaker STJ over the South Pacific Ocean but traces of the PFJ are still apparent south of New Zealand.

Interestingly, the positive composite of PC3 also lacks the strong PFJ which is noticeable in the PC1 composite south of Australia and the South Pacific Ocean, although weak traces of the PFJ are noticeable over the Bellingshausen Sea and the Drake Passage. Comparable to the positive composite of PC1 a strong STJ is visible over all longitudes from the Southern Indian Ocean to the east of South America, although less pronounced than in the positive composite of PC1. The respective negative composite of PC3 shows a clear single jet regime with a strong STJ and a missing PFJ.

Altogether, the positive composite of PSI_{MPI} benefits from the positive contribution of PC1, but lacks the typical split jet structure in the positive PSI_{MPI}

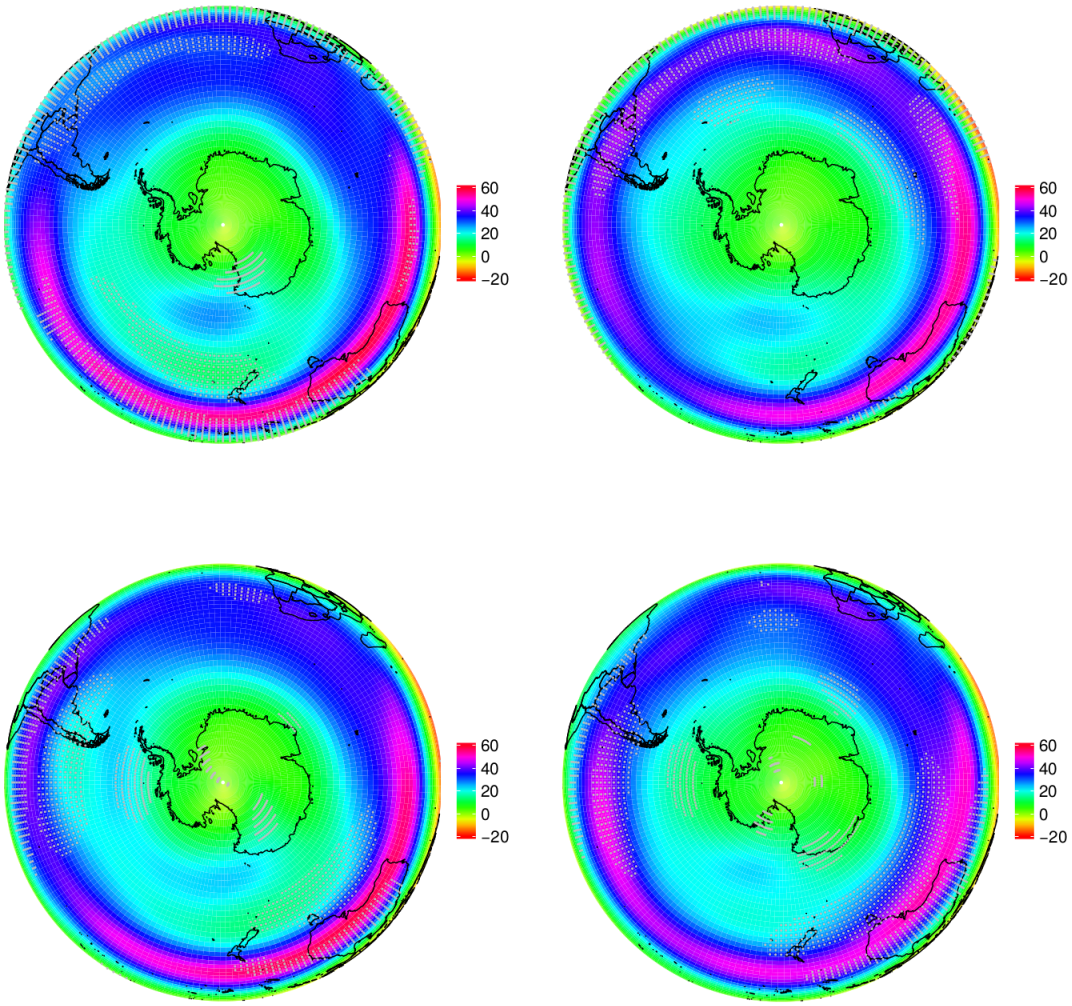

Figure 6.6: *Composites of positive (left) and negative (right) phases of PC1 (first summand of Eq. 6.1; top row) and PC3 (second summand of Eq. 6.1; bottom row) time series of the SH zonal wind in 200 hPa in the MPI-ESM. Gray dotted areas are significant at the $\alpha = 1$ % level.*

composite which is visible in the respective composite in ERA-Interim.

6.4 Aspects of the SH zonal asymmetric circulation in the MPI-ESM

The results of the previous sections suggest that the MPI-ESM lacks substantial portions of variability in the higher order modes of the zonal wind in 200 hPa (U_{200}) during SH winter. These higher order modes were found to be associated with the split jet variability in the ERA-Interim reanalysis. The main objective of this section is thus the identification of potential causes for the deficiencies in the representation of the wintertime SH split jet variability in the MPI-ESM. On this account, climatologies and standard deviations (during Austral winter) of associated fields (U_{200} and Z_{500}), as well as the deviations from the zonal mean of both quantities, will be assessed in the following. The 200 hPa zonal wind field was chosen since it is the level where the split jet is defined. The 500 hPa level of the geopotential height was selected because it represents the middle of the troposphere.

The subsequent six figures are arranged in the same manner: the MPI-ESM plot is shown in the top left panel, the ERA-Interim plot in the top right panel and the differences between both in the bottom row of the according figure. Please note the differing scales of the difference plots in the bottom panels of the respective figures.

Figure 6.7 illustrates the U_{200} climatology for the 1979–2005 period in the MPI-ESM (top left panel), in ERA-Interim (top right panel) and the differences between both fields (i.e. MPI-ESM minus ERA-Interim, bottom panel). While the spatial structure of the zonal wind speed climatology is sufficiently captured by the model particularly concerning the STJ strength, this is not the case for the PFJ. In ERA-Interim a robust PFJ is visible which emerges south of South Africa and circles nearly zonally westwards around the Antarctic continent towards the southern tip of South America. The difference plot reveals therefore a significantly weaker (stronger) PFJ at roughly 65° S (STJ at roughly 30° S) over the whole hemisphere with the greatest differences of the zonal wind anomalies occurring south of Australia.

The standard deviations of the U_{200} fields for the 1979–2005 period can be found in Fig. 6.8. The standard deviation of the MPI-ESM shows great differences particularly over western hemisphere where the standard deviation around the latitude

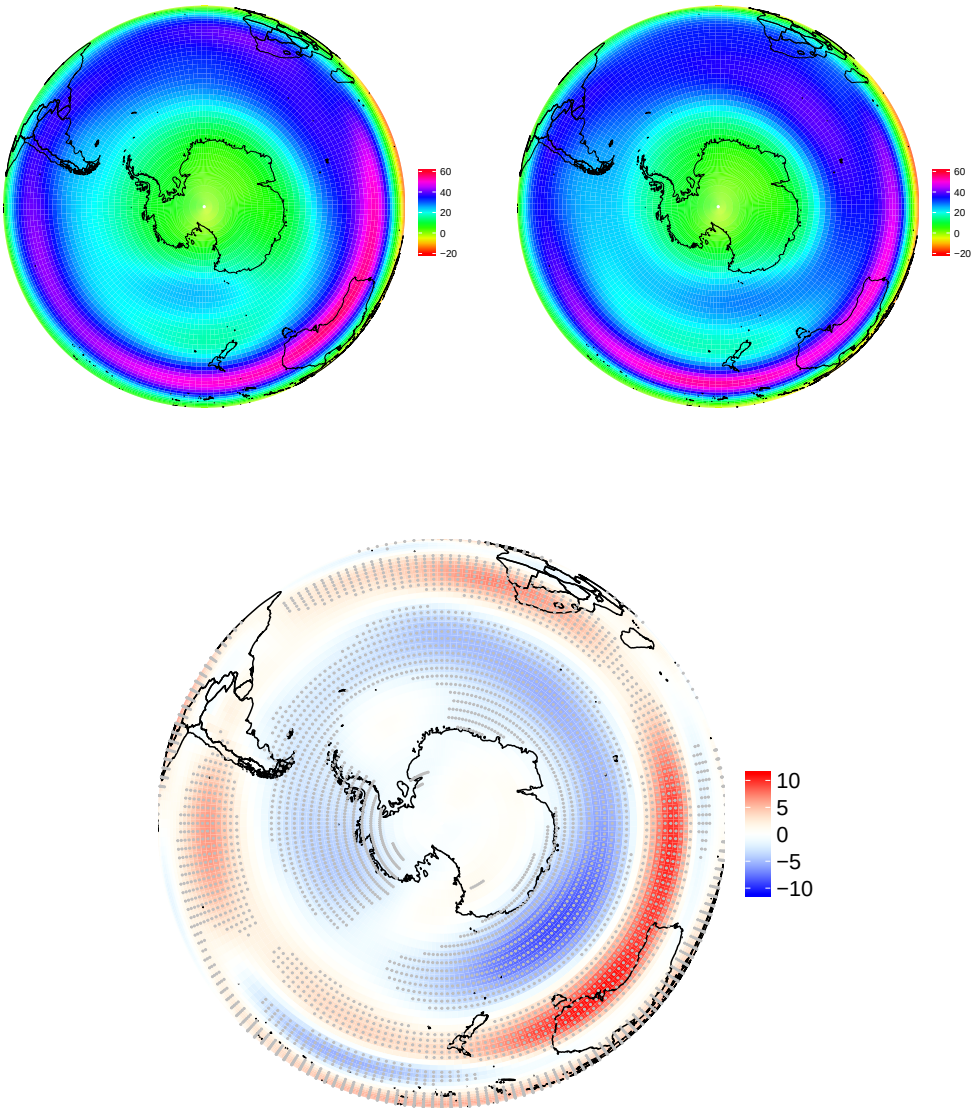

Figure 6.7: *Climatologies of the zonal wind [m/s] at 200 hPa in Austral winter (JAS) for the 1979–2005 period in MPI-ESM (top left panel), in ERA-Interim (top right panel) and the differences between both (bottom panel). Gray dotted areas are significant at the $\alpha = 1$ % level.*

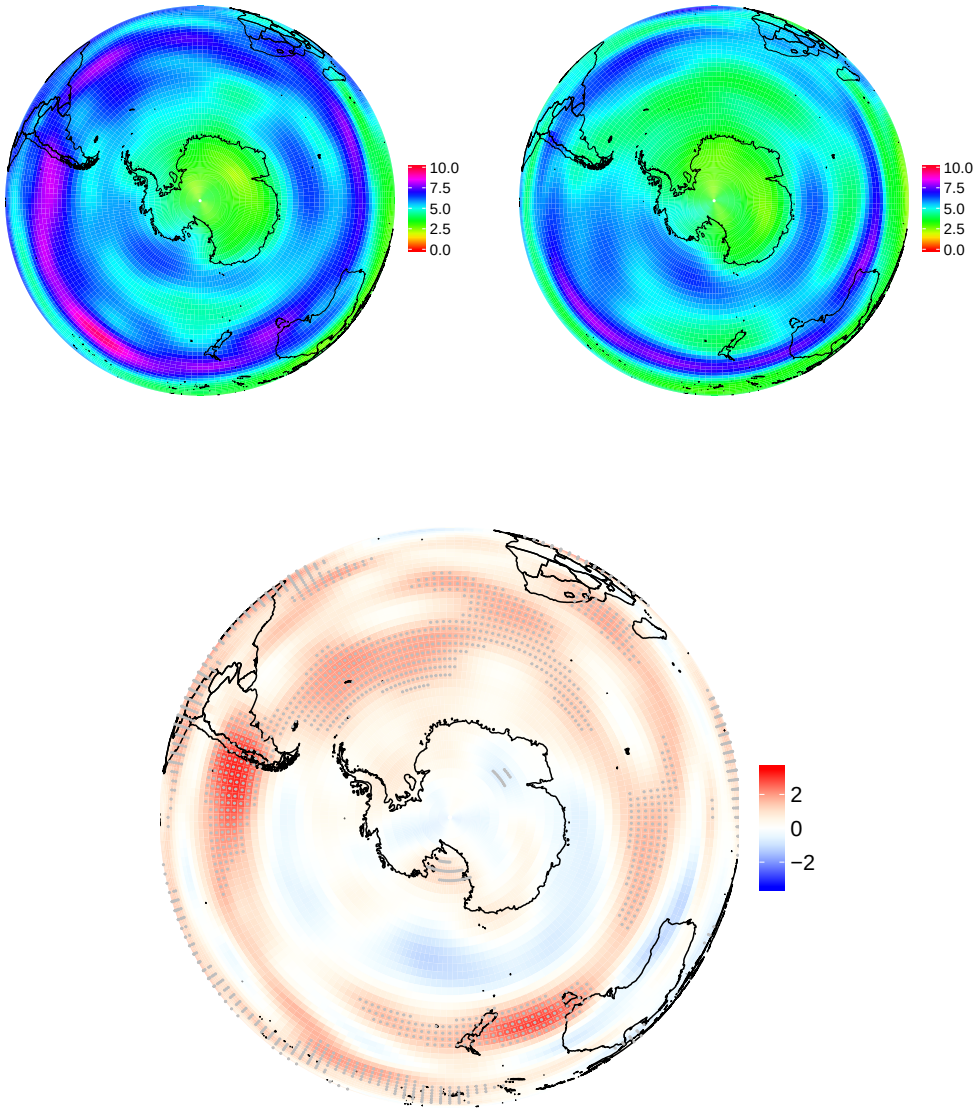

Figure 6.8: *Standard deviations of the zonal wind [m/s] at 200 hPa in Austral winter (JAS) for the 1979–2005 period in MPI-ESM (top left panel), in ERA-Interim (top right panel) and the differences between both (bottom panel). Gray dotted areas are significant at the $\alpha = 1$ % level.*

of 30° S (STJ location) is larger compared to the reanalysis. Southeast of Australia over the Tasmanian Sea where an important region of blocking events excites enhanced variability to the westerly flow (Trenberth and Mo, 1985) the standard deviation is overestimated as well by the model consistent with the enhanced STJ velocities over that region (compare Fig. 6.7). A further distinct detail of the difference plot is a positive standard deviation anomaly west of southern South America where the stronger STJ produces enhanced variability due to orographic effects induced by the Andes. Altogether, the difference plot (MPI-ESM minus ERA-Interim) shows again an underestimation (overestimation) of the PFJ (STJ) variability compared to ERA-Interim. These differences are responsible for the insufficient split jet representation in the model since the variations in strength and position of the jets are the essential part of the split generation and representation. With regard to disentangle the mechanisms responsible for the underestimation (overestimation) of the PFJ (STJ) strength and variability in the MPI-ESM the Z_{500} fields are analysed.

Figure 6.9 and Fig. 6.10 offer the climatologies and standard deviations of the Z_{500} field analogous to the proceeding in the zonal wind (Fig. 6.7 and Fig. 6.8). The most striking difference between the model and ERA-Interim is the underestimated (overestimated) geopotential height over the Antarctic continent (the mid-latitudes). The differences result in a weaker meridional geopotential height gradient which directly affects the zonal wind variability via the thermal wind relation. Consequently, the zonal wind (PFJ) is reduced where the gradient is most restrained in the model (south of Australia). Conversely, the STJ suffers from the reduced PFJ strength and is enhanced farther north (around the latitudes of New Zealand) in the earth system model.

The Z_{500} standard deviation is analysed to identify the causes for the differences in the geopotential height climatologies of the model and the reanalysis. By comparing the spatial distributions of the standard deviation in the model to the reanalysis (Fig. 6.10) it is evident that the wintertime geopotential height variability is most pronounced over the Amundsen and Bellingshausen Seas. In contrast, the MPI-ESM lacks geopotential height variability mainly over that distinct region and west of the Antarctic Peninsula. The region in the vicinity of the Amundsen and Bellingshausen Seas is often studied in literature since it coincides the climatological location of the Amundsen Sea Low (ASL). The variability of the ASL is associated with tropical signals (ENSO teleconnections) in the following way: the absolute depth of the ASL is significantly lower during the La Niña phases compared to El Niño (Raphael et al., 2016). This result hints that a lack of ENSO

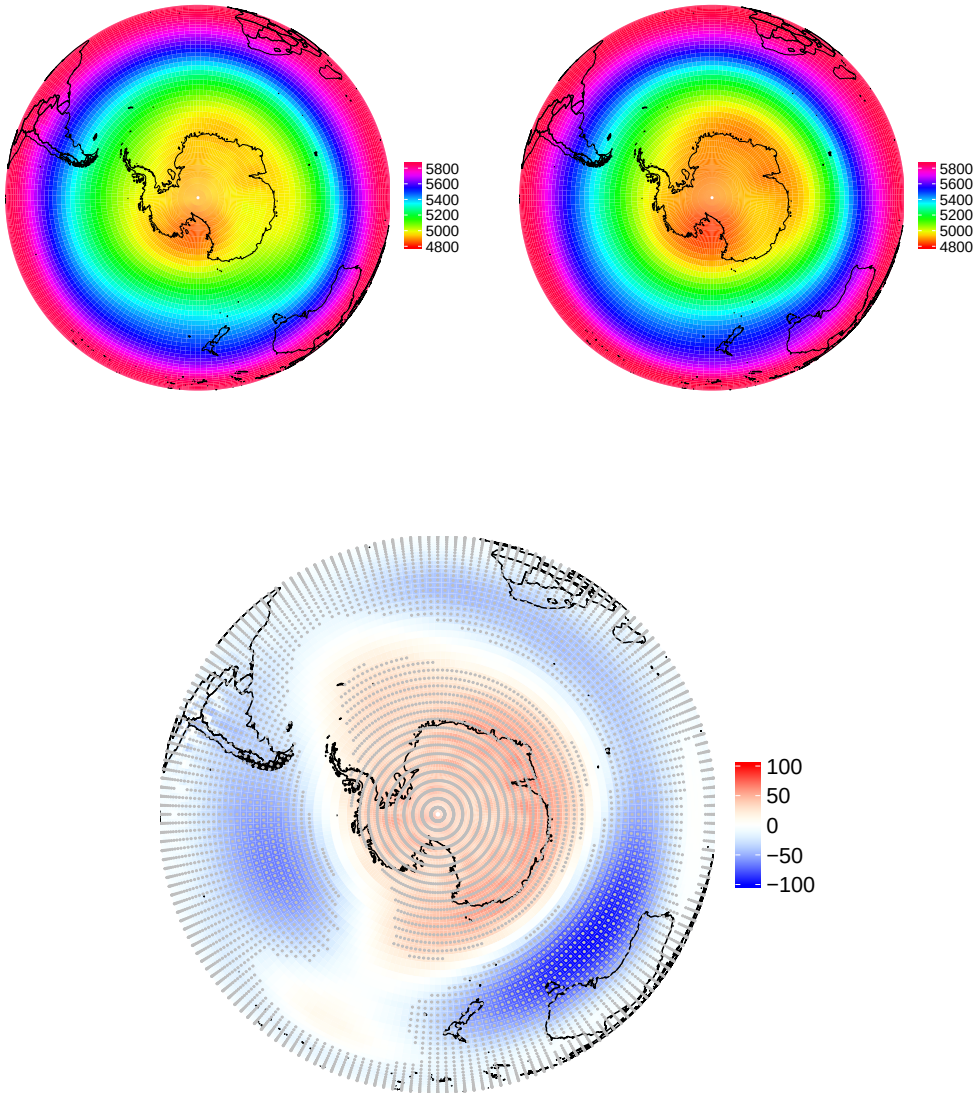

Figure 6.9: *Climatologies of the geopotential height [m] at 500 hPa in Austral winter (JAS) for the 1979–2005 period in MPI-ESM (top left panel), in ERA-Interim (top right panel) and the differences between both (bottom panel). Gray dotted areas are significant at the $\alpha = 1$ % level.*

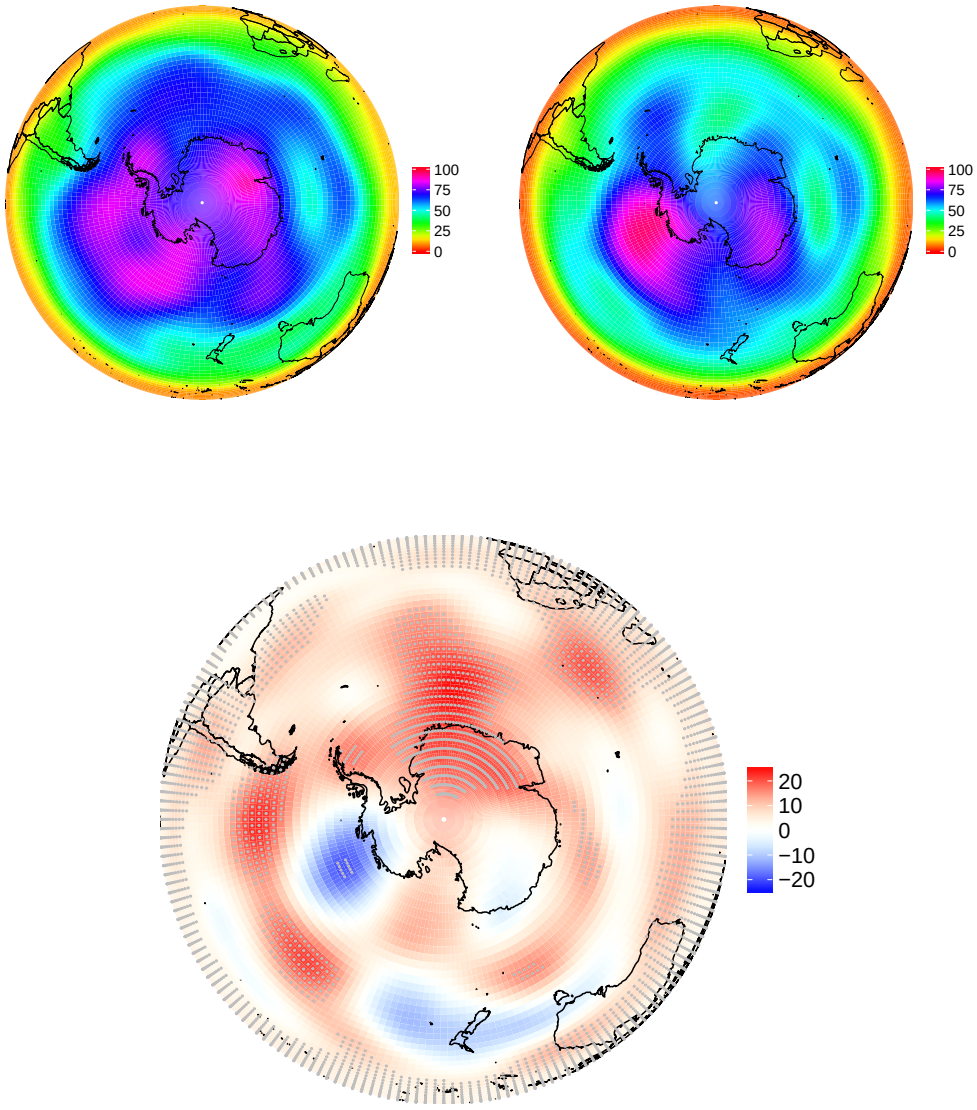

Figure 6.10: *Standard deviations of the geopotential height [m] at 500 hPa in Austral winter (JAS) for the 1979–2005 period in MPI-ESM (top left panel), in ERA-Interim (top right panel) and the differences between both (bottom panel). Gray dotted areas are significant at the $\alpha = 1$ % level.*

variability in the model leads to significant differences in the geopotential height variability over the high-latitudes especially over the western Antarctic Peninsula region. This issue is further discussed in the last section of this chapter (Sec. 6.5).

Consistent with the results from the individual standard deviation plots, the difference plot reveals the greatest differences (between model and reanalysis) over the ASL region where a negative peak points again towards the model's underestimated geopotential height variability. The difference plot exhibits further that the Z_{500} variability is as well underestimated over New Zealand compared to the reanalysis. Since the atmospheric variability over that region is mainly associated with blocking situations which are related to the zonal wavenumber-3-pattern and ENSO in literature (Raphael, 2004; Trenberth and Mo, 1985; Mo et al., 1987; Pook et al., 2013) it is concluded that the MPI-ESM lacks (anticyclonic) geopotential height variability not only over the ASL region but also over New Zealand. Probable origins of these discrepancies are as well discussed in the last section (Sec. 6.5).

In conclusion, the model represents to a large extent the spatial distribution of the geopotential height and zonal wind climatologies and standard deviations as stated by the ERA-Interim reanalysis. Altogether, the model results display an exaggerated zonal symmetry which is absent in the reanalysis (and observations). The most pronounced difference between the climatologies in ERA-Interim and the earth system model is thus a weaker (stronger) PFJ (STJ) over the western Pacific in the model. The reduction (enhancement) of the PFJ (STJ) originates from a reduced geopotential height gradient (over the split jet relevant region) in the model compared to the reanalysis. This leads to significant differences in the zonal wind field between model and reanalysis which are related to the inadequate split jet representation in the MPI-ESM.

6.4.1 Zonal asymmetric SH circulation in the MPI-ESM

The previous section evaluated the ability of the MPI-ESM to represent crucial parts of the (nearly zonally symmetric) SH tropospheric circulation substituted by the associated climatologies and standard deviations of the U_{200} and Z_{500} fields. For the purpose of understanding the lack of regionally (and potentially zonal asymmetric) variability in the MPI-ESM, the deviations from the zonal mean (zonal anomalies) of the zonal wind (in 200 hPa) and the geopotential height (in 500 hPa) are analysed additionally.

Figure 6.11 and Fig. 6.12 show the proportions of the zonal circulation anomalies with respect to the climatologies shown in Fig. 6.7 and Fig. 6.9. The zonal

anomalies (called the "non-zonal" component of the circulation hereafter) arise by removing the respective zonal mean quantity from the respective climatology.

The top right plot in Fig. 6.11 reveals the non-zonal proportion of the U_{200} field in ERA-Interim. Positive (negative) values indicate zonal wind values which are higher (smaller) than the zonal mean value. The most striking feature of this figure is a noticeable zone of positive values which depicts the presence of a broad mid-latitude jet expanding eastward from southern South America towards the South Indian Ocean. Since the transient eddies are well-organised in that mid-latitude jet between 25° and 30° S, the meridional displacement is reduced north and south of that latitudinal band consistent with weaker non-zonal wind speeds over these regions. This structure is broken south of Australia where the broad merged (mid-latitude) jet divides into a separated STJ and PFJ with corresponding higher non-zonal proportions north and south of the mid-latitudes capturing the variabilities in meridional displacement of the separated STJ and PFJ. The MPI-ESM (top left panel of the same figure) shows a similar structure although both, the positive and the negative anomalies of the zonal variations are underestimated in the model over the South Pacific sector compared to ERA-Interim. The difference plot (bottom row) reveals consequently most pronounced differences over that region especially south of Australia and over the South Pacific Ocean.

Figure 6.12 exhibits the respective non-zonal proportion of the geopotential height at the 500 hPa level. The top right panel in this figure shows minimum (maximum) values of the non-zonal variability over most of the eastern (western) hemisphere in ERA-Interim. The spatial structure accounts for the low-pressure systems moving during Austral winter farther south over the eastern hemisphere and for the quasi-stationary anticyclones in the western hemisphere (Pacific sector). The spatial structure in this figure is in agreement with the known zonal wavenumber 1 pattern which is also evident in earlier studies concerning the non-zonal variations of the atmosphere (e.g. Fig. 1 in Hobbs and Raphael (2007)). The spatial distribution of this non-zonal variability is to some extent reproduced by the model, however, the zones of maximum values are shifted. This is again pronounced in the difference plot (bottom row of Fig. 6.12) where the model underestimates the meridional variations south of Australia and over the already addressed ASL region.

By comparing the U_{200} and Z_{500} climatology differences (bottom rows of Fig. 6.7 and 6.9) to the differences in the zonal asymmetric components of these fields (Fig. 6.11 and Fig. 6.12) it is indicative that the spatial distribution of the asymmetric components of both variables resemble largely the structure of the total

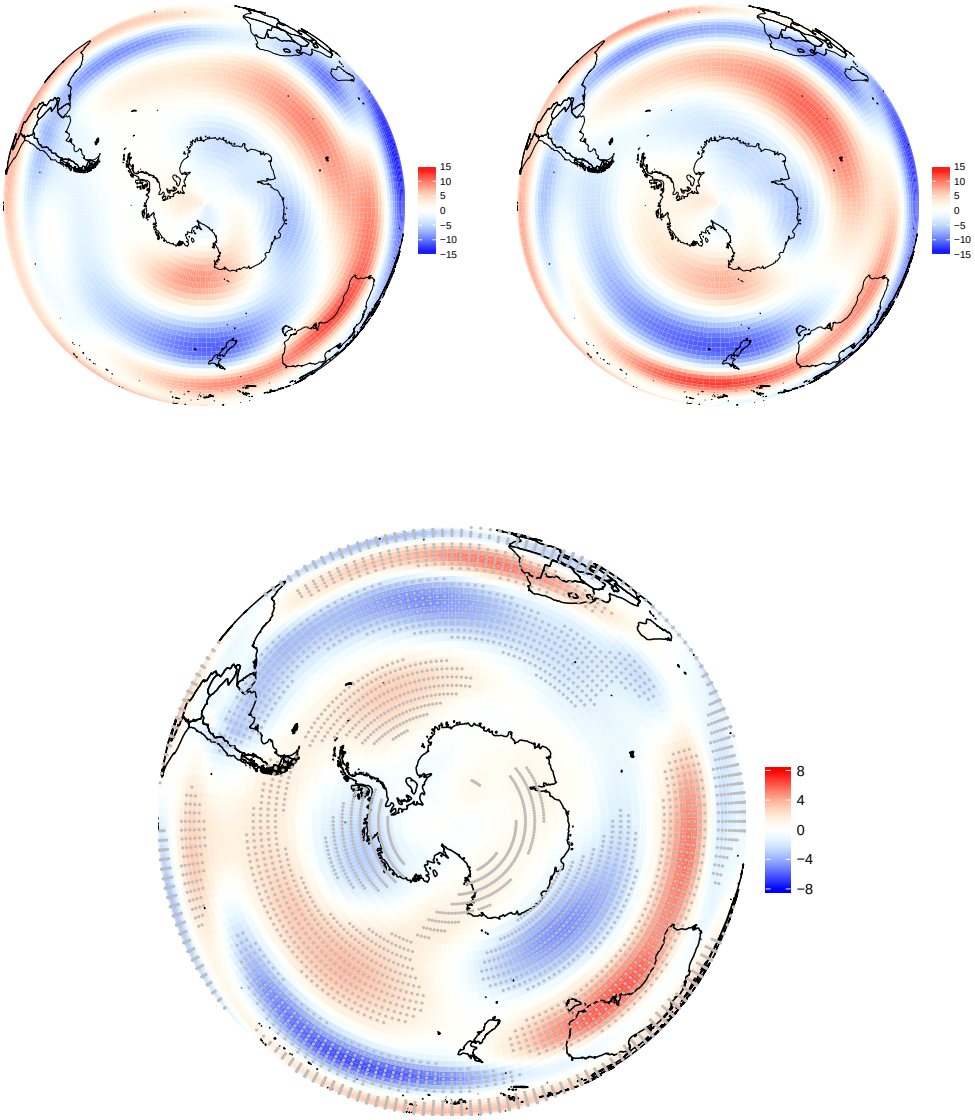

Figure 6.11: *Anomalies w.r.t. the zonal mean of the zonal wind at 200 hPa [m/s] in Austral winter (JAS) for the 1979–2005 period in MPI-ESM (top left panel), for the ERA-Interim (top right panel) and the differences between both (bottom panel). Gray dotted areas are significant at the $\alpha = 1$ % level.*

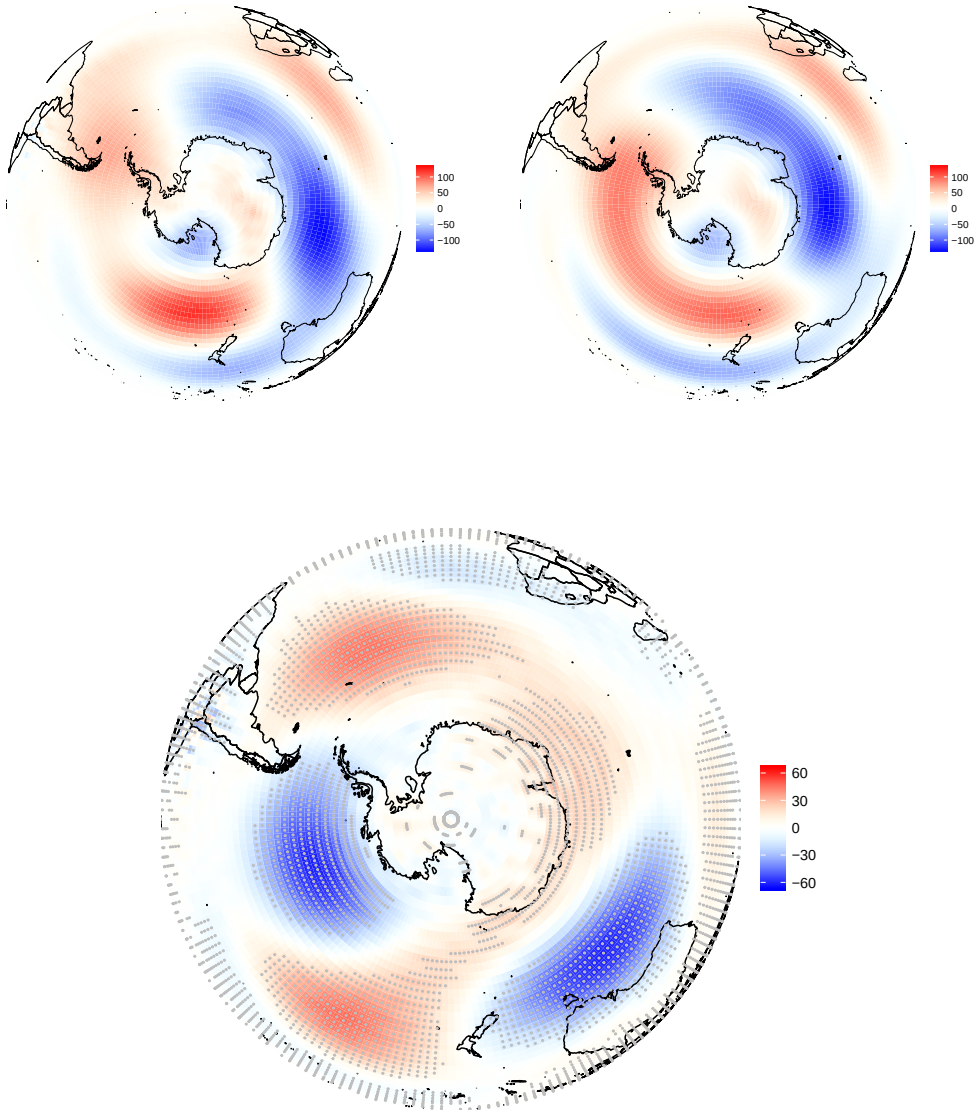

Figure 6.12: *Anomalies w.r.t. the zonal mean of the geopotential height [m] at 500 hPa in Austral winter (JAS) for the 1979–2005 period in MPI-ESM (top left panel), for the ERA-Interim (top right panel) and the differences between both (bottom panel). Gray dotted areas are significant at the $\alpha = 1$ % level.*

differences. It is thus concluded that a great amount of differences between the climatologies of the model and the reanalysis can be attributed to the difficulties of the MPI-ESM to simulate the non-zonal aspects of the circulation.

This is further supported by Figure 6.13 which exposes the correlation maps between the non-zonal Z_{500} field and the respect PSI (i.e. PSI and PSI_{MPI}). By comparing the correlation maps of the asymmetric Z_{500} components of the reanalysis and the model, it is discernible that the relationship between the PSI and the non-zonal Z_{500} field in ERA-Interim differs significantly from the model. The correlation pattern in the ERA-Interim reanalysis (right panel) reveals significant negative (positive) geopotential height anomalies west (east) of the Antarctic Peninsula. This distinct spatial distribution of Pearson's correlation coefficients is absent in the model. This relationship between zonal asymmetric Z_{500} field and split variability is lacking in the MPI-ESM. This result hints that fundamental mechanisms forcing the non-zonal of the circulation are deficient in the MPI-ESM.

Interestingly, the spatial structure of the correlation map between the non-zonal component of the Z_{500} field and the PSI in ERA-Interim resembles approximately the spatial pattern of the Pacific-South American Patterns (PSA, see Sec. 1.2.2). This result suggests that the PSA patterns and the associated tropical forcing is a substantial part of the modulation of the non-zonal component of the geopotential height variability in ERA-Interim. The non-zonal component of the SH circulation is recently discussed to be tropically forced. This has been highlighted in a limited number of studies (Fogt et al., 2012; O'Kane et al., 2017) and will be further discussed in the last chapter (Chap. 7).

6.4.2 Zonal asymmetric AAO component in the MPI-ESM

Figure 4.1 from Chap. 4 shows the spatial patterns of the AAO in the MPI-ESM, in ERA-Interim and the differences between both. As already addressed (Sec. 4.1) the difference plot is indicative of missing temporal geopotential height variability over the Amundsen and Bellingshausen Seas in the earth system model although good agreement in temporal properties (i.e. seasonal cycle and spectral density) of the AAO index was found in the model. Even though in literature the AAO is often referred to as Southern "Annular" Mode, it reveals a considerable portion of "non-annular" (non-zonal) variability (Fogt et al., 2012).

Although the split jet is one of the most prominent asymmetric features of the SH winter circulation (Bals-Elsholz et al., 2001) the PSI was found to be strongly associated with the AAO in ERA-Interim ($\text{r}_{PSI} = 0.81$, see Chap. 5). It is thus

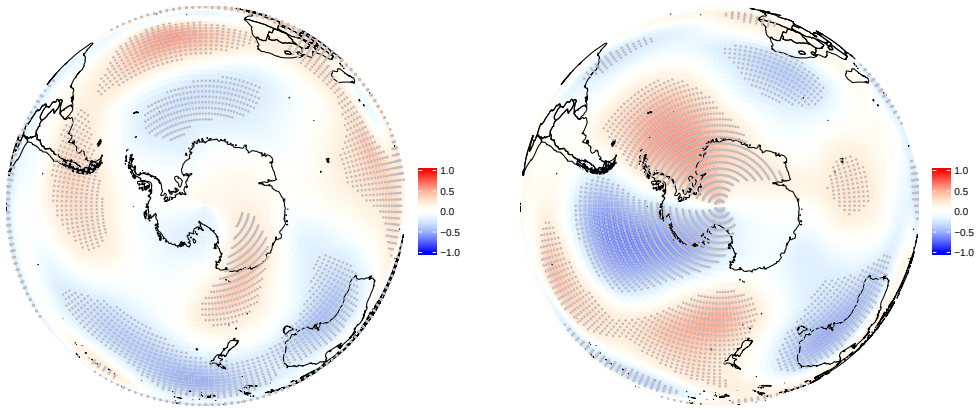

Figure 6.13: *Pearson's correlation coefficients between the zonal anomalies ("non-zonal" component) of the 500 hPa geopotential height and the PSI in the MPI-ESM (left) and the ERA-Interim reanalysis (right). Gray dotted areas are significant at the $\alpha = 1$ % level.*

expected that the non-zonal portion of the AAO is associated as well with the split variability. This motivates the following evaluation of the non-annular portion of the AAO in the MPI-ESM.

The calculation of the zonal asymmetric portion of the AAO is performed by removing both the time and the zonal means from the (700 hPa) geopotential height field prior to the composite calculation (Peixoto and Oort, 1992; Fogt et al., 2012).

Fig. 6.14 shows the positive (left column) and negative (right column) composite of the non-annular AAO composites of the MPI-ESM (top row) and ERA-Interim (bottom row). Generally, Fig. 6.14 highlights again the lacking AAO zonal symmetry which is more pronounced in every other season than the Austral wintertime (e.g. Fogt et al., 2012). The bottom left panel of Fig. 6.14 illustrates the ERA-Interim non-annular part of the AAO. The most striking characteristic of this pattern is a zone of positive (negative) anomalies east (west) of the Antarctic Peninsula. This structure is completely absent in the positive model composite (top left panel). The negative composite in ERA-Interim (bottom right panel) reveals a negative anomaly over the Amundsen and Bellingshausen Seas, in contrast to the negative composite of the MPI-ESM (top right panel) where this pattern is nearly reversed. This is consistent with the mentioned problems in modeling the

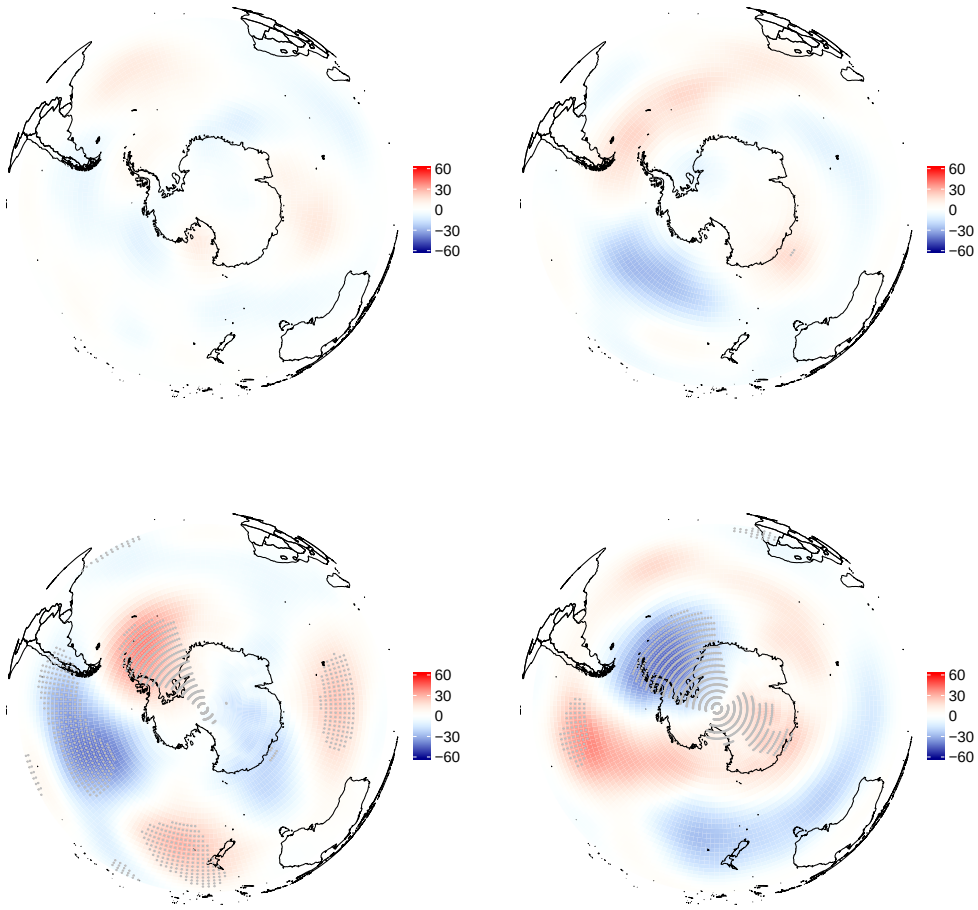

Figure 6.14: *Positive (left column) and negative (right column) composite of the zonal asymmetric portion of the leading EOF in the 700 hPa geopotential height field (i.e. the AAO). Anomalies were calculated w.r.t. the zonal mean of Z_{700} for Austral winter months (JAS) during the 1979–2005 period in MPI-ESM (top row) and in the ERA-Interim (bottom row). Gray dotted areas are significant at the $\alpha = 1$ % le- vel.*

geopotential height variability over that specific region (climatological position of the ASL).

A further discrepancy between model and reanalysis is the absent symmetry between positive and negative composites in the model. While the positive and negative composites of the reanalysis nearly mirror each other, the respective MPI-ESM composites reveal non-linearities (i.e. differences between positive and negative polarities) of the AAO.

Although the MPI-ESM was found to be in general able to reproduce large parts of the AAO spatial structure, this holds not true for the non-annular AAO component where large discrepancies arise between the model and the reanalysis. These are indicative of missing mechanisms forcing the non-zonal AAO part in the MPI-ESM. A potential candidate for these mechanisms are the Pacific South American modes which are in literature assigned to be modulated by ENSO variability (Mo, 2000). Potential causes for these discrepancies will be discussed in the next section.

6.5 Summary and discussion

This chapter aimed the ability of the MPI earth system model to simulate different aspects of the asymmetric component of the SH circulation. The first attempt therefore has been the construction of an index describing a prominent feature of the zonally asymmetric circulation of the SH (the wintertime split jet) in the MPI-ESM analogous to the PSI in ERA-Interim.

It is concluded that the MPI-ESM lacks variance in the higher order modes of the SH zonal wind field at 200 hPa. The modes higher than the first are not distinguishable after North's "rule of thumb" (North et al., 1982). This implicates that the MPI-ESM mixes the variabilities associated with the SH split jet in the higher order modes of the zonal wind variance. This is supported by the fact that two out of three established split jet indices correlate significantly to all five leading PCs except PC2. The mean of all established split jet indices correlates significantly to PC1 and PC3, which was the crucial factor for the PSI_{MPI} definition. Consequently, the PSI_{MPI} is defined as a linear combination of both, PC1 and PC3. The PSI_{MPI} and the mean of all established indices correlate significantly to each other ($r = 0.53$) although the strength of the relationship is modest compared to the reanalysis ($r = 0.76$). A composite analysis of the PSI_{MPI} and its individual components (PC1 and PC3) suggests further that the model misses PFJ variability over the Pacific sector and lacks thus the typical split jet structure as visible in the reanalysis composites.

Interestingly, the fourth PC correlates significantly positive to two (BE, YC) out of the three established split jet indices and negative to the remaining index (IH). The reason for the contrasting relationships to PC4 lies in the definition of the remaining split index (IH) correlating negatively to PC4. The fourth EOF in the MPI-ESM resembles the spatial pattern of EOF3[1] in ERA-Interim and its associated PC is consequently correlated negatively to the BE and YC indices. The split index published by Inatsu and Hoskins (2006) is defined as the difference in zonal mean zonal wind of three overlapping latitudinal boundaries (see Sec. 3.4 for the definitions of the split jet indices) and masks the lacking longitudinal variability over the Pacific sector (especially west of Australia / New Zealand) resulting in a significant positive correlation to PC4 in the MPI-ESM.

A potential cause of the discrepancies in the zonal wind field between the MPI-ESM and the ERA-Interim reanalysis is the insufficient representation of the accurate PFJ latitude especially over the SH (Stevens et al., 2013). Another weakness of the MPI-ESM with possibly unfavorable effects on the accurate representation of the split jet, is the eastward bias in the position of the Amundsen Sea Low (ASL) in the model (Hosking et al., 2013) by acting on the meridional pressure gradient and thus the strength and position of the jets.

To further investigate possible reasons for the discrepancies in the split jet representation and associated zonally asymmetric variability in the model, the climatologies and standard deviations of associated fields, the zonal wind at 200 hPa (U_{200}) and the geopotential height at 500 hPa (Z_{500}), were analysed additionally.

The MPI earth system model performs sufficiently in reproducing the spatial distribution of the geopotential height in a mid-tropospheric level and large portions of the zonal wind climatology. However, the strength of the PFJ (STJ) is underestimated (overestimated) during Austral winter by the MPI-ESM due to a reduced geopotential height gradient compared to the ERA-Interim reanalysis. A difference plot between the model and ERA-Interim shows a lack of variance in Z_{500} over the Amundsen and Bellingshausen Seas which is an important region in terms of cyclonic activity and a known recipient of tropical signals (Turner et al. (2013); Raphael et al. (2016)).

These results hint that a lack of ENSO variability in the model leads to significant differences in the geopotential height variability over the high-latitudes, especially over the West Antarctic region. This assumption is supported by the results from Chap. 4 revealing underestimated ASL variability over that region and by Jungclaus

[1]The leading five EOFs in the U_{200} and Z_{500} fields in ERA-Interim and MPI-ESM can be found in the Appendix.

et al. (2006) who reported the MPI-ESM-MR to simulate much weaker ENSO teleconnections towards the central subtropical South Pacific and tropical western Pacific than observed.

To investigate the model's performance in simulating the non-zonal portions of the SH circulation, the deviations from the zonal means were adducted in the U_{200} and Z_{500} fields. By definition, this non-zonal component of the circulation delineates the transient eddy portion which is an indicator for the strength of meridional heat and momentum transport (e.g. Lorenz, 1967).

The results suggest that the model is partly deficient of non-zonal variability in both fields. The non-zonal Z_{500} field is again indicative of missing (non-zonal) geopotential height variability over the ASL region and south of Australia compared to the reanalysis. In accordance with the stronger geopotential height gradient, a zone of enhanced non-zonal wind anomalies is visible south of Australia in the model. Generally, the difference plot of the zonally asymmetric components of both fields resemble the largest spatial structure of differences in the individual climatology differences. This fact highlights again the exaggerated zonal symmetry in the MPI-ESM compared to the reanalysis. It is concluded that the differences between model and reanalysis climatologies in U_{200} and Z_{500} stem mainly from the lacking non-zonal variations in the model. The ASL region is a recipient of eddies moving southeastward (Turner et al., 2013) and a key component of the non-zonal climatological circulation (Raphael et al., 2016). The model simulates this component insufficiently and is thus deficient in representing the observed geopotential height distribution over the ASL region.

In general, the differences between model and reanalysis of the non-zonal parts of the circulation are most pronounced from the longitudes of Australia towards the east of the Antarctic Peninsula. The geopotential height variability over these longitudes is strongly modulated by the presence of the Pacific South American Patterns (PSA modes). In literature, the PSA modes were traditionally seen as the mechanism by which tropical signals are communicated via stationary Rossby wave trains towards Antarctica (Karoly, 1989). Since the ENSO teleconnections are found to be weaker in the model than observed (Jungclaus et al., 2006), it is plausible that the deficiencies of the model in representing the SH asymmetric circulation originate from the inadequate simulation of the high-latitude ENSO teleconnections.

A more recent interpretation of the PSA variability and its interactions with ENSO is supposed by Irving and Simmonds (2016) who reported that there is only a weak relationship between PSA and ENSO when applying their method

for identifying the PSA pattern. The authors suggest that the PSA pattern can be interpreted as a regional atmospheric response to various trigger mechanisms with ENSO being just one of many players. This is consistent with the idea that the PSA pattern is an integral component of the zonally asymmetric structure of the AAO (Irving and Simmonds, 2016). This finding is in agreement with the result from Chap. 5 which reveals a significant correlation between the PSA-1 mode and a component of the PSI (PC3). It indicates an indirect and non-linear but nevertheless strong (r = 0.75) relationship between the PSA pattern and the SH split variability in ERA-Interim. This relationship is absent in the model pointing towards a lack of mechanisms forcing the PSA patterns and the associated non-annular AAO component.

Fan (2007) demonstrated that at least a part of the non-annular component of the AAO appears due to variations in the Southern Oscillation. A composite analysis of the non-annular portion of the AAO reveals pronounced differences in the model compared to the reanalysis. The positive composite of the non-annular AAO portion in ERA-Interim reveals a deepening of the climatological ASL (and positive anomalies east of the Antarctic Peninsula). This pattern resembles the Antarctic dipole pattern (ADP; (Yuan, 2004)), which was found to be simulated deficiently in the MPI-ESM (see Chap. 4). Consistently, there is a distinct different spatial pattern visible in the model with a positive (negative) anomaly east (west) of the Antarctic Peninsula in the negative composite of the MPI-ESM. It can be concluded that the MPI-ESM lacks considerable non-annular AAO variability in the SH circulation which originates probably from the deficiencies in simulating the tropical forced component that impacts the high-latitude SH atmospheric variability.

7 Discussion

This thesis is dedicated to central aspects of the zonally asymmetric component of the Southern Hemisphere (SH) extra-tropical circulation. Several studies demonstrated the critical importance of the non-zonal part of the circulation to the regional climate, especially when considering seasonal variations (Fogt et al., 2012; O'Kane et al., 2017; Fan, 2007). Particularly the western Antarctic region was found to be sensitive to variations in the non-zonal symmetric circulation (see Introduction, Chap. 1). It is thus highly desirable to (1) understand the physical mechanisms associated with the asymmetric circulation and its impacts on regional weather and climate as observed and (2) to gain an appropriate representation in climate models.

In order to contribute knowledge concerning this matter three major questions are addressed in this thesis: (i) Is the MPI earth system model able to reproduce the spatial patterns of the Antarctic Oscillation (AAO) and related precipitation? (ii) Can a hemispheric index be defined which clarifies the relationships between the SH wintertime split jet variability (i.e. one of the most prominent asymmetric features of the SH circulation) and the large-scale teleconnection indices ENSO, AAO and PSA? And lastly (iii) Is the MPI-ESM able to reproduce the SH wintertime split jet variability?

Therefore, this thesis revises initially the potential of the MPI-ESM to simulate a (nearly zonally symmetric) component of the SH circulation: the AAO which is defined as the leading mode of the tropospheric extra-tropical circulation variability (Thompson and Wallace, 2000). Deviations in representing the AAO which hint towards a lack of (zonally asymmetric) geopotential height variability in the model are discussed. Moreover, the AAO-related precipitation patterns in the MPI-ESM are examined.

Secondly, this thesis provides a novel method to describe the most prominent asymmetric feature of the SH, the Austral wintertime split jet over the longitudes of New Zealand and Australia. A PC based split jet index is introduced and new insights are provided concerning the interactions between the (zonally asymmetric) split jet variability and the large-scale teleconnection patterns AAO, ENSO and

PSA.

Since the presence of the SH wintertime split jet has large impacts on the regional scale, especially over the Pacific sector (Bals-Elsholz et al., 2001), this thesis aims further the ability of the MPI-ESM to represent this zonally asymmetric aspect of the SH tropospheric variability. Reasons for the limited representation of the SH split jet variability in the MPI-ESM are discussed in the context of the non-zonal variability in two associated fields (U_{200} and Z_{500}) and by the utilization of the non-annular (zonally asymmetric) AAO component.

For convenience, these scientific questions are divided into several minor research questions and the corresponding results of the previous chapters are summarised and discussed in the following with respect to these questions posed in Section 1.3.

How is the leading EOF in SH geopotential height at 700 hPa represented in the MPI-ESM?

The MPI-ESM (historical run in MR mode) is in general able to simulate central features of the dominant mode of atmospheric variability in the SH (i.e. the AAO). The ability of the MPI-ESM to reproduce the spatial AAO structure was investigated by comparing properties of the spatial AAO structure to three reanalyses. The spatial patterns are nearly zonally symmetric which is approximately captured by the model. Nevertheless, the AAO's characteristic three centers of action (Mo, 2000) are less pronounced in the MPI-ESM-MR and slightly shifted compared to the reanalysis. This results from the model's exaggerated zonal symmetry which is a common problem of GCMs and ESMs (Fogt et al., 2012).

The annual cycle of AAO index variability with a characteristic peak in the cold season is well reproduced by the MPI-ESM. A spectral analysis of the index time series reveals a lack of variability in the intra-seasonal range (periods of 4 to 5 months). Altogether the model is in general able to reproduce central aspects of the leading mode of the geopotential height variability.

Can mechanisms be identified which cause the deficiencies in the MPI-ESM?

The most pronounced differences (between model and ERA-Interim reanalysis) in the AAO patterns occur over the Amundsen Sea, the Weddell Sea (i.e. the Antarctic Dipole, ADP) and two further regions, the Ross Sea and the southern Indian Ocean. These differences hint towards an inadequate reproduction of the

geopotential height contrast in these locations in the MPI-ESM.

The atmospheric variability over the Amundsen and Weddell Seas were in literature tied to be influenced by the dipolar variability known as the ADP. Since the ADP is in turn triggered by ENSO variability (Yuan, 2004), it is hypothesised that the MPI-ESM lacks portions of ENSO variability. Jungclaus et al. (2013) demonstrated that MPI-ESM-MR is superior in ENSO modeling compared to the CMIP3 version of the MPI model but does not reproduce the correct seasonal modulation of the ENSO strength and nor the right ratio of El Niño and La Niña events. Consequently, improving these ENSO deficits might improve also MPI-ESM-MR's AAO characteristics.

How are the SH precipitation patterns related to the AAO in the MPI-ESM?

This spatial distribution of AAO-related precipitation is to a large extent reproduced by the model, although the MPI-ESM underestimates (overestimates) the precipitation during positive AAO phases over the Antarctic Peninsula (Indonesia). The underestimation of precipitation over the peninsula results from the reduced air-pressure over the Amundsen Sea in MPI-ESM via circulation changes.

The link between the monthly AAO time series and SH precipitation was quantified by correlation plots. The results reveal that the reanalysis correlation patterns are to a large extent reproduced by the model. However, over southern Australia, the Weddell Sea, and the Antarctic Peninsula the MPI-ESM underestimates the strong link between AAO and precipitation. The missing dipolar-like structure in the correlation pattern between Weddell Sea and Antarctic Peninsula on the one hand and Amundsen Sea and West Antarctica on the other hand in the reanalysis is explained by the already mentioned underestimation of the low pressure system over Amundsen Sea (ASL). In climatological mean the ASL contributes wet and warm (cold) air to the eastern (western) part of Antarctic peninsula. This mechanism is less distinct in the model and accounts therefore for missing positive and negative precipitation correlation in the West Antarctic area.

Can a SH wintertime split jet index be found which is superior to the rigid regional definitions used by established indices?

According to the literature review, there are up to now three (past) studies proposing a SH split jet index. All indices use region-based definitions which con-

tradict the assumption that the SH split jet is a hemispheric feature rather than a regional effect. The most important advantage and the novelty of the new PC based split index (PSI) compared to the existing indices is its independence from regional definitions: the PSI is defined by linearly combining the SH second and third principal component of the monthly (JAS) anomalous zonal wind at 200 hPa.

The PSI correlates well to the individual split indices and even the average of all indices gives a significant correlation coefficient of 0.76 to the PSI. From the correlation analysis and the investigation of PSI composites in the 200 hPa zonal wind field, it is apparent that the PC based split index is able to reproduce the SH wintertime split jet structure. Since the PSI captures furthermore the hemispherical nature of the SH split jet, it is superior to the established split jet indices.

Is the SH wintertime split jet related to the large-scale teleconnection indices (i.e. ENSO, AAO and PSA)?

The new PSI shows a significant correlation to the AAO (NOAA's AAO defined at 700 hPa) with r = 0.81. This highly significant relationship between the PSI and the leading mode in geopotential height variability reiterates the importance of the AAO to the PFJ variability (Fyfe (2003), Gallego et al. (2005)). The PFJ strength is enhanced under AAO^+ conditions in accordance with the negative pressure anomalies over the polar region occurring under AAO^+. Since the PFJ variability is more important for the representation of split events (Bals-Elsholz et al., 2001) than its subtropical counterpart, the AAO has a high correlation with the PSI (r = 0.81).

The correlation between the Multivariate ENSO Index (MEI) to the PSI is low, but 7 out of 18 split events occurred during a warm (5) or cold (2) ENSO month. The occurrence of both, warm and cold ENSO events damps the correlation value to the PSI, but the relative frequency of ENSO events is still 30 %. It seems likely that any kind of ENSO flavor is favorable for split events, which results in a nonlinear relation between PSI and ENSO. From earlier studies, it is known that El Niño (La Niña) phases enhance (reduce) the STJ strength over the South Pacific Ocean via advection of mean flow momentum flux (e.g. Chen et al. (1996)). This is consistent with the finding that 5 out of 18 split events occurred during a warm ENSO phase. Otherwise, there are strong ENSO events (El Niño of 1997 and La Niña in 1988) during the analysis period which did not lead to a pronounced split event. Thus, an ENSO event is not necessary to produce a SH split event.

The relationship between the PSA indices and the PSI reveals a small relation-

ship to both indices ($r_{PSA-1} \approx 0.2$ and $r_{PSA-2} = 0.06$). In contrast, the individual PCs of the zonal circulation at 200 hPa correlate significantly to the PSA-1 index. Positive PSA-1 phases are associated with a strong PFJ over the western Pacific sector and the PSA-1 mode is consistently significantly correlated to the PC3 component which is an integral part of the PSI. Negative PSA cases are associated with an enhanced PFJ over the eastern hemisphere which resembles the partly EOF2 variability. It is reasoned that PC3 represents both, AAO as well as PSA variability. However, the connection between the PSA-1 mode and the PSI is canceled out by the PC2 component which is (as well as the PC3 component) negatively correlated to the PSA-1 mode.

Altogether, the strength of the connection between the new PC based SH split jet index and the large-scale modes AAO and ENSO is non-linear. The highly significant relationship to the AAO highlights the importance of the PFJ variability which is a determining factor for the split jet formation while the relation to ENSO and PSA is complex and less important.

Can a PC based split jet index be applied in the MPI-ESM as in ERA-Interim?

In order to evaluate the potential of the MPI-ESM to represent the wintertime SH split jet variability, the procedure for calculating the PSI in ERA-Interim is applied to the model data, i.e. the leading five PCs of the 200 hPa zonal wind are correlated to the established split jet indices. The modes higher than the first are not distinguishable after North's "rule of thumb" (North et al., 1982). This implicates that the MPI-ESM mixes the mechanisms associated with the SH split jet variability in the higher order modes of the zonal wind variance. This is supported by the fact that two out of three established split jet indices correlate significantly to PC1, PC3, PC4 and PC5. The mean of all established split jet indices which was the crucial factor for the PSI_{MPI} definition, correlates significantly to PC1 and PC3.

Thus, the PSI_{MPI} can be defined, in accordance with the PSI in ERA-Interim, as a linear combination of both: PC1 and PC3. The PSI_{MPI} and the mean of all established indices correlate significantly to each other ($r = 0.53$) although the strength of the relationship is modest compared to the reanalysis ($r = 0.76$). The MPI-ESM lacks variance in the higher order modes of the SH zonal wind field at 200 hPa and reproduces thus weaker split variability of the SH winter circulation.

Can causes be identified which account for potential shortcomings of the model in representing the SH split jet variability?

A potential cause of discrepancies in the zonal wind field between the MPI-ESM-MR and the ERA-Interim reanalysis is the insufficient representation of the accurate PFJ latitude (Stevens et al., 2013; Bracegirdle and Marshall, 2012), especially over the SH. This results from the overall reduced meridional geopotential height gradient in the model (see Chap. 4).

Another weakness concerning the geopotential height distribution of the MPI-ESM with a potentially unfavorable effect on the accurate representation of the split jet is the insufficient simulation of ASL variability (e.g. Babian et al., 2016) and longitude (Hosking et al., 2013). Since this region is known to be influenced by ENSO teleconnections, it is argued that a lack of ENSO variability in the model leads to significant differences in the geopotential height variability over the high-latitudes, especially over the western Antarctic Peninsula region. This assumption is supported by Jungclaus et al. (2006) who reported the MPI-ESM-MR to simulate much weaker ENSO teleconnections towards the central subtropical South Pacific and tropical western Pacific than observed.

Are the zonal asymmetric components of the SH circulation depicted by the MPI-ESM?

Generally, the model represents to a large extent the spatial distribution of the geopotential height and zonal wind climatologies and standard deviations as stated by the ERA-Interim reanalysis. The results from Sec. 6.4.1 highlight again the exaggerated zonality in the MPI-ESM compared to the reanalysis. Altogether, the differences between model and reanalysis climatologies in U_{200} and Z_{500} stem mainly from lacking meridional variations in the model.

The differences between model and reanalysis of the non-zonal parts of the circulation are generally most pronounced from the longitudes of Australia towards the east of the Antarctic Peninsula, i.e. a region that is strongly modulated by PSA modes. The PSA modes were traditionally seen as the mechanism by which tropical signals are communicated towards Antarctica (Karoly, 1989). Since the ENSO teleconnections are found to be weaker in the model than observed Jungclaus et al. (2006) it is plausible that the deficiencies of the model in representing the SH asymmetric circulation originate from the inadequate simulation of the ENSO teleconnections in the polar regions.

A composite analysis of the non-annular portion of the AAO reveals pronounced differences in the model compared to the reanalysis. The positive composite of the non-annular AAO portion in ERA-Interim resembles the Antarctic dipole pattern (ADP; (Yuan, 2004)) which was found to be deficiently simulated in the MPI-ESM. Consistently, there is a pronounced difference in the spatial pattern simulated by the model. It can be concluded that the MPI-ESM lacks a part of the non-annular AAO variability in the SH circulation which origins from the deficiencies in simulating the tropical forced component that impacts the high-latitude atmospheric variability.

8 Outlook

This thesis provides results of aspects of the zonally asymmetric SH circulation and the representation in the MPI-ESM. Although representing substantial advances, especially in describing the SH wintertime split jet over the Australia / New Zealand region, there is still potential future work.

One aspect involves the investigation of seasonal variations in the PSI. In the context of a positive summertime trend in the AAO due to ozone depletion, it is likely that the PSI exhibits significant trends at least on seasonal time scales.

Furthermore, the potential of a higher temporal (i.e. daily) resolved index should be explored. A strong split jet can often be considered to be the signature of blocking that occurs over the Australian / New Zealand sector (Trenberth and Mo, 1985; Inatsu and Hoskins, 2006). A daily index would be desirable to describe the processes connected with the blocking activity over that specific region (Australia / New Zealand sector).

In that context, a PC based split index for the Northern Hemisphere (NH) would be as well worthwhile. The NH atmospheric circulation is subject to frequent blocking situations which have a large impact on the synoptic situation of the midlatitudes. Since blocking highs are persistent and quasi-stationary by definition, they affect surface weather and climate in a major way (Dunn-Sigouin and Son, 2013). Especially possible changes in the NH blocking frequency and duration in a warmer climate is a challenging future research question.

The relationships between the SH split jet variability and the large-scale teleconnection indices (AAO, ENSO, PSA) were extensively investigated within this thesis. The interactions between the large-scale modes are highly complex and need further research in order to clarify concurrently the relationship between these patterns and the associated SH split variability. Especially in the context of the interpretation of the PSA patterns as an integral part of the zonally asymmetric AAO component (Irving and Simmonds, 2016), it is of high interest to understand how these patterns are linked.

At this stage, it is not clear what physical mechanisms are responsible for exciting the growth and decay of split and nonsplit events. The PSI time series shows

that the upper-troposphere zonal flow fluctuates between the split and nonsplit regimes on monthly to decadal time scales. An extension of the current work is to understand the life cycle of the SH split jet. An examination of growing and decaying stages of the split jet could provide new insight into the physical processes that govern the evolution, maintenance and dissipation of the split jet. This potentially leads to a better understanding of the variability of the split jet, the PFJ, and the STJ in the SH.

9 References

Baba, K. and Renwick, J. (2017). Aspects of intraseasonal variability of antarctic sea ice in austral winter related to enso and sam events. *Journal of Glaciology*, 63(241):838–846.

Babian, S., Grieger, J., and Cubasch, U. (2017). A new index for the wintertime southern hemispheric split jet. *Atmospheric Chemistry and Physics Discussions*, 2017:1–19.

Babian, S., Rust, H. W., Grieger, J., and Cubasch, U. (2016). Representation of the Antarctic Oscillation and related precipitation in the MPI Earth System Model. *Meteorol. Z.*, 17:12635.

Bals-Elsholz, T. M., Atallah, E. H., Bosart, L. F., Wasula, T. a., Cempa, M. J., and Lupo, a. R. (2001). The wintertime southern hemisphere split jet: Structure, variability, and evolution. *Journal of Climate*, 14(21):4191–4215.

Barnes, E. A. and Hartmann, D. L. (2010). Testing a theory for the effect of latitude on the persistence of eddy-driven jets using cmip3 simulations. *Geophysical Research Letters*, 37(15):n/a–n/a. L15801.

Bengtsson, L., Hodges, K. I., and Roeckner, E. (2006). Storm tracks and climate change. *Journal of Climate*, 19(15):3518–3543.

Berman, A., Silvestri, G., and Compagnucci, R. (2012). Eastern patagonia seasonal precipitation: influence of Southern Hemisphere circulation and links with subtropical South American precipitation. *J. Climate*, 25:6781–6795.

Berman, A., Silvestri, G., and Compagnucci, R. (2013). On the variability of seasonal temperature in southern South America. *Clim. Dyn.*, 40:1863–1878.

Box, G. E. P. and Jenkins, G. M. (1976). *Time Series Analysis: Forecasting and Control*. Prentice Hall, New Jersey.

Bracegirdle, T. J. and Marshall, G. J. (2012). The reliability of antarctic tropospheric pressure and temperature in the latest global reanalyses. *Journal of Climate*, 25(20):7138–7146.

Brockwell, P. J. and Davis, R. A. (1991). *Time series: Theory and Methods*. Springer Series in Statistics. Springer, Berlin.

Carvalho, L., Jones, C., and Ambrizzi, T. (2005). Opposite phases of the Antarctic Oscillation and relationships with intraseasonal to interannual activity in the tropics during the austral summer. *J. Climate*, 18:702–718.

Ceppi, P., Hwang, Y.-T., Frierson, D. M. W., and Hartmann, D. L. (2012). Southern hemisphere jet latitude biases in cmip5 models linked to shortwave cloud forcing. *Geophysical Research Letters*, 39(19):n/a–n/a. L19708.

Chen, B., Smith, S. R., and Bromwich, D. H. (1996). Evolution of the Tropospheric Split Jet over the South Pacific Ocean during the 1986–89 ENSO Cycle. *Monthly Weather Review*, 124:1711–1731.

Climate Prediction Center (2014). Website. Available online at http://www.cpc.noaa.gov; visited on March 8th 2014.

Codron, F. (2007). Relations between annular modes and the mean state: Southern hemisphere winter. *Journal of the Atmospheric Sciences*, 64(9):3328–3339.

Dee, D. P., Uppala, S. M., Simmons, A. J., Berrisford, P., Poli, P., Kobayashi, S., Andrae, U., Balmaseda, M. A., Balsamo, G., Bauer, P., Bechtold, P., Beljaars, A. C. M., van de Berg, L., Bidlot, J., Bormann, N., Delsol, C., Dragani, R., Fuentes, M., Geer, A. J., Haimberger, L., Healy, S., Hersbach, H., Holm, E. V., Isaksen, L., Kållberg, P., Koehler, M., Matricardi, M., McNally, A. P., Monge-Sanz, B. M., Morcrette, J.-J., Park, B.-K., Peubey, C., de Rosnay, P., Tavolato, C., Thepaut, J.-N., and Vitart, F. (2011). The ERA-Interim reanalysis: configuration and performance of the data assimilation system. *Quart. J. Roy. Meteor. Soc.*, 137(656):553–597.

deLeeuw, J. (1992). Akaike (1973) information theory and an extension of the maximum likelihood principle. In Kotz, S. and Johnson, N. L., editors, *Breakthroughs in Statistics*, volume 1, pages 599–609. Springer, London.

Ding, Q., Steig, E. J., Battisti, D. S., and Wallace, J. M. (2012). Influence of the tropics on the southern annular mode. *Journal of Climate*, 25(18):6330–6348.

Ding, R., Li, J., Tseng, Y.-h., Ha, K.-J., Zhao, S., and Lee, J.-Y. (2016). Interdecadal change in the lagged relationship between the Pacific–South American pattern and ENSO. *Climate Dynamics*, 47(9):2867–2884.

Dunn-Sigouin, E. and Son, S.-W. (2013). Northern hemisphere blocking frequency and duration in the CMIP5 models. *Journal of Geophysical Research: Atmospheres*, 118(3):1179–1188.

Fan, K. (2007). Zonal asymmetry of the antarctic oscillation. *Geophysical Research Letters*, 34(2):n/a–n/a. L02706.

Fogt, R. L., Jones, J. M., and Renwick, J. (2012). Seasonal zonal asymmetries in the southern annular mode and their impact on regional temperature anomalies. *Journal of Climate*, 25(18):6253–6270.

Fyfe, J. C. (2003). Separating extratropical zonal wind variability and mean change. *Journal of Climate*, 16(5):863–874.

Fyfe, J. C., Boer, G. J., and Flato, G. M. (1999). The arctic and antarctic oscillations and their projected changes under global warming. *Geophysical Research Letters*, 26(11):1601–1604.

Gallego, D., Ribera, P., Garcia-Herrera, R., Hernandez, E., and Gimeno, L. (2005). A new look for the Southern Hemisphere jet stream. *Climate Dynamics*, 24(6):607–621.

Galvin, J. F. P. (2007). The weather and climate of the tropics part 2 –the subtropical jet streams. *Weather*, 62(11):295–299.

Gerber, E., Polvani, L., and Ancukiewicz, D. (2008). Annular mode time scales in the intergovernmental panel on climate change fourth assessment report models. *Geophysical Research Letters*, 35(22).

Gillett, N., Kell, T., and Jones, P. (2006). Regional climate impacts of the Southern Annular Mode. *Geophys. Res. Lett.*, 33:L23704.

Giorgetta, M. A., Jungclaus, J., Reick, C. H., Legutke, S., Bader, J., Böttinger, M., Brovkin, V., Crueger, T., Esch, M., Fieg, K., Glushak, K., Gayler, V., Haak, H., Hollweg, H.-D., Ilyina, T., Kinne, S., Kornblueh, L., Matei, D., Mauritsen, T., Mikolajewicz, U., Mueller, W., Notz, D., Pithan, F., Raddatz, T., Rast, S., Redler, R., Roeckner, E., Schmidt, H., Schnur, R., Segschneider, J., Six,

K. D., Stockhause, M., Timmreck, C., Wegner, J., Widmann, H., Wieners, K.-H., Claussen, M., Marotzke, J., and Stevens, B. (2013). Climate and carbon cycle changes from 1850 to 2100 in MPI-ESM simulations for the Coupled Model Intercomparison Project phase 5. *J. Adv. Model. Earth Syst.*, 5(3):572–597.

Gong, D. and Wang, S. (1999). Definition of Antarctic Oscillation Index. *Geophysical Research Letters*, 26(4):459–462.

Hall, A. and Visbeck, M. (2002). Synchronous Variability in the Southern Hemisphere Atmosphere, Sea Ice, and Ocean Resulting from the Annular Mode. *J. Climate*, 15:3043–3057.

Hannachi, A., Jolliffe, I. T., and Stephenson, D. B. (2007). Empirical orthogonal functions and related techniques in atmospheric science: A review. *Int. J. Climatol.*, 27(9):1119–1152.

Hendon, H. H., Thompson, D. W. J., and Wheeler, M. C. (2007). Australian Rainfall and Surface Temperature Variations Associated with the Southern Hemisphere Annular Mode. *J. Climate*, 20:2452–2467.

Hio, Y. and Hirota, I. (2002). Interannual variations of planetary waves in the southern hemisphere stratosphere. *Journal of the Meteorological Society of Japan. Ser. II*, 80(4B):1013–1027.

Hobbs, W. R. and Raphael, M. N. (2007). A representative time-series for the southern hemisphere zonal wave 1. *Geophysical Research Letters*, 34(5):n/a–n/a. L05702.

Hobbs, W. R. and Raphael, M. N. (2010). Characterizing the zonally asymmetric component of the sh circulation. *Climate Dynamics*, 35(5):859–873.

Hosking, J. S., Orr, A., Marshall, G. J., Turner, J., and Phillips, T. (2013). The influence of the amundsen–bellingshausen seas low on the climate of west antarctica and its representation in coupled climate model simulations. *Journal of Climate*, 26(17):6633–6648.

Ilyina, T., Six, K. D., Segschneider, J., Maier-Reimer, E., Li, H., and Núñez Riboni, I. (2013). Global ocean biogeochemistry model HAMOCC: Model architecture and performance as component of the MPI-Earth system model in different CMIP5 experimental realizations. *J. Adv. Model. Earth Syst.*, 5(2):287–315.

Inatsu, M. and Hoskins, B. J. (2006). The seasonal and wintertime interannual variability of the split jet and the storm-track activity minimum near New Zealand. *Journal of the Meteorological Society of Japan*, 84(3):433–445.

Irving, D. and Simmonds, I. (2016). A new method for identifying the pacific–south american pattern and its influence on regional climate variability. *Journal of Climate*, 29(17):6109–6125.

Jolliffe, I. T. (2002). *Principal Component Analysis*. Springer Series in Statistics. Springer, New York, 3rd edition.

Jungclaus, J. H., Fischer, N., Haak, H., Lohmann, K., Marotzke, J., Matei, D., Mikolajewicz, U., Notz, D., and von Storch, J. S. (2013). Characteristics of the ocean simulations in the Max Planck Institute Ocean Model (MPIOM) the ocean component of the MPI-Earth system model. *J. Adv. Model. Earth Syst.*, 5(2):422–446.

Jungclaus, J. H., Keenlyside, N., Botzet, M., Haak, H., Luo, J.-J., Latif, M., Marotzke, J., Mikolajewicz, U., and Roeckner, E. (2006). Ocean circulation and tropical variability in the coupled model ECHAM5/MPI-OM. *J. Climate*, 19:3952–3972.

Kalnay, E., Kanamitsu, M., and Kistler, R. (1996). The NCEP/NCAR 40-Year Reanalysis Project. *Bull. Amer. Meteor. Soc.*, 77:437–471.

Karoly, D. J. (1989). Southern hemisphere circulation features associated with el niño-southern oscillation events. *Journal of Climate*, 2(11):1239–1252.

Kidson, J. W. (1988). Indices of the southern hemisphere zonal wind. *Journal of Climate*, 1(2):183–194.

Kidson, J. W. (1999). Principal Modes of Southern Hemisphere low-frequency variability obtained from NCEP-NCAR reanalyses. *J. Climate*, 12:2808–2830.

Kidston, J. and Gerber, E. P. (2010). Intermodel variability of the poleward shift of the austral jet stream in the cmip3 integrations linked to biases in 20th century climatology. *Geophysical Research Letters*, 37(9):n/a–n/a. L09708.

Kim, B.-M., Choi, H., Kim, S.-J., and Choi, W. (2017). Amplitude-dependent relationship between the southern annular mode and the el niño southern oscillation in austral summer. *Asia-Pacific Journal of Atmospheric Sciences*, 53(1):85–100.

Kistler, R., Kalnay, E. M., and Collins, W. (2001). The NCEP/NCAR 50-Year Reanalysis: Monthly Means CD-ROM and documentation. *Bull. Amer. Meteor. Soc.*, 82:247–268.

Kitoh, A. (1994). Tropical Influence on the South Pacific Double Jet Variability. *Proc. NIPR Symp. Polar Meteorol. Glaciol.*, 8:34–45.

Kohyama, T. and Hartmann, D. L. (2016). Antarctic sea ice response to weather and climate modes of variability. *Journal of Climate*, 29(2):721–741.

Kruschke, T., Rust, H. W., Kadow, C., Leckebusch, G., and Ulbrich, U. (2014). Evaluating decadal predictions of northern hemispheric cyclone frequencies. *Tellus A*, 66:22830.

Kruschke, T., Rust, H. W., Kadow, C., Müller, W., Pohlmann, H., Leckebusch, G., and Ulbrich, U. (2015). Probabilistic evaluation of decadal predictions for northern hemisphere winter storms. *Meteorol. Z.*, this issue.

Kwok, R. and Comiso, J. C. (2002). Spatial patterns of variability in antarctic surface temperature: Connections to the southern hemisphere annular mode and the southern oscillation. *Geophysical Research Letters*, 29(14):50–1–50–4.

Lee, S. and Kim, H. (2003). The dynamical relationship between subtropical and eddy-driven jets. *Journal of the Atmospheric Sciences*, 60(12):1490–1503.

Lefebvre, W., Goosse, H., Timmermann, R., and Fichefet, T. (2004). Influence of the southern annular mode on the sea ice–ocean system. *Journal of Geophysical Research: Oceans*, 109(C9):n/a–n/a. C09005.

Limpasuvan, V. and Hartmann, D. L. (1999). Eddies and the annular modes of climate variability. *Geophysical Research Letters*, 26(20):3133–3136.

Lorenz, D. J. and Hartmann, D. L. (2001). Eddy–Zonal Flow Feedback in the Southern Hemisphere. *Journal of the Atmospheric Sciences*, 58:3312–3327.

Lorenz, E. (1967). *The Nature and Theory of the General Circulation of the Atmosphere*. WMO: TP. World Meteorological Organization.

Lu, R., Li, Y., and Buwen, D. (2007). Arctic oscillation and antarctic oscillation in internal atmospheric variability with an ensemble agcm simulation. *Advances in Atmospheric Sciences*, 24(1):152–162.

Marotzke, J., Mueller, W. A., Vamborg, F. S. E., Becker, P., Cubasch, U., Feldmann, H., Kaspar, F., Kottmeier, C., Marini, C., Polkova, I., Prömmel, K., Rust, H. W., Stammer, D., Ulbrich, U., Kadow, C., Köhl, A., Kröger, J., Kruschke, T., Pinto, J. G., Pohlmann, H., Reyers, M., Schröder, M., Sienz, F., Timmreck, C., and Ziese, M. (2016). MiKlip - a National Research Project on Decadal Climate Prediction. *Bull. Amer. Meteor. Soc.*

Marshall, G. J. and Bracegirdle, T. J. (2015). An examination of the relationship between the southern annular mode and antarctic surface air temperatures in the cmip5 historical runs. *Climate Dynamics*, 45(5):1513–1535.

Marsland, S. J., Haak, H., Jungclaus, J. H., Latif, M., and Roeske, F. (2003). The Max-Planck-Institute global ocean/sea-ice model with orthogonal curvilinear coordinates. *Ocean Modelling*, 5:91–127.

Mechoso, C. R., O'Neill, A., Pope, V. D., and Farrara, J. D. (1988). A study of the stratospheric final warming of 1982 in the southern hemisphere. *Quarterly Journal of the Royal Meteorological Society*, 114(484):1365–1384.

Meneghini, B., Simmonds, I., and Smith, I. (2007). Association between Australian rainfall and the Southern Annular Mode. *Int. J. Climatol.*, 27:109–121.

Mo, K. C. (2000). Relationships between Low-Frequency Variability in the Southern Hemisphere and Sea Surface Temperature Anomalies. *J. Climate*, 13:3599–3610.

Mo, K. C. and Higgins, R. W. (1998). The pacific–south american modes and tropical convection during the southern hemisphere winter. *Monthly Weather Review*, 126(6):1581–1596.

Mo, K. C. and Paegle, J. N. (2001). The pacific–south american modes and their downstream effects. *International Journal of Climatology*, 21(10):1211–1229.

Mo, K. C., Pfaendtner, J., and Kalnay, E. (1987). A gcm study on the maintenance of the june 1982 blocking in the southern hemisphere. *Journal of the Atmospheric Sciences*, 44(8):1123–1142.

Moy, C. M., Moreno, P. I., Dunbar, R. B., Kaplan, M. R., Francois, J.-P., Villalba, R., and Haberzettl, T. (2009). Climate Change in Southern South America During the Last Two Millennia. In Vimeux, F., Sylvestre, F., and Khodri,

M., editors, *Past Climate Variability in South America and Surrounding Regions*, volume 14 of *Developments in Paleoenvironmental Research*, pages 353–393. Springer Netherlands.

Müller, W., Baehr, J., Haak, H., Jungclaus, J., Kröger, J., Matei, D., Notz, D., Pohlmann, H., von Storch, J., and Marotzke, J. (2012). Forecast skill of multi-year seasonal means in the decadal prediction system of the Max Planck Institute for Meteorology. *Geophys. Res. Lett.*, 39:L22707.

North, G. R., Bell, T. L., Cahalan, R. F., and Moeng, F. J. (1982). Sampling errors in the estimation of empirical orthogonal functions. *Mon. Wea. Rev.*, 110:699–706.

O'Kane, T. J., Monselesan, D. P., and Risbey, J. S. (2017). A multiscale re-examination of the pacific–south american pattern. *Monthly Weather Review*, 145(1):379–402.

Peixoto, J. P. and Oort, A. H. (1992). *Physics of climate / Jose P. Peixoto and Abraham H. Oort ; foreword by Edward N. Lorenz*. American Institute of Physics New York.

Pezza, L. B., Durrant, T., Simmonds, I., and Smith, I. (2008). Southern Hemisphere Synoptic Behavior in Extreme Phases of SAM, ENSO, Sea Ice Extent, and Southern Australia Rainfall. *J. Climate*, 21:5566–5584.

Pohlmann, H., Müller, W. A., Kulkarni, K., Kameswarrao, M., Matei, D., Vamborg, F. S. E., Kadow, C., Illing, S., and Marotzke, J. (2013). Improved forecast skill in the tropics in the new MiKlip decadal climate predictions. *Geophys. Res. Lett.*, 40:5798–5802.

Pook, M. J., Risbey, J. S., McIntosh, P. C., Ummenhofer, C. C., Marshall, A. G., and Meyers, G. A. (2013). The seasonal cycle of blocking and associated physical mechanisms in the australian region and relationship with rainfall. *Monthly Weather Review*, 141(12):4534–4553.

Priestley, M. B. (1992). *Spectral Analysis and Time Series*. Academic Press, London.

R Core Team (2013). *R: A Language and Environment for Statistical Computing*. R Foundation for Statistical Computing, Vienna, Austria.

Raddatz, T. J., Reick, C. H., Knorr, W., Kattge, J., Roeckner, E., Schnur, R., Schnitzler, K. G., Wetzel, P., and Jungclaus, J. H. (2007). Will the tropical landbiosphere dominate the climate-carbon cycle feedback during the twenty-first century? *Clim. Dyn.*, 29:565–574.

Raphael, M. N. (2004). A zonal wave 3 index for the southern hemisphere. *Geophysical Research Letters*, 31(23):n/a–n/a. L23212.

Raphael, M. N., Marshall, G. J., Turner, J., Fogt, R. L., Schneider, D., Dixon, D. A., Hosking, J. S., Jones, J. M., and Hobbs, W. R. (2016). The amundsen sea low: Variability, change, and impact on antarctic climate. *Bulletin of the American Meteorological Society*, 97(1):111–121.

Rashid, H. A. and Simmonds, I. (2005). Southern hemisphere annular mode variability and the role of optimal nonmodal growth. *J. Atmos. Sci.*, 62:1947–1961.

Reason, C. J. C. and Rouault, M. (2005). Links between the Antarctic Oscillation and winter rainfall over western South Africa. *Geophys. Res. Lett.*, 32(7).

Renwick, J. and Thompson, D. (2006). The Southern Annular Mode and New Zealand climate. *Water and Atmosphere*, 14:24–25.

Renwick, J. A. (2002). Southern hemisphere circulation and relations with sea ice and sea surface temperature. *Journal of Climate*, 15(21):3058–3068.

Renwick, J. A., Katzfey, J. J., Nguyen, K. C., and McGregor, J. L. (1998). Regional model simulations of new zealand climate. *Journal of Geophysical Research: Atmospheres*, 103(D6):5973–5982.

Rogers, J. C. and Van Loon, H. (1982). Spatial variability of sea level pressure and 500 mb height anomalies over the southern hemisphere. *Monthly Weather Review*, 110(10):1375–1392.

Sahai, A. K., Chattopadhyay, R., Joseph, S., Abhilash, S., Borah, N., and Goswami, B. N. (2014). A new method to compute the principal components from self-organizing maps: An application to monsoon intraseasonal oscillations. *International Journal of Climatology*, 34(9):2925–2939.

Seager, R., Harnik, N., Kushnir, Y., Robinson, W., and Miller, J. (2003). Mechanisms of hemispherically symmetric climate variability. *Journal of Climate*, 16(18):2960–2978.

Silvestri, G. E. and Vera, C. S. (2003). Antarctic Oscillation signal on precipitation anomalies over southeastern South America. *Geophys. Res. Lett.*, 30(21).

Silvestri, G. E. and Vera, C. S. (2009). Non-stationary impacts of the Southern Annular Mode on Southern Hemisphere climate. *J. Climate*, 22:6142–6148.

Stevens, B., Giorgetta, M., Esch, M., Mauritsen, T., Crueger, T., Rast, S., Salzmann, M., Schmidt, H., Bader, J., Block, K., Brokopf, R., Fast, I., Kinne, S., Kornblueh, L., Lohmann, U., Pincus, R., Reichler, T., and Roeckner, E. (2013). Atmospheric component of the MPI-M Earth System Model: ECHAM6. *J. Adv. Model. Earth Syst.*, 5(2):146–172.

Taljaard, J. (1972). *Synoptic Meteorology of the Southern Hemisphere*. Meteorological Monographs, Boston, 13 edition.

Taylor, K. E., Stouffer, R. J., and Meehl, G. A. (2012). An overview of CMIP5 and the experiment design. *Bull. Amer. Meteor. Soc.*, 93:485–498.

Thompson, D. and Wallace, J. M. (2000). Annular modes in the extratropical circulation. Part I: Month-to-month variability. *J. Climate*, 13:1000–1016.

Trenberth, K. E. and Caron, J. M. (2000). The southern oscillation revisited: Sea level pressures, surface temperatures, and precipitation. *Journal of Climate*, 13(24):4358–4365.

Trenberth, K. F. and Mo, K. C. (1985). Blocking in the southern hemisphere. *Monthly Weather Review*, 113(1):3–21.

Turner, J., Phillips, T., Hosking, J. S., Marshall, G. J., and Orr, A. (2013). The amundsen sea low. *International Journal of Climatology*, 33(7):1818–1829.

Ummenhofer, C. and England, M. (2007). Interannual extremes in New Zealand precipitation linked to modes of Southern Hemisphere climate variability. *J. Climate*, 20:5418–5440.

Uppala, S. M., Kållberg, P. W., Simmons, A. J., Andrae, U., da Costa Bechtold, V., Fiorino, M., Gibson, J. K., Haseler, J., Hernandez, A., Kelly, G. A., Li, X., Onogi, K., Saarinen, S., Sokka, N., Allan, R. P., Andersson, E., Arpe, K., Balmaseda, M. A., Beljaars, A. C. M., van de Berg, L., Bidlot, J., Bormann, N., Caires, S., Chevallier, F., Dethof, A., Dragosavac, M., Fisher, M., Fuentes, M., Hagemann, S., Holm, E., Hoskins, B. J., Isaksen, L., Janssen, P. A. E. M., Jenne,

R., McNally, A. P., Mahfouf, J.-F., Morcrette, J.-J., Rayner, N. A., Saunders, R. W., Simon, P., Sterl, A., Trenberth, K. E., Untch, A., Vasiljevic, D., Viterbo, P., , and Woollen, J. (2005). The ERA-40 re-analysis. *Quart. J. Roy. Meteor. Soc.*, 131:2961–3012.

Valcke, S. (2013). The OASIS3 coupler: a European climate modelling software. *Geoscientific Model Development*, 6:373–388.

van den Broeke, M. R. and van Lipzig, N. P. M. (2004). Changes in Antarctic temperature, wind and precipitation in response to the Antarctic Oscillation. *Ann. Glaciol.*, 39:119–126.

Venables, W. N. and Ripley, B. D. (2002). *Modern Applied Statistics with S*. Springer, New York, fourth edition. ISBN 0-387-95457-0.

Wilks, D. S. (2011). *Statistical methods in the atmospheric sciences*. Academic Press, San Diego, CA, 3rd edition.

Yang, X. and Chang, E. K. M. (2006). Variability of the Southern Hemisphere Winter Split Flow – A Case of Two-Way Reinforcement between Mean Flow and Eddy Anomalies. *Journal of Atmospheric Sciences*, 63(1987):634–650.

Yuan, X. (2004). Enso-related impacts on antarctic sea ice: a synthesis of phenomenon and mechanisms. *Antarctic Science*, 16:415–425.

Zhang, Z., Gong, D., Kim, S., Mao, R., and Yang, J. (2014). Is the antarctic oscillation trend during the recent decades unusual? *Antarctic Science*, 26(4):445–451.

Appendix

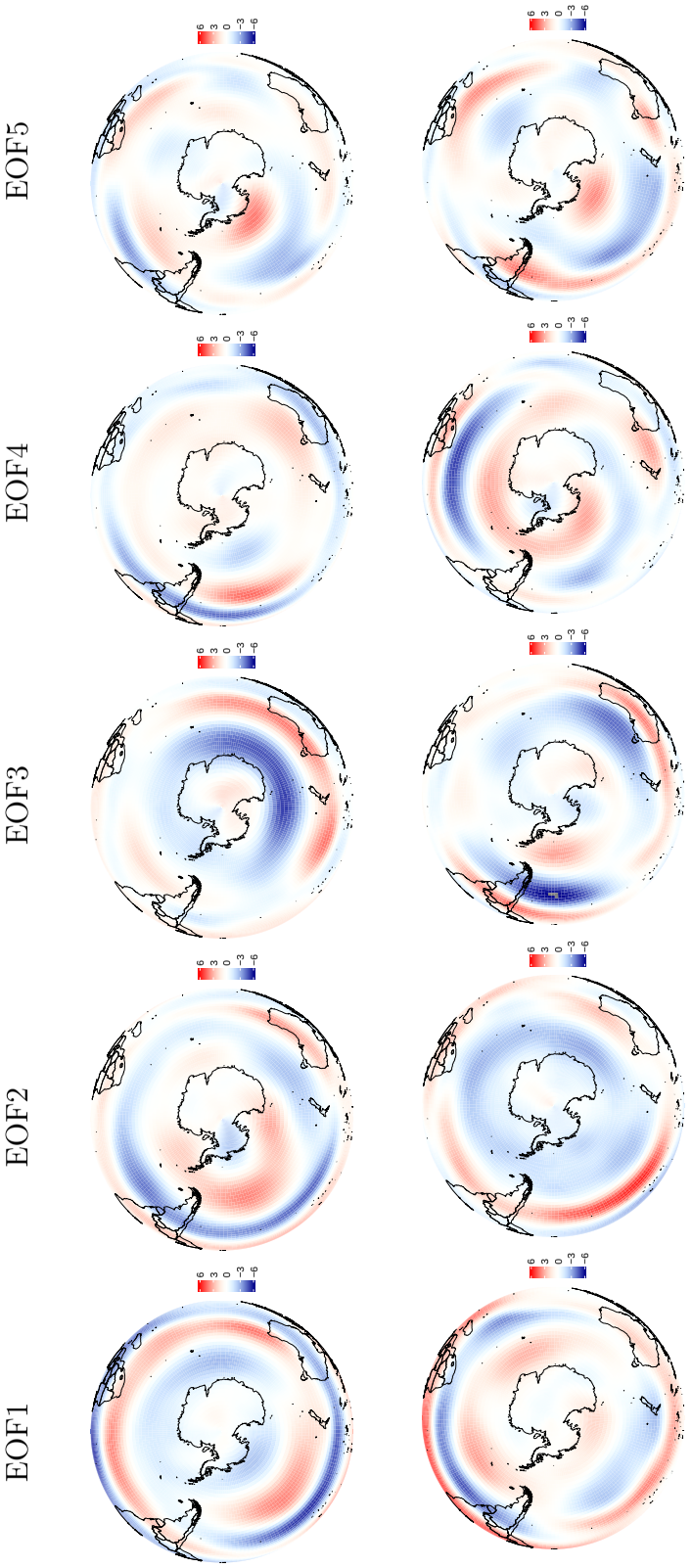

Figure 1: *The leading 5 EOF patterns of the zonal wind (m/s) at 200 hPa in Austral winter (JAS) for the 1979–2005 period in ERA-Interim (top row) and the MPI-ESM-MR (bottom row).*

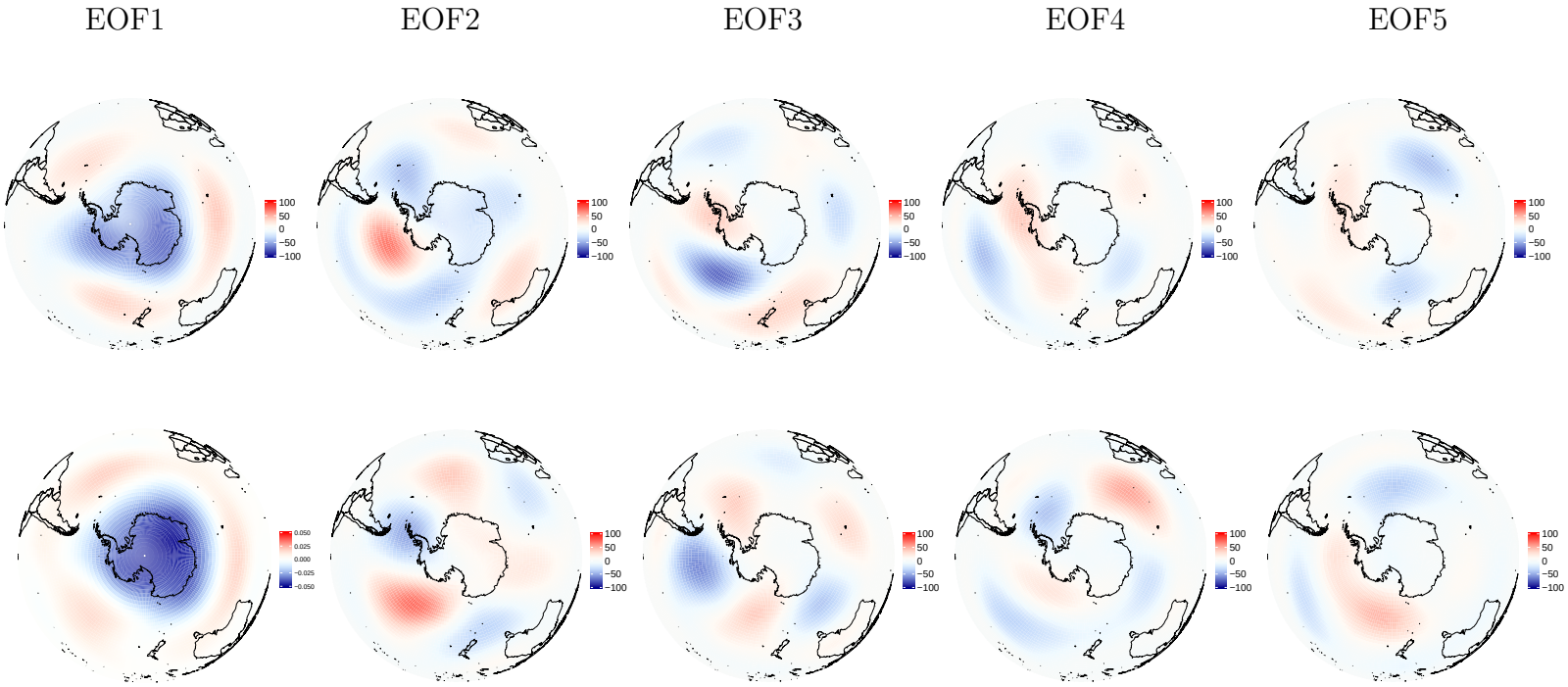

Figure 2: *The leading 5 EOF patterns of the geopotential height (m) at 500 hPa in Austral winter (JAS) for the 1979–2005 period in ERA-Interim (top row) and the MPI-ESM-MR (bottom row).*

List of Figures

List of Tables

Curriculum Vitae

Der Lebenslauf ist aus Gründen des Datenschutzes in der Online-Version nicht enthalten.